A PARAMETRIC AND PHYSICS-BASED APPROACH TO STRUCTURAL WEIGHT ESTIMATION OF THE HYBRID WING BODY AIRCRAFT

A Thesis
Presented to
The Academic Faculty

by

Trevor W. Laughlin

In Partial Fulfillment
of the Requirements for the Degree
Master of Science in the
School of Aerospace Engineering

Georgia Institute of Technology
December 2012

A PARAMETRIC AND PHYSICS-BASED APPROACH TO STRUCTURAL WEIGHT ESTIMATION OF THE HYBRID WING BODY AIRCRAFT

Approved by:

Professor Dimitri N. Mavris,
Committee Chair
School of Aerospace Engineering
Georgia Institute of Technology

Dr. Neil Weston
Aerospace Systems Design Laboratory
Georgia Institute of Technology

Dr. Vivek Mukhopadhyay
Langley Research Center
National Aeronautics and Space Administration

Date Approved: 24 August 2012

To my parents

ACKNOWLEDGEMENTS

First and foremost, I thank God for giving me the skills, strength, and perseverance to complete this work.

I would like thank my adviser Prof. Dimitri Mavris for his guidance and support throughout the course of this work. The events leading me to ASDL were unexpected but it has been a wonderful experience and I will always be grateful for the opportunity. I am thankful for all the research engineers who I have had the pleasure of learning from while at ASDL including Dr. Jung-ho Lewe and Dr. Hernando Jimenez.

This work would have not been possible without the technical guidance provided by so many talented and inspiring NASA engineers at the Langley Research Center: Dr. Vivek Mukhopadhyay, Mr. Craig Nickol, Dr. Frank Gern, Ms. Sharon Padula, Mr. Jay Robinson, Mr. Andy Hahn, Dr. Lloyd Eldred, and Dr. Jamshid Samareh.

I wish to also thank all my friends and colleagues here at ASDL. Although we were all at times completely overwhelmed and frustrated, we always found a way to get things done and enjoy ourselves a little bit in the process. I wish you all the best of luck and I hope to work with you again in the future.

I wouldn't have had this opportunity if it wasn't for all the love and support from my parents throughout my entire life. My academic success and any in the future is due in large part to the work ethic you instilled in me and I am forever grateful. Thank you Mom and Dad.

Trevor Laughlin

August, 2012

TABLE OF CONTENTS

LIST OF TABLES

LIST OF FIGURES

LIST OF ABBREVIATIONS AND SYMBOLS

ANN	Artificial Neural Network.
ANOVA	Analysis of Variance.
BWB	Blended Wing Body.
CAD	Computer-Aided Design.
CFD	Computational Fluid Dynamics.
DDTBDM	Discrete Data Transfer Between Dissimilar Meshes.
FEA	Finite Element Analysis.
FEM	Finite Element Model.
FLOPS	Flight Optimization System.
HWB	Hybrid Wing Body.
LaRC	Langley Research Center.
M&S	Modeling and Simulation.
MFE	Model Fit Error.
MRE	Model Representation Error.
NASA	National Aeronautics and Space Administration.
OML	Outer Mold Line.
PMARC	Panel Method Ames Research Center.
psi	Pounds per square inch.
VSP	Vehicle Sketch Pad.
$\{\varepsilon\}$	Vector of membrane strains.
$[A]$	Extensional stiffness matrix.
$A^{(i)}$	Area of i^{th} element.
α	Angle of attack.
AR	Aspect ratio.
A_{total}	Total area of all elements.

$[B]$	Bending stiffness matrix.
b	Wingspan.
b_{ow}	Span of the outboard wing section.
C_L	Lift coefficient.
$C_{L,req}$	Required lift coefficient.
$C'_{L,req}$	Required lift coefficient corrected for compressibility effects.
C_p	Pressure coefficient.
C'_p	Incompressible pressure coefficient.
$c_{r,cb}$	Chord length at root of centerbody section.
$c_{r,ow}$	Chord length at root of outboard wing section.
$c_{t,cb}$	Chord length at tip of centerbody section.
$c_{t,ow}$	Chord length at tip of outboard wing section.
$[D]$	Bending-extensional coupling stiffness matrix.
E_c	Compression modulus of isotropic material.
E_{c1}	Compression modulus of composite material in fiber direction.
E_{c2}	Compression modulus of composite material perpendicular to fiber direction.
E_t	Tensile modulus of isotropic material.
E_{t1}	Tensile modulus of composite material in fiber direction.
E_{t2}	Tensile modulus of composite material perpendicular to fiber direction.
g	Gravitational acceleration.
G	Shear modulus of isotropic material.
G_{12}	In-plane shear modulus of composite material.
G_{13}	Interlaminar shear modulus of composite material (13-direction).

G_{23}	Interlaminar shear modulus of composite material (23-direction).
K	Calibration constant.
$\{k\}$	Vector of bending strains.
K_{cb}	Calibration factor for centerbody section.
K_{ow}	Calibration factor for outboard wing section.
K_{rc}	Calibration factor for rear centerbody section.
K_{tw}	Calibration factor for trapezoidal wing section.
K_{vs}	Variable sweep constant.
λ	Wing taper ratio.
$\Lambda_{LE,cb}$	Sweep angle of centerbody leading edge.
$\Lambda_{LE,ow}$	Sweep angle of outboard wing leading edge.
l_{cabin}	Length of the centerbody cabin.
L/D	Lift-to-drag ratio.
M_∞	Freestream Mach number.
$\{M\}$	Vector of bending moments.
M_{inc}	Incompressible Mach number used for PMARC analysis.
n	Limit load factor.
$\{N\}$	Vector of membrane loads.
n_{bay}	Number of centerbody cabin bays.
$N_{x,T}^{(i)}$	Tensile membrane load of i^{th} element.
n_{pax}	Number of passengers.
ν_c	Poisson ratio of isotropic material (compression).
ν_{c12}	Poisson ratio of composite material (compression).
ν_t	Poisson ratio of isotropic material (tension).
ν_{t12}	Poisson ratio of composite material (tension).
$\overline{N}_{x,T}$	Area weighted average tensile membrane load.

P	HWB nominal cabin pressure (9.2 psi).
ϕ_{ow}	Twist angle at tip of outboard wing.
ρ_∞	Freestream density.
ρ	Material density.
S_{cabin}	Area of the passenger cabin.
σ_{cu1}	Ultimate compressive strength of composite material in fiber direction.
σ_{cu2}	Ultimate compressive strength of composite material perpendicular to fiber direction.
σ_{cy}	Yield strength of isotropic material (compression).
$\sigma_{N_{x,T}}$	Area weighted standard deviation of tensile membrane loads.
σ_{su}	Ultimate shear strength of isotropic material.
σ_{su12}	In-plane ultimate shear strength of composite material.
σ_{su13}	Interlaminar ultimate shear strength of composite material (13-direction).
σ_{su23}	Interlaminar ultimate shear strength of composite material (23-direction).
σ_{su3}	Through thickness ultimate shear strength of composite material.
σ_{tu}	Ultimate tensile strength of isotropic material.
σ_{tu1}	Ultimate tensile strength of composite material in fiber direction.
σ_{tu2}	Ultimate tensile strength of composite material perpendicular to fiber direction.
σ_{ty}	Yield strength of isotropic material (tension).
S_{wing}	Wing area.
$(t/c)_r$	Airfoil thickness-to-chord ratio at wing root.
$(t/c)_{r,cb}$	Thickness-to-chord ratio at root of centerbody.
$(t/c)_{r,ow}$	Thickness-to-chord ratio at root of outboard wing.

$(t/c)_{t,cb}$	Thickness-to-chord ratio at tip of centerbody.
$(t/c)_{t,ow}$	Thickness-to-chord ratio at tip of outboard wing.
θ_{ow}	Dihedral angle of outboard wing.
V_∞	Freestream velocity.
ε_{cu1}	Ultimate compressive straing of composite material in fiber direction.
ε_{cu2}	Ultimate compressive strain of composite material perpendicular to fiber direction.
ε_{su12}	In-plane ultimate shear strain of composite material.
ε_{tu1}	Ultimate tensile strain of composite material in fiber direction.
ε_{tu2}	Ultimate tensile strain of composite material perpendicular to fiber direction.
$W_{airframe}$	Total airframe structural weight.
w_{bay}	Width of centerbody cabin bay.
W_{cabin}	Weight of centerbody cabin structure.
w_{cabin}	Width of the centerbody cabin.
W_{cb}	Structural weight of centerbody section.
W_E	Aircraft empty weight.
W_{ow}	Structural weight of outboard wing section.
W_{rc}	Structural weight of rear centerbody section.
W_{TO}	Aircraft takeoff gross weight.
W_{tw}	Structural weight of trapezoidal wing section.
$x_{r,ow}$	Point along outboard wing root chord that aligns with the centerbody rear wall.
$y_{rib,ow}$	Outboard wing rib spacing.
$y_{rib,tw}$	Trapezoidal wing rib spacing.

SUMMARY

Estimating the structural weight of a Hybrid Wing Body (HWB) aircraft during conceptual design has proven to be a significant challenge due to its unconventional configuration. Aircraft structural weight estimation is critical during the early phases of design because inaccurate estimations could result in costly design changes or jeopardize the mission requirements and thus degrade the concept's overall viability. The tools and methods typically employed for this task are inadequate since they are derived from historical data generated by decades of tube-and-wing style construction. In addition to the limited applicability of these empirical models, the conceptual design phase requires that any new tools and methods be flexible enough to enable design space exploration without consuming a significant amount of time and computational resources. This thesis addresses these challenges by developing a parametric and physics-based modeling and simulation (M&S) environment for the purpose of HWB structural weight estimation. The tools in the M&S environment are selected based on their ability to represent the unique HWB geometry and model the physical phenomena present in the centerbody section. The new M&S environment is used to identify key design parameters that significantly contribute to the variability of the HWB centerbody structural weight and also used to generate surrogate models. These surrogate models can augment traditional aircraft sizing routines and provide improved structural weight estimations.

CHAPTER I

INTRODUCTION

1.1 Motivation

Aircraft are typically configured as a "tube-and-wing" design where the main function of the tube, or fuselage, is containing the cargo or passengers and the wing is the main mechanism for generating lift. For decades this configuration has proven to be an effective and viable design and there has been little need for change. Incremental improvements in areas such as weight reduction, engine performance, and aerodynamics have resulted in the production of increasingly larger and fuel efficient aircraft. An example of these incremental improvements culminating in a recent tube-and-wing design is the Boeing 787 Dreamliner, which consists of approximately fifty percent composite materials by weight and claims to emit twenty percent less emissions than any other aircraft of its size[36]. Using lift-to-drag ratio (L/D) as the figure of merit, the impact of these evolutionary advancements over a long period of tube-and-wing style construction can be seen in Figure 1. While there has been a significant amount of improvement since the early days of flight, the last forty years of data show no revolutionary improvement in the large jet category. Although they have enabled the airline industry to endure fluctuating economic conditions and demanding environmental regulations, following a typical technology "S-curve" these evolutionary improvements are more difficult to achieve successively over time due to physics-based limitations.

In 1988, NASA engineer Dennis Bushnell posed the question: "Is there a renaissance for the long-haul transport?"[17]. Aircraft manufacturer McDonnell Douglas

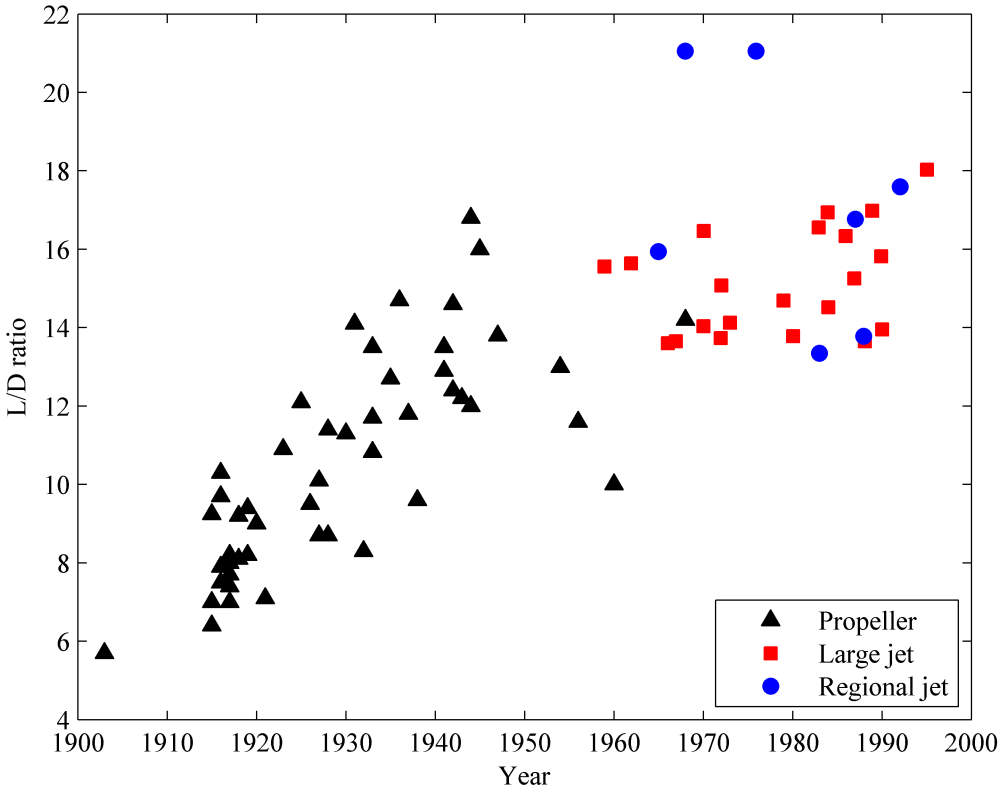

Figure 1: A sample of aircraft L/D ratios between 1903 and 1998[2, 18, 4].

responded with a design study to create and evaluate unconventional aircraft configurations. One result of this early study is shown in Figure 2(a), where the wings are blended around a pair adjacent tubes that serve as the fuselage. Preliminary results showed the potential for a lighter design and higher L/D ratios when compared to a conventional aircraft sized for the same mission. Cylindrical tubes were chosen since they efficiently handled the internal pressure, but it became apparent that this constraint was driving the design back towards a conventional tube-and-wing. Requiring the use of cylindrical cross-sections was eventually abandoned based on the assumption that an alternative structural concept with non-circular cross-sections could be developed with minimal weight penalties. This proved to be a critical design decision and led to the more familiar configurations where high-lift wings are merged with

a wide airfoil shaped fuselage. This design is commonly referred to as the Hybrid Wing Body (HWB), or Blended Wing Body (BWB). An example of this configuration is Boeing's BWB-450 design shown in Figure 2(b) which has shown the potential for a thirty-two percent reduction in fuel burn per seat compared to a conventional tube-and-wing aircraft[17]. Although the cost and risk associated with committing to a radically new aircraft configuration can be prohibitive, NASA has recently established a set of ambitious goals for the next generation of subsonic transport aircraft including a seventy-five percent reduction in emissions and a forty percent reduction in fuel burn[26]. These goals, coupled with economic instability and rising fuel costs, have made unconventional configurations such as the HWB a more viable alternative since they potentially offer revolutionary performance benefits compared to their tube-and-wing counterparts.

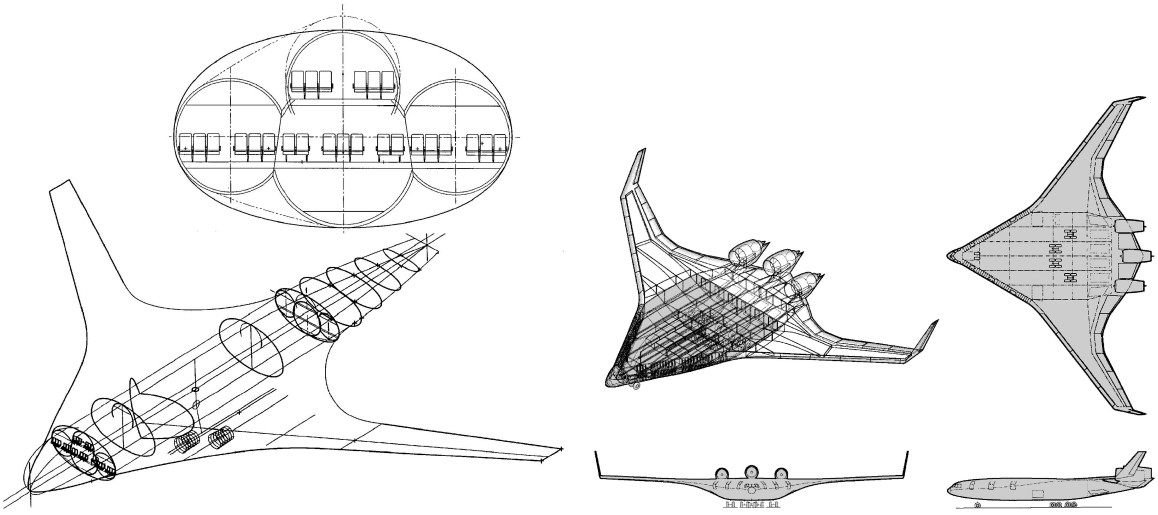

(a) Early 1988 configuration (b) Boeing BWB-450 configuration

Figure 2: Hybrid wing body configurations (a) after a 1988 McDonnell Douglas design study and (b) a more recent Boeing configuration[17].

To enable an accurate evaluation of the HWB concept and a meaningful comparison to traditional aircraft, the tools and methods used during conceptual design for mission analysis and aircraft sizing should be capable of capturing the unique design characteristics of the configurations under study. It is during this initial design

phase that first-order estimations are made that define the aircraft's required size, shape, and weight to perform the desired mission. Estimating the structural weight of an aircraft during the early phases of design has traditionally been accomplished by utilizing historical data generated by decades of tube-and-wing style construction. Statistical curve-fit equations derived from this data are used to estimate an aircraft's empty weight given its type (e.g., jet transport) and estimated takeoff gross weight. More sophisticated empirical methods decompose the aircraft into its various components and can be a function of parameters such as planform area, wetted area, and wing sweep angle. Regardless of the level of detail, their applicability is limited to configurations that are present in the historical database which clearly presents a problem when considering unconventional configurations such as the HWB.

The HWB will have some commonality with the tube-and-wing design, such as the outboard wing section, and empirical relationships can be used when appropriate. Of particular concern is the HWB centerbody section, which is the functional equivalent of a tube-and-wing's fuselage, which must perform as a wing but also contain internal pressure. The use of non-circular cross-sections to contain pressure and the biaxial loading conditions present in this component are a significant structural challenge. While much effort has been devoted to developing innovative structural concepts to satisfy these structural loading conditions, the abilities of current conceptual design tools to model these concepts and their impact on the vehicle's total structural weight are limited. The uncertainty surrounding HWB centerbody weight estimates has been identified as a "high-risk" item since inaccurate weight estimations could jeopardize mission requirements and degrade the HWB's overall viability[24].

The main factors challenging conceptual level HWB structural weight estimation can be categorized into three general areas. These three areas are considered when formulating research objectives and when constructing the modeling and simulation environment.

1. **Physics**: The HWB centerbody section serves as both a wing and a fuselage and presents unique loading conditions and structural requirements. The physics inherently embedded in historical data for either a wing or fuselage do not capture this scenario.

2. **Geometry**: The HWB planform is unique in shape and size. The structural layout in the centerbody section is not comparable to a conventional wing or fuselage.

3. **Computational Effort**: During conceptual design the tools and methods should be computationally inexpensive to enable design space exploration.

Semi-empirical methods calibrated to historical data will be applicable to the HWB outboard wings, where the structural layout and loading conditions will be similar to those existing in the historical database, but major challenges are presented by the HWB centerbody section from both a physics and geometric perspective. The three-axis loading conditions are a critical design aspect and a function of both the centerbody section and the outboard wings. The internal structural loads that result from this loading condition are difficult to derive analytically, which is why many approaches assumed a separate pressure shell concept in an attempt to decouple the analysis. While theoretically derived semi-empirical approaches typically idealize structural components as equivalent beams or plates, this approximation may not be applicable in the centerbody section due to its size, depth, and unique structural configuration.

As higher-order analysis tools are being applied during the conceptual design phase, computational effort becomes a key consideration. During the iterative aircraft sizing process the geometry and estimated gross weight will change several times, and for each iteration a drag polar and empty weight estimate must be generated to perform mission analysis. Higher-order tools, such as finite element analysis or

computational fluid dynamics, are usually avoided during this initial sizing loop since they require a significant amount of computation effort and are typically less robust. Long execution times are a significant drawback and the geometry is typically not yet of sufficient detail to produce such models.

While the ideal conceptual level HWB structural weight estimation tool would employ geometry-driven and physics-based tools that are computationally inexpensive, these attributes are often in direct conflict with one another. In order to improve HWB structural weight estimation methods and enable design space exploration, a modeling framework must be developed that provides an adequate balance between these challenge areas.

1.2 Research Objectives

The work in this thesis addresses the current limitations to HWB structural weight estimation by formulating and implementing a parametric and physics-based modeling and simulation (M&S) environment. The tools in the M&S environment are selected based on their ability to represent the unique HWB geometry as well as their ability to model the physical phenomena present in the centerbody section. This analysis capability is intended to provide improved structural weight estimations and enable a more accurate evaluation of the HWB concept. The main goals of this thesis can be summarized by the three research objectives discussed below.

Objective 1: Develop a parametric and physics-based modeling and simulation environment for HWB structural weight estimation.

With no historical data available for HWB type aircraft, the M&S environment must utilize physics-based tools that adequately model the unique loading conditions and structural configuration. In the context of aircraft structural weight estimation, the term *physics-based* implies that the tools do not rely only on historical data,

although they may be calibrated by it. The environment is intended for use during conceptual design and therefore must be parametric in order to enable design space exploration.

Objective 2: Identify the design parameters that dominate the variability of the HWB centerbody structural weight.

Of particular interest throughout the course of this work is the HWB centerbody section due to its novel design. The fuselage and wing components of a conventional tube-and-wing aircraft can be virtually decoupled to simplify the analysis process, at least during the conceptual design phase. This is not the case for the HWB and it is important to study the relationship between the components in order to fully understand the trades within the design space. Identifying parameters that have a significant influence on certain aspects of the design is of critical importance during conceptual design where the most design freedom exists. The goal of the second research objective is to identify parameters of the HWB outboard wings that have a significant impact on the centerbody structural weight and provide insight into the interactions between the two components.

Objective 3: Provide a computationally inexpensive and robust alternative to the physics-based M&S environment.

Although the physics-based M&S environment developed as part of the first objective could be integrated into an aircraft sizing routine, it will most likely result in undesirably long execution times. The goal of the third objective is to derive analytical models that can accurately replicate the results of the M&S environment but at a fraction of the computational cost. These analytical models can augment traditional

aircraft sizing routines to establish an initial design point which can then be refined in the M&S environment.

1.3 Organization of Thesis

The general layout of the thesis is as follows. Chapter 2 provides relevant background material relating to traditional aircraft structural weight estimation, structural challenges of the HWB concept, and current HWB structural weight estimation capabilities.

Formulation of the HWB structural weight estimation M&S environment is presented in Chapter 3. This chapter provides justification for the chosen analysis tools and relevant assumptions relating to their use. A thorough description of the parametric geometry, the detail of the structural model, and the selected sizing criteria is presented.

Validating the environment by applying the same process and tools to a number of conventional aircraft wings is presented in Chapter 4. This chapter also includes a mesh sensitivity study and definition and calibration of the baseline HWB aircraft.

Results from the M&S environment are presented in Chapter 5. A vehicle scaling study is performed and compared to the results from another recently developed HWB weight estimation methodology. This chapter also presents the key design parameters identified by Research Objective 2 and the surrogate models that developed from Research Objective 3.

Finally, Chapter 6 concludes the thesis. This chapter summarizes the contributions of this work and provides suggestions for future work.

CHAPTER II

BACKGROUND

The intent of this chapter is to review any material that is relevant to this research work and to provide a foundation for formulating the HWB modeling and simulation environment. First, techniques for structural weight estimation of conventional aircraft are examined to establish an understanding of their typical application and limitations. Next, structural challenges presented by the HWB configuration are discussed in order to identify critical loading scenarios and potential structural concepts. A review of current HWB structural weight estimation methodologies is provided in the last section.

2.1 Overview Aircraft Weight Estimation

A brief examination of any aircraft performance calculation reveals that most are influenced by the aircraft weight. Performance characteristics such as landing and takeoff distances, range, and maximum velocity are adversely affected if the weight of the aircraft increases. Niu[27] states that an additional pound of aircraft empty weight may require an additional ten pounds of gross weight for an aircraft to maintain the same performance characteristics. In addition to these impacts on performance, an aircraft's cost is typically related to its weight and inaccurate estimations could result in severe economic consequences. During the conceptual design process, weight estimation is a critical function since it is during this stage that an aircraft manufacturer may guarantee a set of mission and economic characteristics to the customer.

Key factors affecting weight include the aircraft's size and geometry, the internal structural arrangement, the limit load factor, and the choice of material. Additional characteristics that affect weight include things such as fuselage pressurization, fuel

carried in the wing, or engine mounts and cutouts[15]. The challenge during conceptual design is accounting for all these factors with limited knowledge about the design. Most weight estimation procedures can account for the aircraft's geometry, structural arrangement, limit load factor, and materials since this information, or at least a reasonable estimation, is usually available even during the early stages of design. When secondary factors are considered the amount of information required is typically unavailable but is usually accounted for by non-optimum factors derived from historical data and model calibration.

2.1.1 Empirical and Semi-Empirical Methods

A variety of structural weight estimation methodologies exist for conventional aircraft and are categorized into the three general groups seen in Table 1. The appropriate method is usually determined by many factors including the design stage, the complexity of the vehicle, and desired level of visibility. Statistical methods were among the first to be developed and are still widely used as more aircraft are added to the historical database from which they are derived. The simplest statistical methods provide predictions of an aircraft's empty weight given its type and estimated takeoff gross weight. One form that these types of equations can take is shown in Equation 3 below

$$\frac{W_E}{W_{TO}} = A W_{TO}^{\beta} K_{vs}$$

where,

W_{TO} = aircraft takeoff gross weight

W_E = aircraft empty weight

A, β = values determined from historical trends

K_{vs} = variable sweep factor

Example values for A and β for a conventional jet transport given by Raymer[30] are

1.02 and -.06, respectively. The applicability of these types of relationships is usually limited to the early stages of design given their level of abstraction, but they are useful for first-order estimates of overall weight fractions and initial feasibility checks.

Table 1: Conventional aircraft weight estimation methodologies[5].

Method	Description
Statistical	Parametric variations of statistical weight or physical feature relationships. Usually given as a single fraction of W_{TO} or at the component level.
Semi-empirical	Weight estimates are generated from a theoretical foundation. Non-optimum factors are applied to theoretical weight.
Actual	Weight calculated given the part volume and material density.

More advanced statistical methods provide equations for estimating weight at the functional group level such as the wing, horizontal tail, vertical tail, or fuselage as a function of planform characteristics, applied loading, and aircraft takeoff gross weight. These relationships are more useful for parametric analysis and trade studies since they are sensitive to more degrees of freedom. The form of the statistical equation must contain the appropriate terms to reflect changes in design parameters that have a significant influence on the weight. As an example, the general form of the wing weight equation given by Shanley[32] is

$$W_{wing} = A\cos^2\Lambda_{c/4} + B\cos\Lambda_{c/4} + \frac{C}{\cos\Lambda_{c/4}} + \frac{D}{\cos^2\Lambda_{c/4}} + J_{lt}S_{wing} \tag{1}$$

where,

W_{wing} = wing weight

$\Lambda_{c/4}$ = wing sweep at quarter-chord

J_{lt} = unit weight of leading and trailing edge structure in terms of wing area

S_{wing} = wing area

and the relative size of the factors is shown in Table 2. The load term for bending is a key driver of the total weight and together with the secondary structure may account for as much as eighty-four percent of the total wing weight.

Table 2: Description and relative size of the terms in the general wing weight equation[5].

Term	Size	Description
$A\cos^2\Lambda_{c/4}$	<1%	Rib flange term
$B\cos\Lambda_{c/4}$	7%	Rib shear size term plus rib shear load term
$C/\cos\Lambda_{c/4}$	9%	Shear size and load terms plus rib shear size term
$D/\cos^2\Lambda_{c/4}$	59%	Load term for bending
$J_{lt}S_{wing}$	25%	Secondary structure

After some substitutions and variable transformations the general wing weight expression of Equation 1 can be written as

$$W_{wing} = K(W_{TO}n_u)^{\beta_1}S_{wing}^{\beta_2}AR^{\beta_3}(t/c)_r^{\beta_4}(1+\lambda)^{\beta_5}(\cos\lambda_{c/4})^{\beta_6}(w_{box}/c)_r^{\beta_7}S_{cs}^{\beta_8} \qquad (2)$$

where,

K, β = statistically determined constants

AR = aspect ratio

$(t/c)_r$ = airfoil thickness-to-chord ratio at the wing root

λ = wing taper ratio

$(w_{box}/c)_r$ = width of the structural wing box divided by the wing chord at the root

S_{cs} = area of wing mounted control surfaces

and the K and β are commonly determined using constrained regression methods and historical data[34]. Although these statistical methods can be formulated using sophisticated regression techniques, embedded in all of them are certain technology

levels, manufacturing techniques, and variable bounds that constrain their applicability.

Semi-empirical methods are another approach to weight estimation where the theoretical weights of the most basic elements of the structure are determined and then non-optimum factors and weight penalties are applied. The non-optimum factors and weight penalties are used to correlate the theoretical weight to existing data and account for things such as cutouts, splices and joints, and any other unique features of the structural component under study. Secondary weight, such as leading and trailing edges or control surfaces, can be determined separately using statistical techniques. If derived and applied properly, semi-empirical methods provide more sensitivity to the engineering parameters that drive the major component weights of a group and enable more accurate trade studies and technology projections. An example of this type of weight estimation methodology can be found in References [3] and [35].

2.1.2 Finite Element Model Based Methods

With advancements in computer processing power and Computer-Aided Design (CAD) software, advanced structural analysis techniques such as Finite Element Analysis (FEA) are common practice for aircraft design. Depending on the design stage and available information, a Finite Element Model (FEM) will typically model the load-carrying structure using idealized elements. Given the appropriate material and stiffness properties, these idealized elements can represent the actual structure and determine internal structural loads and optimum load paths. Since the actual structure is modeled as idealized elements, weight estimation using FEMs is simply not a matter of the material density multiplied by the FEM volume. For example, a spar cap modeled as a simple rod element will not include fillets, additional land for fasteners, or any required splice plates. A number of calibration factors based on historical data and an engineer's experience will be applied to the theoretical FEM weight to

determine an estimate of the actual as-built weight. The amount of actual weight modeled by a FEM can vary greatly as shown in Figure 3 and can depend on the type of structure as well as the detail of the model. Calibration factors of 1.25 to 2.0 are common values when predicting the actual weight as a function of the theoretical FEM weight.

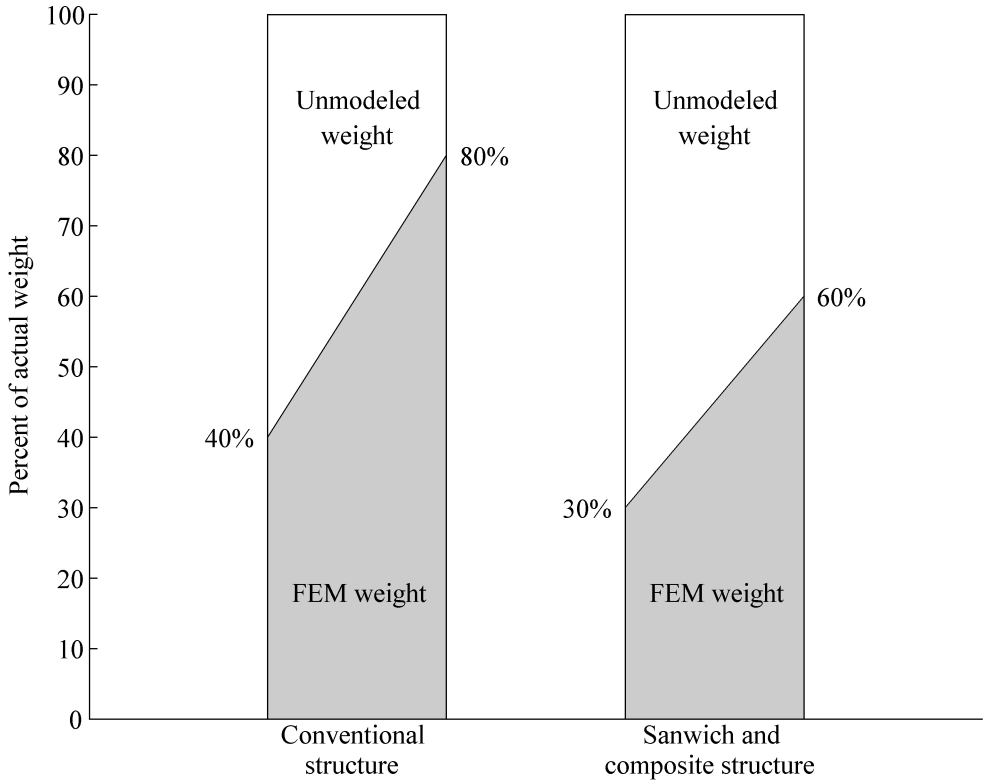

Figure 3: FEM theoretical weight as a percent of actual as-built weight[29].

A FEM based approach during conceptual design would be similar to a semi-empirical technique where the theoretical weight of the load-carrying structure is correlated to an estimate of the actual weight. The challenge with any analysis-based, or physics-based, approach is accounting for all the design details and all of the criteria that will eventually size the individual structural components. Non-optimum load paths from structural cutouts will adversely affect the weight and other considerations

such as damage criteria or fatigue are difficult to address during conceptual design. However, basic strength and stiffness based methods will capture approximately sixty-five to seventy-five percent of the total weight and are useful for predicting trends in the design space[1]. In most cases, these challenges are exacerbated when using FEM based methods because of the additional complexity of constructing the model itself, although they may be well-suited for the hyperstatic nature of many unconventional configurations.

2.2 Structural Considerations of the HWB Aircraft

Velicki[37] states that the primary challenge of the HWB configuration is producing a centerbody section that is not only lightweight, but also economical to manufacture. The HWB centerbody section presents a number of unique challenges since it must perform as a wing, generating approximately twenty percent of the overall lift, and also contain internal cabin pressure as a fuselage[39]. In conventional tube-and-wing aircraft, these functions are virtually decoupled where the wing structure is responsible for wing bending loads while a circular fuselage efficiently handles internal pressure through hoop stress. Mukhopadhyay[20] shows that in non-circular cross-sections, such as those present in the HWB centerbody, large bending stresses are induced from this internal pressure and present a critical loading condition. In addition to this large out-of-plane pressure loading, during maneuvers the skin panels of the centerbody section also experience in-plane biaxial loading conditions that can be approximately equal in magnitude. This differs from a conventional circular fuselage where the longitudinal direction is the dominant loading direction as a result of empennage loads. This biaxial loading condition implies that the structural concept employed in the centerbody section should have continuous load paths in each direction as well as the capability to efficiently contain internal pressure[16, 40, 37].

A wide variety of structural concepts have been proposed for the HWB centerbody. Some of the first HWB designs proposed by Liebeck[17] used traditional skin and stringer arrangements where the stringers were approximately five to six inches deep. In an attempt to take advantage of circular cross-sections, later designs used separate pressures shells to contain the cabin pressure and a separate outer skin to handle the wing bending loads as shown in Figure 4(a). Preliminary studies by Mukhopadhyay[21] showed that this design was lighter than comparable flat sandwich panel concepts but still almost twice as inefficient as a purely cylindrical structure. While this separate pressure shell may partially decouple the internal pressure and wing bending loads, it introduced a number of other challenges. The outer skin would still need to be designed to contain the internal pressure in case of an inner skin failure and would also need a sufficient level of bending stiffness to limit deformation that could degrade aerodynamic performance[22]. The redundancy of the inner and outer skin makes this concept much less weight efficient. Both light honeycomb material and cross-ribbed concepts have been proposed to connect the inner and outer skin but the large amount of honeycomb material required would create negative weight penalties. It is also common in the aerospace industry to avoid honeycomb material in primary flight structures due to debonding, local crippling, moisture egress, crack propagation, and inspection problems[20].

Another structural concept for the HWB centerbody utilizes flat sandwich panels where a deep sandwich shell with composite skins and honeycomb core simultaneously handle the internal pressure and wing bending loads. While the deep sandwich shell increases the cross-section's bending stiffness in both the longitudinal and lateral direction, large bending moments are induced on the relatively flat panels. Studies revealed this concept to be heavier than the separate pressure shell and the use of honeycomb material in the primary structure caused concern for the same reasons mentioned above[21]. A notional example of this configuration can be seen in Figure

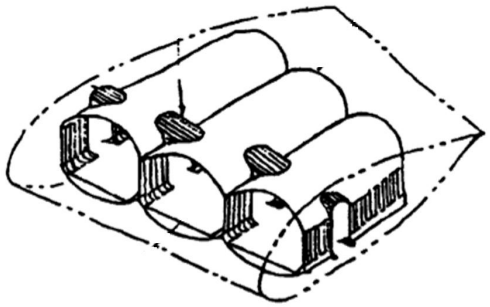

(a) Separate pressure shell

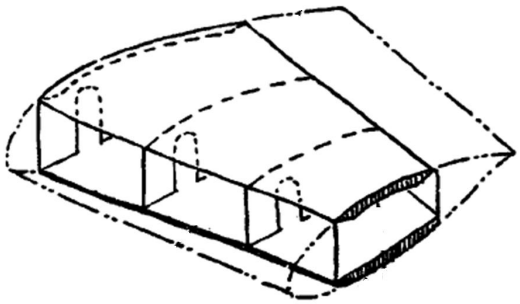

(b) Integrated skin and shell

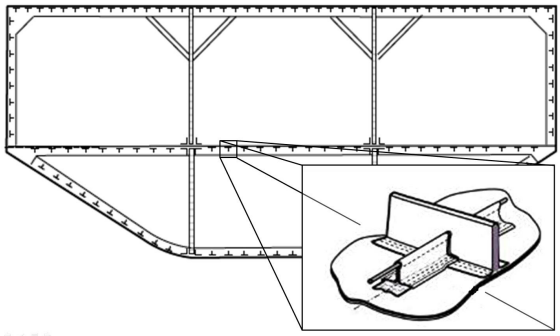

(c) PRSEUS

Figure 4: Structural concepts considered for the HWB centerbody section include a (a) separate pressure shell[17], (b) an integrated skin and shell[17], and (c) the PRSEUS concept[40].

4(b).

Velicki[37] noted that a structural concept was needed that was tailored to the complex three-axis loading conditions produced by the HWB pressure cabin. Evolving from the cross-ribbed separate pressure shell concept came what is known as the Pultruded Rod Stitched Efficient Unitized Structure, or PRSEUS. This is an all composite concept where the components are highly integrated and stitched together to form a single element with more efficient load paths, lower part counts, and fewer joints. The main components of the PRSEUS concept, shown in Figure 4(c), are a composite skin, lateral frames with inner foam cores, and longitudinal stringers with

pre-cured rods that increase the strength and stability of the panel section. Stitching the components together provide a number of advantages such as forming a self-supporting preform which eases manufacturing, arresting damage propagation, and handling out-of-plane loads since it no longer relies primarily on bonded or co-cured laminate interfaces[38]. Preliminary results by Velicki[39] show that this concept may offer a twenty-eight weight savings as compared to sandwich panel designs.

2.3 Current HWB Structural Weight Estimation Methodologies

Howe[13] develops an "empirically weighted theoretical approach" assuming that the airframe weight may be first calculated primarily as a wing, and then corrections and penalties are applied for the payload carrying centerbody. This semi-empirical approach is derived from the author's previous work referred to as the "F" method, where first-order principles are used to determine the material required to resist the spanwise bending moment and the stiffness needed to prevent overall compression failure of the wing skin[12]. In application to the HWB, the planform is idealized into an outer and inner wing where weight correction functions can be applied independently. Based on the result of an earlier HWB study by Smith[33], a separate pressure shell concept is assumed for the centerbody section. Results for a notional HWB configuration yield a structural weight fraction of approximately twenty-four percent of maximum takeoff weight for light alloys, and eighteen percent for carbon fiber-reinforced polymers.

Giles[9, 10] has developed an equivalent plate formulation to model and analyze critical elements of metallic or composite wing structures during conceptual design. The analysis procedure is based on the Ritz method, in which the deflection of the structure is assumed to be described by a set of polynomial displacement functions. The wing box structure is represented by an equivalent plate which consists of multiple trapezoidal segments described by properties such as wing depth, airfoil camber,

and skin thickness. The procedure became the Equivalent Laminated Plate Solution (ELAPS) computer program and has been applied to a HWB configuration. Again, a separate pressure shell concept was assumed where the outer centerbody skin will carry only the wing bending loads[11]. The structural weight is determined by assuming a material density, multiplying that be the volume of the equivalent plate model, and applying a correction factor to the resulting weight. Giles recommends finding this correction factor by applying this equivalent plate analysis to a pre-existing aircraft with known structural weights.

Bradley[6] fits an equation to data generated from finite element analysis that relates the HWB centerbody structural weight to the vehicle's takeoff gross weight and payload cabin area. A number of finite element models were created for a range of HWB passenger classes consisting of the outboard wing box and centerbody skin, ribs, and passenger deck. The finite element models used plate elements where the strength and stiffness of the elements were equivalent to a skin and z-section stringer concept. Load cases included a positive 2.5g maneuver with an assumed trapezoidal lift distribution and internal cabin pressure. For each finite element model and for a range of takeoff gross weights, the thickness of the shell elements were manually adjusted until a specified stress and deflection criteria were met. Changing the thickness of the shell elements corresponds to adjusting parameters of the skin and z-section stringer concept such as skin and stringer thicknesses, stringer depth, and stringer spacing. This process generates trends for cabin weight as a function of takeoff gross weight and cabin area. Regression analysis of this data provides the relationship below

$$W_{cabin} = K \times 0.316422(W_{TO})^{0.166552}(S_{cabin})^{1.061158} \tag{3}$$

where,

W_{cabin} = Weight of centerbody cabin structure

K = calibration constant

S_{cabin} = area of the passenger cabin

Using a Boeing proprietary study the calibration constant K was determined to be approximately 5.7 to estimate the as-built structural weight. This approach was first implemented in NASA's Flight Optimization System (FLOPS) Version 6.03.

Gern[8] developed a scalable HWB centerbody weight estimation tool that integrates a number of higher-order analysis tools. A parametric conceptual level FEM represents the load-carrying structure of the centerbody and outboard wing sections and a doublet-lattice aerodynamic module calculates the external loads for a $+2.5g$ and $-1.0g$ maneuver. An internal cabin pressure load case is also considered the element thicknesses are optimized until all strength and deflection criteria are satisfied. The FEM theoretical weight is calibrated to a Boeing study to provide estimates of the actual as-built structural weight. The main advantage of this type of procedure is its scalability and the degrees of freedom provided by the various physics-based analysis tools.

CHAPTER III

FORMULATION OF MODELING AND SIMULATION ENVIRONMENT

This chapter provides the theoretical background and overall approach to formulating the HWB structural weight estimation M&S environment. The first section discusses the process used to define the overall framework of the environment as well as the justification for the selection of any existing analysis tools. The remaining sections describe each modeling component in more detail and include any relevant assumptions about the analysis tool itself or how it is applied in the overall environment.

3.1 Definition of Modeling Components and Selection of Analysis Tools

The background information presented in Chapter 2 serves as the foundation for formulating an approach to HWB structural weight estimation. The applicability of empirical aircraft weight estimation methodologies is clearly limited since there is currently no database of HWB aircraft to derive the statistical relationships. Certain components of the HWB aircraft, such as the outboard wing, are geometrically similar to existing designs and empirical methods may be applicable, but other aspects may not be so comparable. Things such as the spanwise load distribution or the amount of lift produced by only the outboard wing sections may be difficult to estimate and may not compare with the physics embedded in the historical data. Semi-empirical methods can better represent the physics of the problem and are typically more sensitive to parameters that significantly affect the structural weight. These methods usually rely upon idealizing the structure as beams or plates so that basic structural analysis methods can be applied. The HWB centerbody poses a challenge for this

type of approach given its size, depth, structural configuration, and complex loading conditions. FEM based methods are becoming more common and successful applications have been shown by Gern[8] and Padula[28], among others. The main challenges to overcome with this type of approach are the complexity of creating the model and the robustness of the numerical solution.

The first step is defining the general modeling components within the M&S environment and its overall architecture. This process begins by first identifying the objective of the environment (i.e., structural weight) and determining the information needed to achieve the desired objective. This process was continued in a "bottom-up" fashion using the previously defined modeling component as the objective. This bottom-up formulation can be seen on the left side of Figure 5 where structural weight was the initial objective. In order to estimate the structural weight a structural sizing routine is needed to size the design parameters of the structural model. The structural sizing routine will require a set of internal loads that result from the externally applied loads for each considered load case. These external loads are applied to a structural model that is derived from the aircraft's geometry. The general components of the M&S environment identified using this bottom-up approach are integrated and then implemented in a "top-down" fashion. The general function, or task, of each component can be seen on the right side of Figure 5, starting with the aircraft geometry and ending with the structural weight.

With the general M&S components defined, specific analysis tools can be selected that will provide the needed information. There are many things to consider when choosing the appropriate analysis tools. First and foremost, they must represent the given problem in terms of the general challenge areas discussed in Section 1.1. Any structural analysis tools must be capable of capturing the three-axis loading conditions present in the HWB centerbody section resulting from the internal cabin pressure and loads from the outboard wing. Semi-empirical wing weight estimation

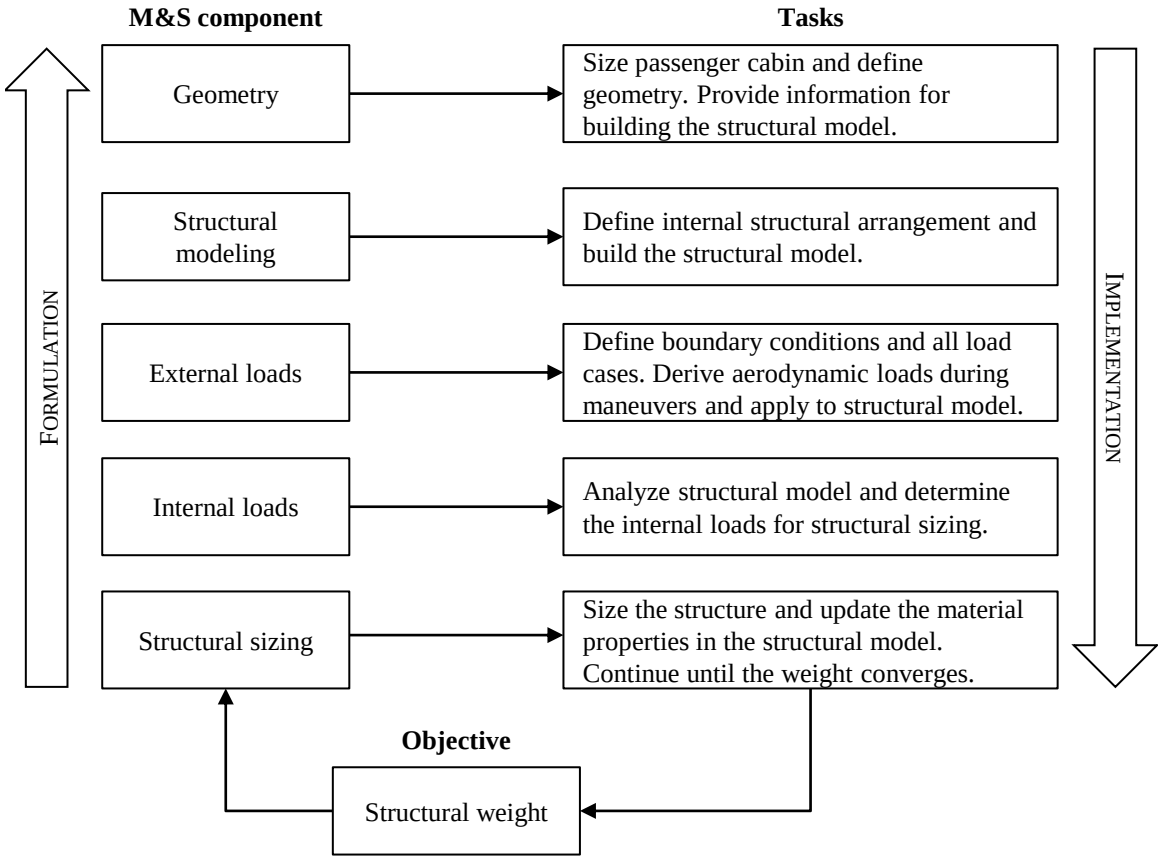

Figure 5: Formulation and implementation of the M&S environment.

techniques may sometimes prescribe a lift distribution and size the wing box by a "station-cut" analysis where the wing box is sized at a number of spanwise stations. Given the size and shape of the centerbody section, the freedom to size the structure as a function of both the spanwise and chordwise position will be a critical feature. In addition to these requirements, the structural analysis tools must be able to consider advanced materials and structural concepts such as PRSEUS. A matrix of alternatives was constructed to first identify potential analysis tools and can be seen in Table 3. The first column of the matrix is the general components in the M&S environment and each row contains the potential analysis tools.

While it is important that the geometry modeling and analysis tools are capable of capturing the physics of the problem, there are additional aspects to consider

Table 3: Matrix of alternatives for selection of the analysis tools in M&S environment.

Component	1	2	3	4	5
Geometry	VSP	AMS-ketcher	AVID PAGE	CATIA	Solid-Works
Structural modeling	VSP	Patran	Femap	Hyper-Mesh	
External loads	VORLAX	PMARC	PanAir	STAR-CCM	Overflow
Internal loads	CalculiX	Nastran Sol 101	ANSYS	Abaqus	
Structural sizing	Hyper-Sizer	Nastran Sol 200	ANSYS	Abaqus	

when selecting the various analysis tools. When integrating a number of independently developed analysis tools, translation of the data and preparation of the input files from one component to another is inevitable. Using analysis tools where the input and output data from one modeling component to the next is of a similar format should ease the data transfer process since large data transformations can be avoided. For example, a high-order computational fluid dynamics (CFD) code will typically construct the outer mold line (OML) with a fine grid of x, y, and z points. If the structural model is idealized as a simple beam with aerodynamic loads distributed along a spanwise reference line such as the wing quarter-chord, a large data transformation is required to translate the pressure coefficients on the detailed aerodynamic grid to the simple structural model. These types of large data transformations can be avoided and the integration process simplified if all the analysis tools use the same type of data format and coordinate system. More simply put, the format used to define the model and the required level of detail should be similar between all the various analysis tools. In addition to simplifying the integration process, the advantages of using a high-order aerodynamic tool may be less significant if used in conjunction with a low-order structural model, or vice-versa. For example, depending on the detail of the structural model the theoretical weight estimated by a semi-empirical or FEM

based wing weight methodology may require a calibration factor on the order of 1.5 to 2.0. If the use of a high-order aerodynamic tool results in only a small change in this calibration factor, it may be unnecessary considering its added complexity and computational cost. Additional considerations may include things such as the availability of the tool, previous examples of successful application, or its capability to be executed in automation mode.

The purpose of the geometry component is to define the planform and OML and to provide this information to the other analysis components. The geometry must be parametric and it should ideally be defined by parameters that are typically important to aircraft design engineers during the conceptual design stage. While CAD software such as CATIA and SolidWorks have been applied in integrated multidisciplinary analysis environments, they were deemed too complex for this research effort and their availability was limited. Vehicle Sketch Pad (VSP) is an open source parametric aircraft geometry tool developed by NASA where aircraft models are defined by common aircraft engineering parameters such as wing area, aspect ratio, taper ratio, etc. VSP also provides the capability to export the geometric models to many different file formats which then can be easily translated for use by a variety of aerodynamic analysis tools.

The structural modeling component will be responsible for creating the internal structural arrangement of the HWB aircraft given the OML from the geometry component. A FEM based approach provides a better representation of both the load-carrying structure and the internal load paths, particularly in the centerbody section. The selected structural modeling tool is MSC Patran which is a common FEA pre/post-processing program in the aerospace industry. Patran provides its own custom scripting language that can be used to run the program in batch mode. Given that the environment is intended for use during the conceptual design phase, the stringers and frames of any stiffened panels will not be discretely modeled but

rather their stiffness properties will be represented by an equivalent thin plate. This greatly simplifies the FEM construction process and allows any stringer or frame variables to remain free for structural sizing.

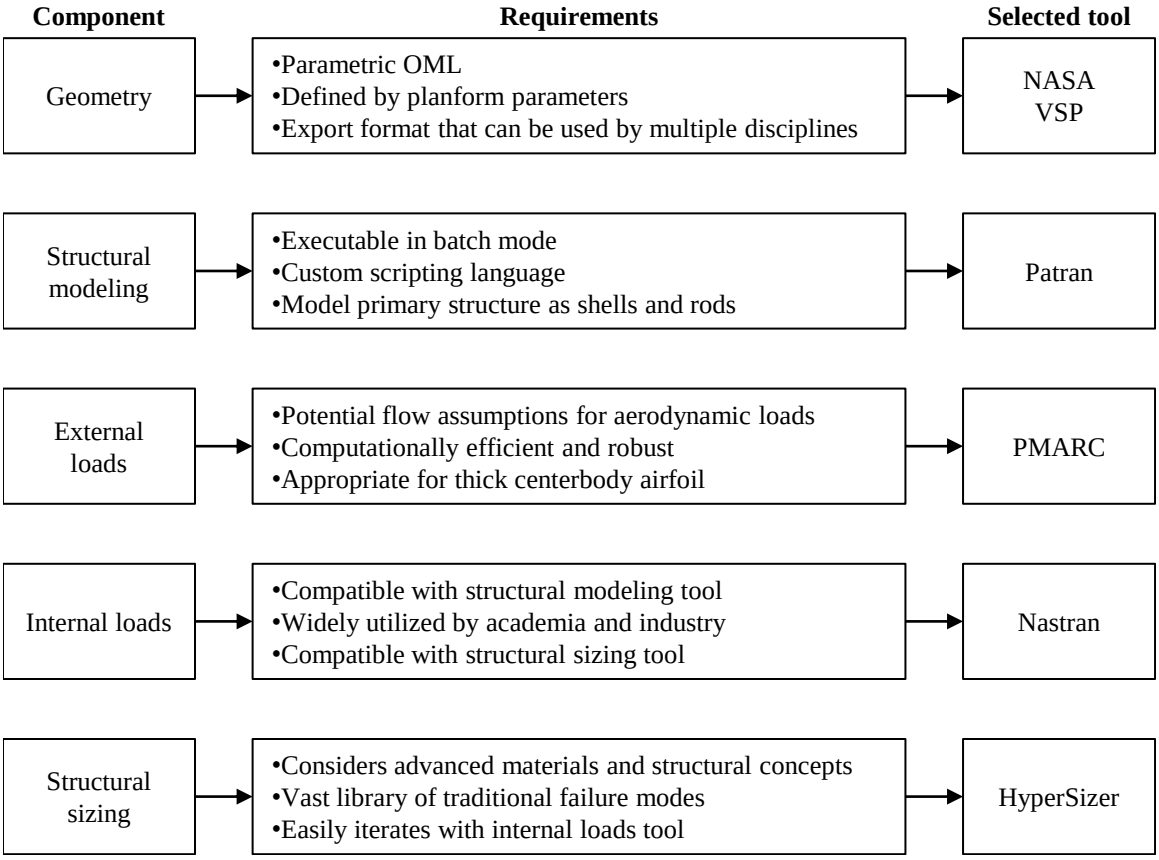

Figure 6: Selected tools for the M&S environment.

With the geometry and structural model defined, the next step is determining the external loads for all the considered load cases. A more thorough discussion will be had in Section 3.4 regarding the considered load cases, but for now the focus is on selection of an appropriate aerodynamic tool for the purpose of generating aerodynamic loads during a specified maneuver. As mentioned earlier, it is common for semi-empirical wing weight estimation methods to prescribe a lift distribution rather than deriving one from an aerodynamic analysis. A elliptical, triangular, or

Schrenk distribution can usually be used to determine the spanwise loading of conventional subsonic transport wings for preliminary structural analysis. Due to the HWB planform shape and centerbody size, a lift distrusting that is a function of only the spanwise location may not be of sufficient detail. Obtaining a more representative lift distribution is done by incorporating a suitable physics-based aerodynamic analysis tool given the size, shape, and thickness of the HWB. Very high-order CFD tools such as OVERFLOW or STAR-CCM may provide more accurate results, but their complexity and computational cost make them infeasible for the desired approach. Since lift is the primary concern, aerodynamic tools based on potential flow theory will be capable of providing a representative lift distribution while also improving the computational speed and robustness of the aerodynamic modeling component. Panel Method Ames Research Center (PMARC) is a three-dimensional aerodynamic panel code based on potential flow theory. While more complex than a vortex-lattice code such as VORLAX, it is capable of more accurately modeling the HWB centerbody with its airfoil thickness-to-chord ratio of fifteen to seventeen percent. Also, the coordinates of the panels in the aerodynamic model will more closely match those of the structural model and simplify the loads transfer process between the two dissimilar meshes.

With the structural model and external loads defined, the internal loads for sizing the structure can be determined. During conceptual and even preliminary design, coarsely meshed structural models are typically used to derive the internal loads using a linear static solution. While many FEA tools are available to perform this task, it was decided that a commercial tool that is widely utilized by both academia and industry should be chosen to avoid verification and validation of the tool itself. Since the selected structural modeling tool, Patran, works conveniently with MSC Nastran, this FEA tool was chosen to determine the internal loads for structural sizing.

Sizing the structure to determine the structural weight is the last step in the

M&S environment. While most commercial FEA tools have their own design and optimization routines, they are typically used to only size the thickness of the elements or the cross-sectional area. HyperSizer by Collier Research was chosen since it easily integrates with Nastran and has a vast library of stiffened panel concepts and failure modes. After sizing the structure, HyperSizer will update the material properties in the FEM and rerun the FEA analysis to update the internal loads. This process continues until the structural weight converges.

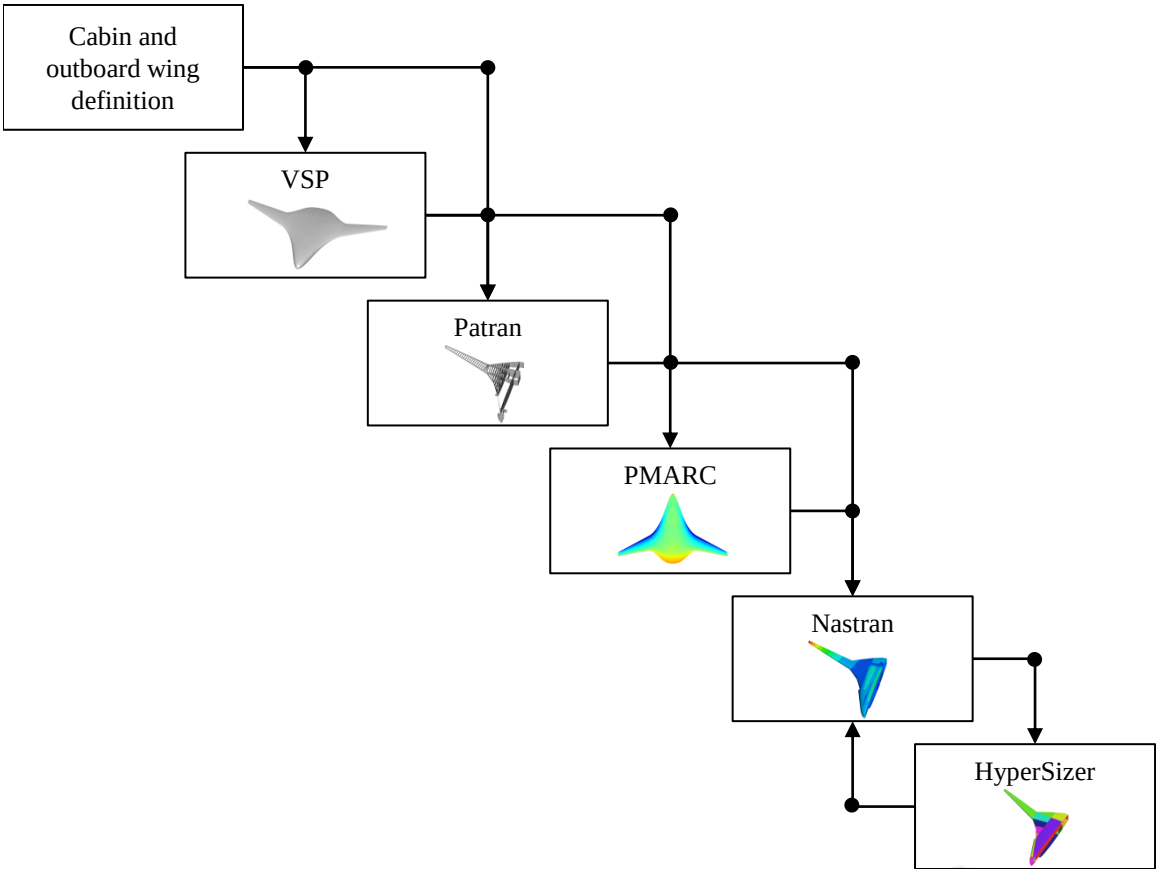

Figure 7: M&S environment design structure.

The overall structure of the M&S environment can be seen in Figure 7 and is integrated using Phoenix Integration's ModelCenter. The process begins with definition of the HWB cabin and outboard wing. A VSP model is constructed providing the OML to both Patran and PMARC. The aerodynamic loads determined by PMARC

will then be transferred to the FEM by a discrete data transfer algorithm. Finally, the iterative sizing process between Nastran and HyperSizer will determine the structural weight and report the results. The following sections describe each of the modeling components in more detail and any relevant assumptions regarding their application.

3.2 Parameterization of HWB Outer Mold Line

The M&S environment begins with definition of the HWB planform and OML using VSP. While more recent versions of VSP included modifications for generating HWB models, it was found to be difficult to produce scalable and smooth planform shapes with a limited number of design variables. For this reason, a custom procedure was developed that would write a VSP file as a simple wing component rather than using the HWB module. The HWB planform is divided into the four different sections shown in Figure 8. The sections are abbreviated as shown in the legend and any parameters with these abbreviations as subscripts specify which section the parameter is associated with. The red centerbody section is the pressurized passenger cabin and will be sized by the number of passengers or amount of cargo. The outboard wing section in green can be specified independently of the centerbody section since it is shaped as a conventional wing. If an existing wing was to be used for the outboard wing section, this allows the dimensions to be specified and then attached to the centerbody section by the trapezoidal wing section shown in blue. The rear centerbody section shown in gray is not pressurized and is where any engines may be attached or embedded.

The HWB cabin is first sized by the number of passengers of amount of cargo using the methodology developed by Bradley[6] to determine the cabin length (l_{cabin}), cabin width (w_{cabin}), centerbody root chord length ($c_{r,cb}$), and centerbody tip chord length ($c_{t,cb}$). Note that $c_{r,cb}$ and $c_{t,cb}$ include the length of the centerbody and rear centerbody sections and are determined by the airfoil thickness-to-chord ratio and

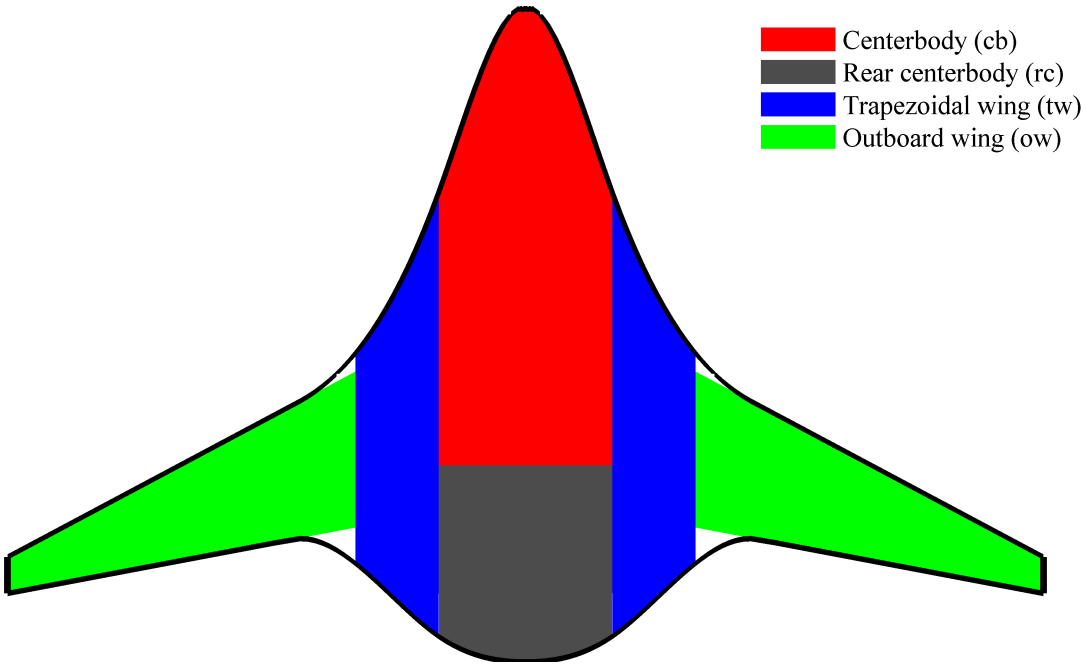

Figure 8: HWB planform groups shown by color.

required cabin height. Piecewise cubic splines are used to define the blended leading and trailing edges of the HWB planform and the control points can be seen in Figure 9. Assuming that the nose of the aircraft is located at the origin, the first two control points along the leading and trailing edges are found by

$$x_{TE}^{(1)} = x_{LE}^{(1)} + c_{r,cb} \tag{4a}$$

$$y_{TE}^{(1)} = y_{LE}^{(1)} \tag{4b}$$

$$y_{LE}^{(2)} = y_{LE}^{(1)} + \frac{w_{cabin}}{2} \tag{4c}$$

$$x_{LE}^{(2)} = x_{LE}^{(1)} + \frac{w_{cabin}}{2} \times \tan(\Lambda_{LE,cb}) \tag{4d}$$

$$y_{TE}^{(2)} = y_{LE}^{(2)} \tag{4e}$$

$$x_{TE}^{(2)} = x_{LE}^{(2)} + c_{t,cb} \tag{4f}$$

where $\Lambda_{LE,cb}$ is the sweep angle of the centerbody leading edge. With the centerbody control points defined, the next step is positioning of the outboard wing section.

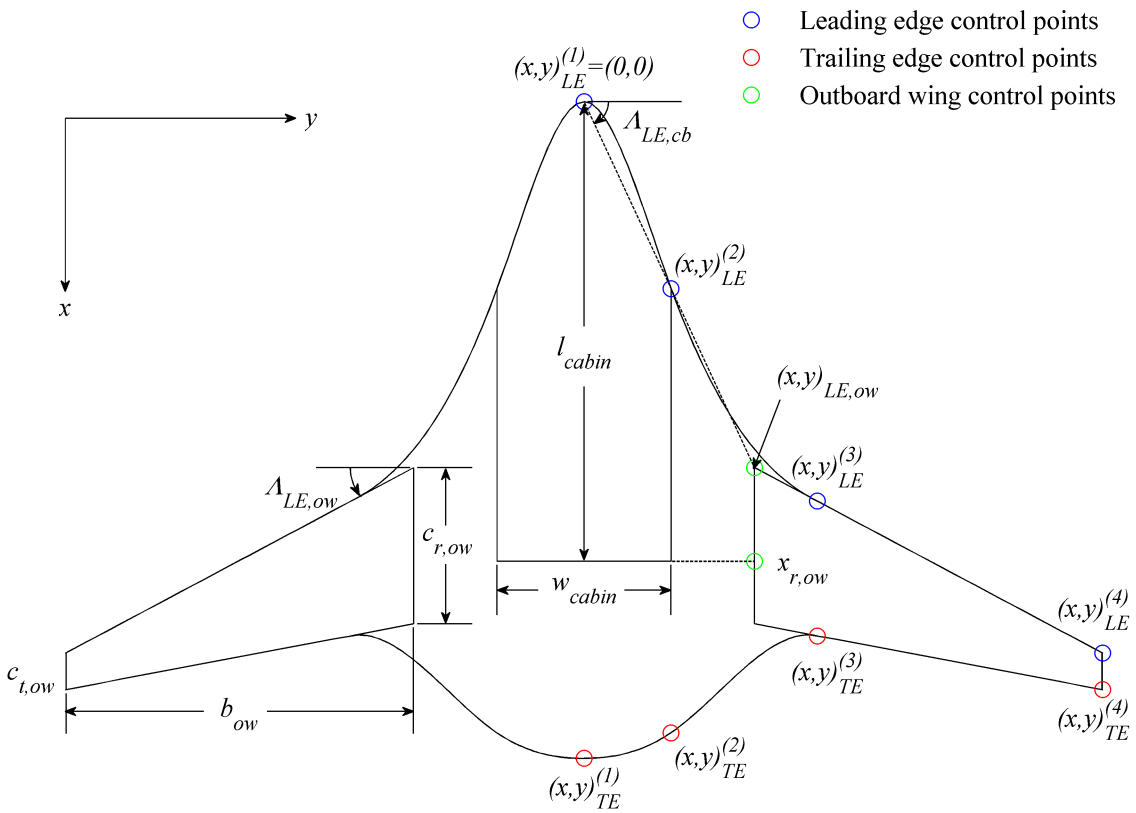

Figure 9: Variables used to define the planform leading and trailing edges and the outboard wing.

The position of the outboard wing section will be affected by many things such as the structural arrangement and stability and control considerations. The main assumption in this procedure is that a point along the root of the outboard wing section ($x_{r,ow}$) will align with the rear wall of the centerbody and is specified as a fraction of root chord length of the outboard wing ($c_{r,ow}$). With the longitudinal position now fixed, the lateral position is found by the intersection of the leading edge of the outboard section and a line extending from the centerbody leading edge

and shown in Figure 9. These outboard wing control points are determined by

$$x_{LE,ow} = l_{cabin} - x_{r,ow} \times c_{r,ow} \tag{5a}$$

$$y_{LE,ow} = \frac{x_{LE,ow}}{\tan(\Lambda_{LE,cb})} \tag{5b}$$

which can be used to determine the third leading and trailing edge controls points and define all the points used for construction of the piecewise cubic splines. The third control points can be positioned down the span of the outboard wing section to control the transition between the trapezoidal and outboard wing section. A piecewise cubic spline defining the leading edge of the centerbody and trapezoidal wing section can now be generated where the slope at $(x, y)^{(1)}_{LE}$ is zero and the slope at $(x, y)^{(3)}_{LE}$ equals the leading edge sweep angle of the outboard wing section ($\Lambda_{LE,ow}$). The same procedure is used for the trailing edge but the slope at $(x, y)^{(3)}_{LE}$ must equal the trailing edge sweep angle of the outboard wing section. The leading and trailing edge control points at the tip of the outboard wing section are determined by the span (b_{ow}), sweep, and tip chord length ($c_{t,ow}$) of the outboard wing section. These points are found by

$$x^{(4)}_{LE} = x^{(3)}_{LE} + b_{ow} \times \tan(\Lambda_{LE,ow}) \tag{6a}$$

$$y^{(4)}_{LE} = y^{(3)}_{LE} + b_{ow} \tag{6b}$$

$$x^{(4)}_{TE} = x^{(4)}_{LE} + c_{t,ow} \tag{6c}$$

$$y^{(4)}_{TE} = y^{(4)}_{LE} \tag{6d}$$

and are used to create linear leading and trailing edges for the outboard wing section. A similar procedure can be performed to create a HWB planform with a linear centerbody leading edge rather than a blended one as shown in Figure 10. If using a linear centerbody leading edge the length and width of the flight deck must be specified and a cubic spline is used to define the leading edge.

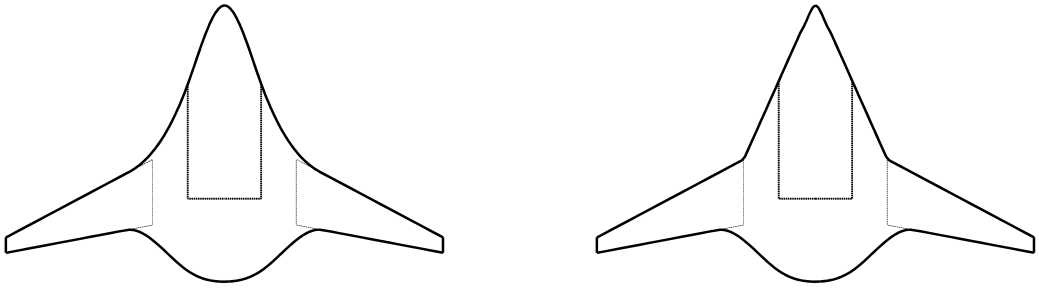

(a) Blended (b) Linear

Figure 10: The two types of centerbody leading edge types are a (a) blended and (b) linear leading edge.

With the HWB planform fully defined, an OML can be generated by VSP given an airfoil stack that describes the airfoils as a function of the span location. The planform is sliced into a number of sections and at each section the coordinates of the OML are determined given the section chord length and normalized airfoil coordinates. The airfoil stack must contain at least two airfoils and two-dimensional linear interpolation is used to determine the airfoil coordinates if the planform section is between the airfoil stations given in the airfoil stack. An example of a VSP model generated using this procedure can be seen in Figure 11.

Only a small number of parameters defining the centerbody cabin and outboard size are needed to define the HWB planform. The procedure is fully scalable and allows a fixed outboard wing section to be logically positioned even as the passenger cabin changes size. Table 4 summarizes all the design variables that define the HWB planform and OML. The HWB VSP is provided to both the structural and aerodynamic model in the form of a Hermite file. This file defines the OML of the model by specifying the x, y, and z-coordinates at a number of spanwise stations.

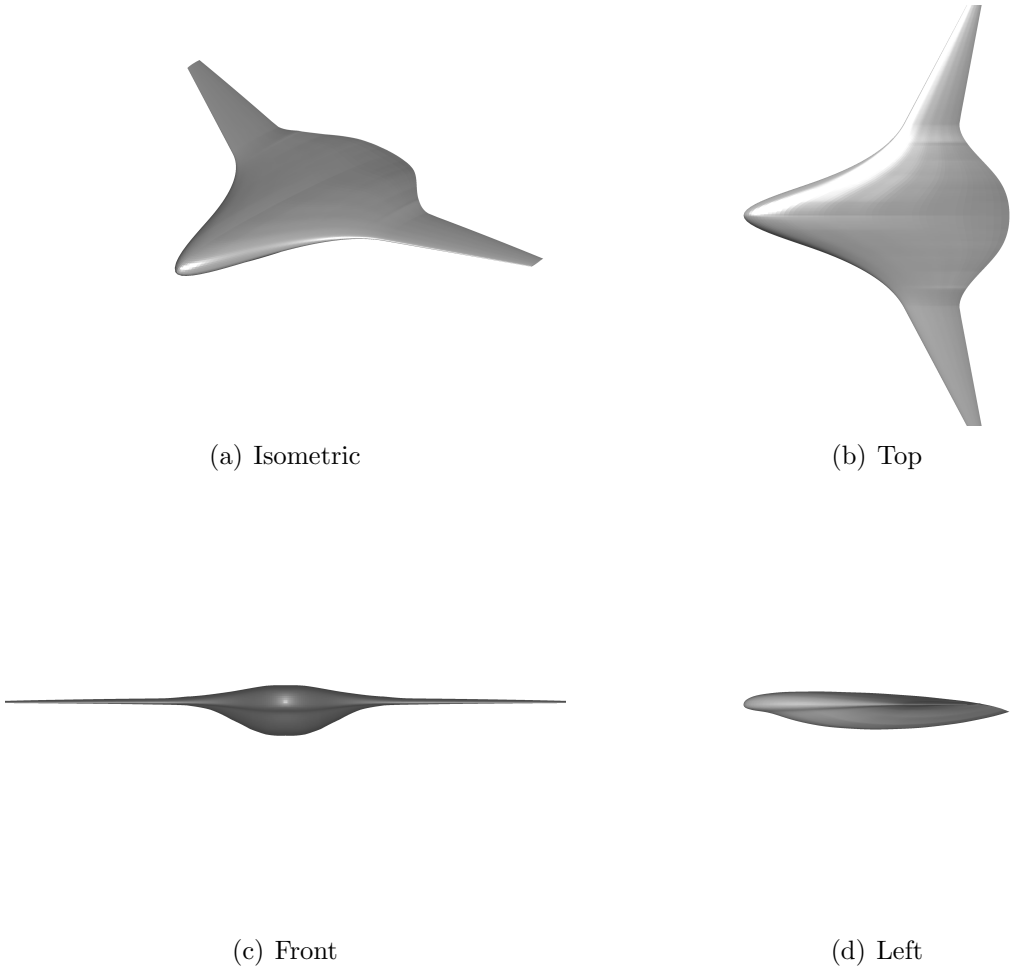

(a) Isometric

(b) Top

(c) Front

(d) Left

Figure 11: An example HWB VSP model using the procedure developed for the M&S environment.

Table 4: Design variables defining the HWB planform and OML.

Variable	Description
$\Lambda_{LE,cb}$	Sweep angle of centerbody leading edge
l_{cabin}	Length of centerbody cabin
w_{cabin}	Width of centerbody cabin
$(t/c)_{r,cb}$	Thickness-to-chord ratio at root of centerbody
$(t/c)_{t,cb}$	Thickness-to-chord ratio at tip of centerbody
b_{ow}	Span of outboard wing section
$\Lambda_{LE,ow}$	Sweep angle of outboard wing leading edge
$\Lambda_{LE,ow}$	Sweep angle of outboard wing leading edge
$c_{r,ow}$	Chord length at root of outboard wing
$c_{t,ow}$	Chord length at tip of outboard wing
$(t/c)_{r,ow}$	Thickness-to-chord ratio at root of outboard wing
ϕ_{ow}	Twist angle at tip of outboard wing
θ_{ow}	Dihedral angle of outboard wing

3.3 Structural Parameterization and Finite Element Modeling

With the HWB VSP model providing the OML, the next step in the M&S environment is defining the internal structure and constructing the FEM. The procedure begins by first defining the internal structural components in each one of the HWB sections shown in Figure 8. A custom modeling component was developed that will determine the boundary points of the structure given the component's beginning and ending points. For example, defining a wing spar only requires the spar's beginning and ending points in terms of its x- and y-coordinates. The points are usually normalized by the wing semispan and local chord length so all the coordinates are between zero and one. The main advantage to this approach is that almost all the internal structural components can be defined this way, providing a very fast way of specifying new components since small pieces of code can be reused. Figure 12 shows the result of this structural layout routine with the skin and floor panels in the centerbody section not shown. Currently the M&S environment only models the load-carrying structure of the HWB aircraft since it will account for the majority of the structural weight. Accounting for secondary structure is a challenge since the critical loads for this type of structure may be difficult to determine with a conceptual level structural model. Vertical tails are not modeled at this point for the same reason. The assumption with this approach is that the load-carrying structure will provide useful global trends in the design space with only a limited number of critical load cases. The following paragraphs discuss in greater detail what parts of the HWB structure are considered, the available design variables, and any relevant assumptions.

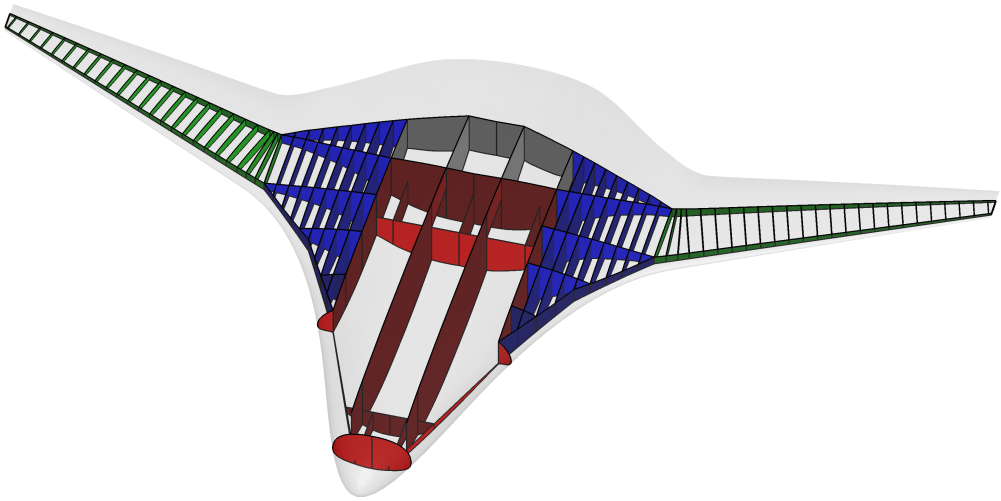

Figure 12: Structural layout of notional HWB configuration.

The HWB outboard wing shape and structural arrangement is similar to a conventional aircraft. The structural wingbox consists of a front and rear spar, multiple evenly spaced ribs that are perpendicular to the rear spar, and an upper and lower wing skin. Structural design parameters include the location of the front and rear spars as a percent of the chord length and the rib spacing. Typical locations of the front and rear spars are twelve and sixty percent, respectively.

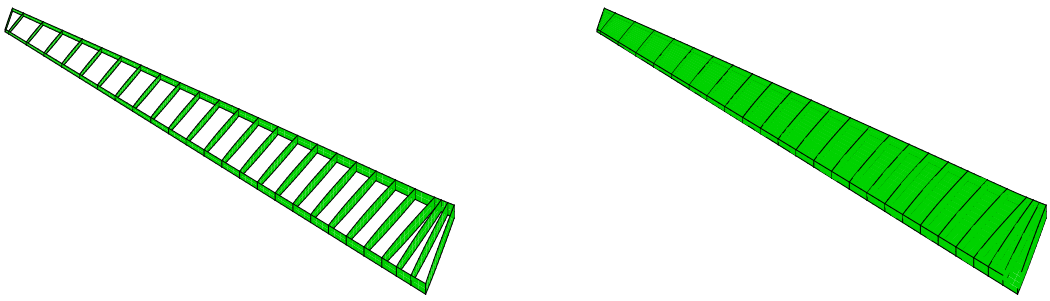

(a) Internal structure (b) Skin panels

Figure 13: Structure of the outboard wing section.

The trapezoidal wing structure transitions between the centerbody and outboard wing and consists of multiple spars, ribs, and an upper and lower skin. One spar is always attached between the rear spar of the outboard wing and rear wall of the centerbody cabin and serves as the main load-carrying component. Another spar is attached to the front spar of the outboard wing and the side-wall of the centerbody. Front and rear spar locations are specified as a percent chord and the front spar is allowed to break at the midpoint if a blended leading edge is used to maintain a reasonable depth. This feature is shown in Figure 14(a). Intermediate spars are inserted if the distance between the required spars is greater than some specified allowance. Ribs are oriented in the streamwise direction and are evenly spaced.

(a) Internal structure (b) Skin panels

Figure 14: Structure of the trapezoidal wing section.

The HWB centerbody is the most unique structural feature of the aircraft and the most difficult to model since it must handle wing bending loads as a wing and internal cabin pressure as a fuselage. Although circular cross-sections efficiently contain pressure loads through hoop stress, utilizing a separate inner skin to contain pressure and an outer skin to maintain the aerodynamic shape and handle wing bending loads does not provide a weight efficient solution. For this reason, a single outer skin is used for the centerbody and advanced structural concepts and materials will be utilized to achieve the desired weight efficiency. A curved leading edge skin, shown in Figure

15(b), is used to contain the internal pressure rather than a flat front spar that is the full depth of the OML. Large bay walls are modeled that divide the cabin bays and decrease the span distance for the pressure containing skins. Some landing gear support structure is modeled and the lower skin is cutout where the landing gear bay doors would be located. This was done in order to provide a more realistic load path in the lower skin since the landing gear bay doors would typically not be considered as part of the load-carrying structure. Although not shown in Figure 15(a), a main cabin floor is modeled and is positioned based on a desired cabin height. Although a cabin floor is typically not considered a load-carrying structure, it was modeled in this approach since the floor would provide a support point for the cabin side and rear walls. By decreasing the span distance, this additional support decreases the bending moments induced in the cabin side and rear walls when containing internal pressure. In the areas above the nose and main landing gear bays, the floor panels are also responsible for containing the internal pressure. The floor containing the internal pressure in some areas was the reason for modeling some of the landing gear structure since it provides additional support in those areas. An upper and lower skin and bulkhead make up the flight deck structure. Structure design parameters in the centerbody include the number of cabin bays, the location of the front spar, and the size of the landing gear bays.

The rear centerbody section is not pressurized and consists of upper and lower skins, rear bay walls, and a rear spar. The rear bay walls are defined by the location of the centerbody bay walls and the rear spar location is specified as a percent chord of the centerline chord length.

With the structural arrangement and the boundary points of all the structural components defined, the finite element model can be constructed in Patran. An automated procedure written in the Patran Command Language (PCL) will create the structural geometry using the boundary points of the structural components defined

(a) Internal structure (floor panels not shown) (b) Skin panels

Figure 15: Structure of the centerbody section.

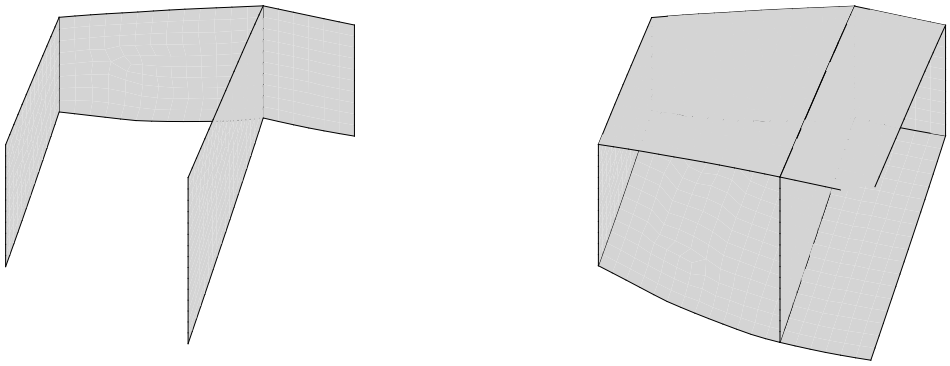

(a) Internal structure (b) Skin panels

Figure 16: Structure of the rear centerbody section.

by the structural arrangement procedure. The boundary points are used to create upper and lower curves which are then used to create the surface of the structural component. These upper and lower curves eventually become the spar or rib caps and the surface becomes the spar or rib web. Using these curves the skin panels can be created by identifying which curves enclose a skin surface. All spar and rib webs and skin panels are meshed with quadrilateral CQUAD4 elements having plate properties and triangular CTRIA3 elements are used in transition areas. Although avoiding the use of CTRIA3 elements would be ideal since they typically overestimate the stiffness, this is a consequence of the automated meshing routine and the desired robustness

of the overall procedure. Also, some parts might sometimes be modeled with pure shear elements, such as the rib webs, but this usually required a more tedious meshing process which was difficult to achieve within the automated environment. Spar and rib caps are modeled with CBAR elements. Stiffeners are not discretely modeled but the equivalent properties of any stiffened panels will be reflected in the element's plate properties. This allows for structural sizing variables such as stringer spacing or height to be free during structural sizing. This process results in a FEM such as the one shown in Figure 17.

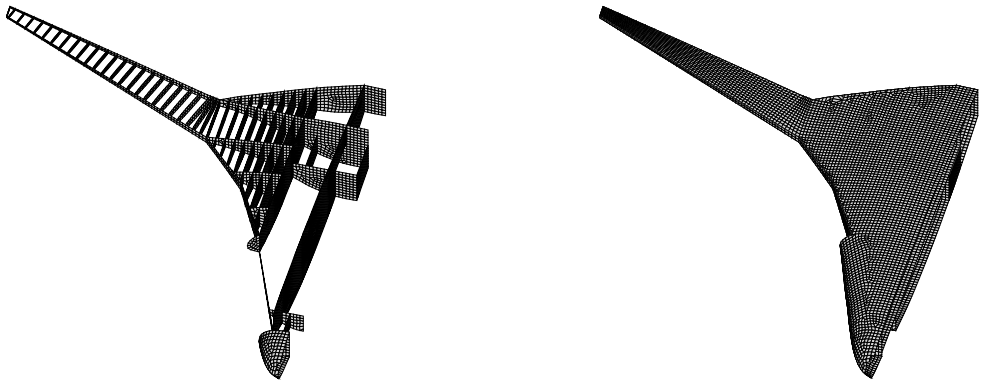

(a) Internal structure (b) Skin panels

Figure 17: FEM mesh of notional HWB configuration.

The M&S currently only considers symmetric load cases so the FEM models half of the structure and symmetric boundary conditions are applied at the centerline. In addition to these symmetric boundary conditions, the model must be constrained in the z-direction since external forces applied the maneuver loads will not equal the modeled weight plus its inertia (i.e., the loads are not balanced). A nodal displacement constraint is placed near the rear cabin wall where a significant amount of structure is located in order to distribute the concentrated reactions forces and limit the influence on the structural sizing routine. Obtaining an initial set of internal loads for the structural sizing routine requires applying temporary material properties to the FEM. Aluminum 7075 is applied to the entire model to generate the first set

of internal loads. After the structure has been sized, the materials will be updated accordingly. At the end of the FEM construction process, the nodes and elements on the FEM OML are exported to the structural loads modeling component to enable the aerodynamic/structure data transfer process.

3.4 External Loads

Thousands of load cases will eventually be used to size the various structural components and include flight loads, ground handling loads, propulsion system loads, landing loads, fuel slosh, and many more. An advantage of purely statistical weight estimation methodologies is that all of these load cases are accounted for in the historical data. On the other hand, a physic-based approach requires that each of these load cases be identified and modeled one by one. This problem is exacerbated by the limited amount of knowledge available during the early phases of design. For this research effort, a limited number of load cases were selected assuming they would account for a majority of the structural weight and provide useful trends in the design space.

As discussed in Chapter 2, the internal cabin pressure presents a critical loading condition for the HWB centerbody and must be included to appropriately size the centerbody structure. Nominal HWB cabin pressure during normal operation is assumed to be 9.2 pounds per square inch (psi) with an ultimate cabin pressure of 18.4 psi $(2P)$[1][19]. The ultimate 2P cabin pressure load is a static load case and accounts for all safety factors. Two symmetric maneuver load cases are considered and are based on the regulations found in Federal Aviation Regulations Part 25 Section 337. These regulations specify maneuvering limit load factors (n) of positive 2.5 and negative 1.0 times the design maximum takeoff weight, respectively, at design cruise speeds. Both of these maneuvers will include a nominal cabin pressure of $1P$. During each

[1] P=9.2 psi

of these load cases, an equal and opposite inertia load will be applied to the model to capture bending relief from the modeled airframe, fuel in the outboard wing, and cabin payload. The payload weight is determined by the number of passengers and is evenly distributed across the cabin floor using concentrated mass elements. The fuel weight in the outboard wing is determined by finding the approximate volume between each outboard wing rib and multiplying it by a fuel volume efficiency factor of 0.9 and an assumed fuel weight of 6.8 pounds per gallon. A summary of the load cases is provided in Table 5. Both maneuver load cases are performed at the design cruise speed and maximum takeoff weight.

Table 5: Summary of load cases used for structural sizing.

Load Case	**Limit Load Factor**	***P* (psi)**	**Inertia Loads**	**Safety Factor**
1	$+2.5g$	9.2	$-2.5g$ (airframe, fuel, payload)	1.5
2	$-1.0g$	9.2	$+1.0g$ (airframe, fuel, payload)	1.5
3	N/A	18.4	N/A	1.0

Each maneuver load case requires an aerodynamic analysis to derive the aerodynamic loads that are applied to the structural model. The panel code PMARC was selected for this application for its computational speed and robustness. Although it is based on potential flow theory, assuming inviscid, incompressible, and irrotational flow, it is still suitable for deriving aerodynamic loads for structural analysis and is also capable of modeling the thickness of the centerbody airfoil. PMARC uses a time-stepping wake model, but for the purposes of this research an initial wake was specified two wingspans downstream from the trailing edge assuming this would provide steady-state results. A PMARC input file is generated from the VSP geometry and given the flight conditions, limit load factor, wing reference area, and vehicle

weight a required lift coefficient can be determined by

$$C_{L,req} = \frac{W_{TO} \times n}{\frac{1}{2}\rho_\infty V_\infty^2 S_{wing}} \tag{7}$$

where,

$C_{L,req}$ = required lift coefficient

n = limit load factor

ρ_∞ = freestream density

V_∞ = freestream velocity

S_{wing} = wing area

and the freestream conditions are determined by the altitude and Mach number (M_∞). Since PMARC is limited to incompressible flow, the inverse of the Prandtl-Glauert compressibility correction is used to obtain a new required lift coefficient determined by

$$C'_{L,req} = C_{L,req} \times \frac{\sqrt{1 - M_\infty^2}}{\sqrt{1 - M_{inc}^2}} \tag{8}$$

where,

$C'_{L,req}$ = required lift coefficient corrected for compressibility effects

M_{inc} = incompressible Mach number used for PMARC analysis

PMARC is then executed at an upper and lower angle of attack (α) to develop a linear relationship between C_L and α. These two data points are used to determine the angle of attack required to achieve $C'_{L,req}$. For each load case, PMARC is executed at the required angle of attack using an incompressible Mach number and the pressure coefficients (C_p) at each panel are extracted. These pressure coefficients are then transformed by the Prandtl-Glauert compressibility correction to obtain the pressure coefficients that will be used to determine the loads for the structural model. This transformation is given by

$$C_p = C'_p \times \frac{\sqrt{1 - M_{inc}^2}}{\sqrt{1 - M_\infty^2}} \tag{9}$$

where,

C'_p = incompressible pressure coefficient

C_p = pressure coefficient

The resulting pressure coefficients provide the required C_L for the given maneuver and are eventually integrated over the area of the panel to determine forces and moments for the structural model. An overview of this process can be seen in the lower part of Figure 18.

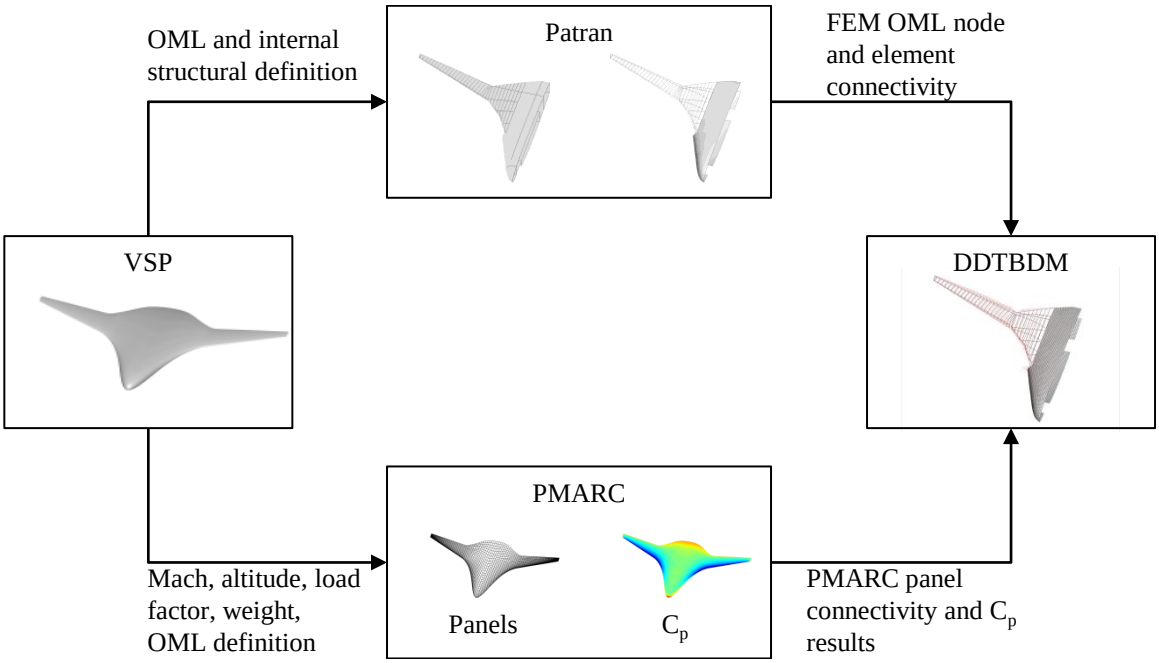

Figure 18: Process used for determining the aerodynamic loads and transferring them to the structural model.

Transferring the aerodynamic results to the structural model is accomplished by the code Discrete Data Transfer Between Dissimilar Meshes (DDTBDM)[31]. The pressure coefficients on the aerodynamic model are integrated and transferred to the structural model as equivalent forces and moments. On the outboard and trapezoidal wing sections, the loads are transferred to only where spars or ribs exist, rather than

directly to the skin as seen in Figure 19. In the centerbody and rear centerbody sections, the loads are transferred directly to the skin.

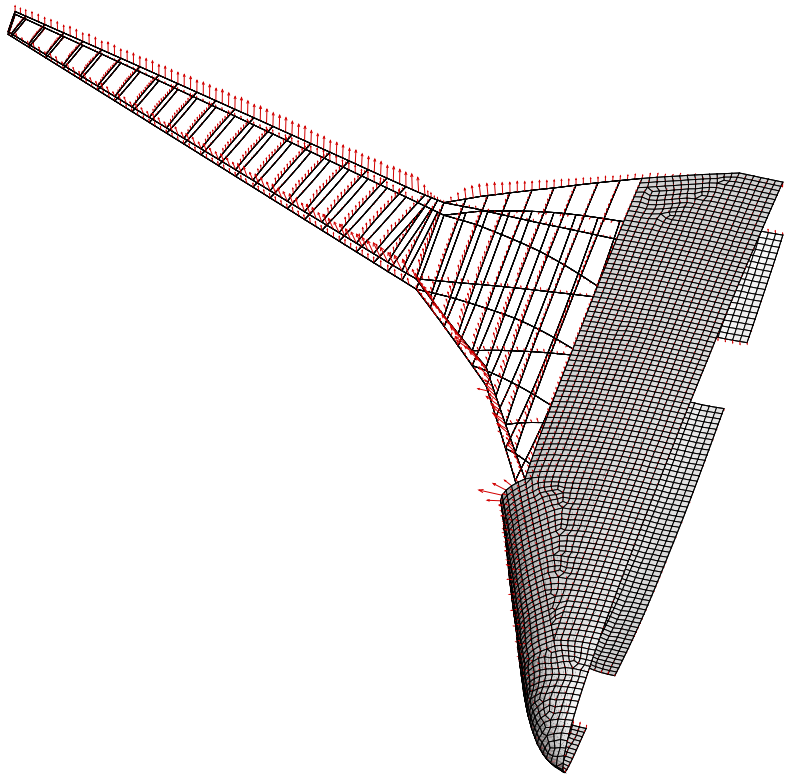

Figure 19: Force vectors on the structural model for the $+2.5g$ load case (moments not shown).

Not shown is an additional step required where the original PMARC results are transferred to a refined aerodynamic mesh. Due to limitations on the number of panels within PMARC the aerodynamic mesh is much coarser than the structural mesh, especially in the centerbody section. If this original PMARC mesh is used for the loads transfer, concentrated forces arise on the structural model that coincides with the corner points of the PMARC panels. To remedy this, the PMARC mesh is refined so that the centerbody panels are approximately equal in size the structural mesh size, and the original C_p values are interpolated to the refined mesh. Although

the DDTBDM tool provides the capability to transfer the deflections back to the aerodynamic model after structural analysis, a rigid-body aerodynamic model is assumed and aeroelastic effects are not considered.

3.5 Finite Element Analysis and Structural Sizing

Determining the internal structural loads for structural sizing is accomplished by finite element analysis. Nastran is the FEA tool selected for this research given its extensive use by both industry and academia. A linear static solution is performed given the structural model created by Patran and the loads generated by PMARC. Depending on the size of both the aircraft and the structural mesh, the analysis can usually be executed in less than one minute. The result of this analysis is the internal loads at each element in the FEM which are then extracted by the structural sizing routine.

Sizing the structure and determining the structural weight is done by HyperSizer developed by Collier Research. HyperSizer extends classical laminated plate theory to stiffened panels by "smearing" the stiffness properties into an equivalent plate[7]. This allows structural cross-sections with general shapes and materials to be analyzed as plates and used in a vehicle-scale finite element analysis. HyperSizer will determine the equivalent stiffness of a panel or beam and solve for the strains and curvatures using the design-to loads extracted from the FEA solution as shown in Equation 10.

$$\begin{bmatrix} \{\varepsilon\} \\ \{k\} \end{bmatrix} = \begin{bmatrix} [A] & [B] \\ [B] & [D] \end{bmatrix}^{-1} \begin{bmatrix} \{N\} \\ \{M\} \end{bmatrix} \tag{10}$$

where,

$\{\varepsilon\}$ = vector of membrane strains

$\{k\}$ = vector of bending strains

$[A]$ = extensional stiffness matrix

$[B]$ = bending stiffness matrix

$[D]$ = bending-extensional coupling stiffness matrix

$\{N\}$ = vector of membrane loads

$\{M\}$ = vector of bending moments

Design-to membrane loads $\{N\}$ and bending moments $\{M\}$ are determined by a statistical loading method using the element loads and moments that are part of the larger panel. A stiffened panel or beam in HyperSizer will consist of many elements in the FEM and a single set of design-to loads must be derived. This is done by finding the average of all the element loads in the panel and choosing the number of standard deviations from the mean to use as the design-to load. As an example, the area weighted average tensile membrane load and standard deviation are given by

$$\overline{N}_{x,T} = \frac{\sum N_{x,T}^{(i)} A^{(i)}}{A_{total}} \tag{11a}$$

$$\sigma_{N_{x,T}} = \sqrt{\frac{\sum \left(N_{x,T}^{(i)} A^{(i)} - \overline{N}_{x,T} \right)^2}{A_{total}}} \tag{11b}$$

where,

$\overline{N}_{x,T}$ = area weighted average tensile membrane load

$N_{x,T}^{(i)}$ = tensile membrane load of i^{th} element

$A^{(i)}$ = area of i^{th} element

A_{total} = total area of all elements

$\sigma_{N_{x,T}}$ = area weighted standard deviation of tensile membrane loads

and the statistical loading options are 0σ (mean), 1σ, and 2σ. This statistical loading methodology provides an added level of conservatism the design-to loads in addition to the safety factor of 1.5.

After defining the variables bounds on each of the parameters describing a particular structural concept, HyperSizer will generate a pool of candidate designs and sort them on their unit weight. HyperSizer will analysis each candidate using the design-to loads, starting with the lightest solution, and continue until it reaches a design

that provides positive margins of safety for all specified failure criteria. Variables for stiffened panels include skin, web, and flange thicknesses, overall panel height, flange widths, stiffener spacing and height, etc. The candidate designs are created by a full factorial combination of all the cross-sectional parameters at a given number of levels, although this can lead to the number of candidates to quickly become unmanageable. A balance must be achieved between the number of candidate designs and ensuring that the variable bounds are suitable for a wide range of vehicle sizes.

HyperSizer provides an extensive library of failure criteria but only a select few were chosen in order to improve execution time. The active failure criteria are described below and apply to both panels and beams.

Panel buckling Overall buckling of the stiffened panel where the buckling lengths are determined by the location of the elements that make up the panel. Buckling lengths are automatically updated if needed, such as the spanwise buckling length of the panels along the centerline if a bay wall it not present.

Local buckling Each object in the stiffened panel is independently analyzed for local buckling by treating each object as a simply supported plate or shell. This includes the flanges, webs, skin sections between stiffeners, etc. Local buckling is treated as a failure, except for the PRSEUS concept where local postbuckling of the skin is permitted up to a fraction of the ultimate load.

Crippling The collapse of short, thin-walled columns after the web and flanges have locally buckled. Johnson-Euler buckling interaction is used for metallics and MIL-HDBK-17-3E for composites.

Isotropic strength (metallic) Material strength of all objects in longitudinal, transverse, and shear directions. The von Mises yield criterion is

also included.

Maximum strain (composite) Maximum strain in the longitudinal, transverse, and shear directions. Tsai-Hill interaction if using discrete laminates.

Each panel and beam component will be sized independently which results in discontinuous stringer spacing or height between panels. Although these variables can be linked within HyperSizer, this feature dramatically increases the execution time and was not utilized for this research. The independently sized panels and beams included in the model are shown in Figure 20, where the various color represent the components.

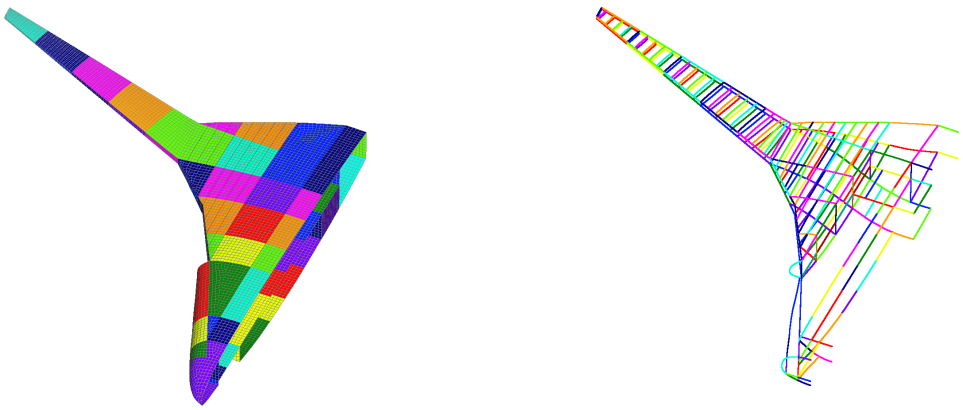

(a) Panels (b) Beams

Figure 20: Example of the independently sized panel and beams components in a HyperSizer model.

After the structural components have been sized, the equivalent stiffness properties are updated in the FEM and the structural analysis is repeated to obtain new internal loads. This process continues until the internal loads, and hence structural weight, converge. Convergence is usually achieved after three iterations. The total structural weight will be

$$W_{airframe} = K_{ow}W_{ow} + K_{tw}W_{tw} + K_{cb}W_{cb} + K_{rc}W_{rc} \tag{12}$$

where,

$W_{airframe}$ = total airframe structural weight

K_{ow} = calibration factor for outboard wing section

W_{ow} = structural weight of outboard wing section

K_{tw} = calibration factor for trapezoidal wing section

W_{tw} = structural weight of trapezoidal wing section

K_{cb} = calibration factor for centerbody section

W_{cb} = structural weight of centerbody section

K_{rc} = calibration factor for rear centerbody section

W_{rc} = structural weight of rear centerbody section

and the calibration factors are yet to be determined.

CHAPTER IV

IMPLEMENTATION OF MODELING AND SIMULATION ENVIRONMENT

This chapter describes implementation of the M&S environment by first examining the impact the structural mesh size has on the weight results. Next, the same overall process and tools discussed in Chapter 3 are applied to a number of conventional aircraft wings for model validation. The last section of this chapter describes the baseline configuration used to determine the calibration factors in Equation 12.

4.1 Mesh Sensitivity Study

The convergence of any numerical process should always be verified to avoid erroneous results. The trends developed by the M&S environment should be a function of only the physics of the problem and not be a function of the mesh size. The structural mesh of the FEM is of primary concern since it will have the most significant impact on the design-to loads used by HyperSizer for structural sizing. The baseline HWB configuration, described later in Section 4.3, was created to investigate the sensitivity of the structural weight with respect to the structural mesh size and statistical loading options. The mesh size of the FEM was varied between 4 and 24 inches with all other parameters held constant and the change in weight of each section was observed. For each HWB section , the data is presented as a percentage of the section's maximum structural weight, which always results in the 4 inch mesh size and 2σ loading conditions being one hundred percent. In this way, both the sensitivity of the structural weight with respect to the mesh size and the relative difference between the statistical loading options are clearly observable.

The results of this study are presented in Figures 21 through 24. One of the most noticeable observations is the impact of the statistical loading methods, where the 0σ method is typically twenty to thirty percent below the maximum 2σ value. In general, the 0σ and 1σ methods appear to be the least sensitive to the mesh size, not considering the largest mesh sizes where all the methods appear to be fairly erratic. Areas of the FEM where transitions between structural components occur or where many components intersect may result in irregularly shaped surfaces. With large mesh sizes, the finite elements meshed on these surfaces may have poor characteristics in terms of element aspect ratios and skew angles. These elements will inaccurately model the internal loads and may be unable to any capture critical load concentrations, thus impacting the structural weight. A rather concerning trend with the 2σ loading method is that the weight appears to continuously increase as the mesh decreases in size, rather than converging to a constant value. Although this study used a fixed vehicle and varying mesh size, this would be equivalent to fixing the mesh size and scaling up the vehicle so the mesh becomes smaller relative to the structural model. This is an undesirable characteristic since the M&S environment is intended to be fully scalable and artificial sensitivities in the design space due to this behavior would adversely affect the quality of the results. Clearly the design-to loads determined by the HyperSizer 2σ statistical loading methodology are increasing as the mesh size decreases. This may be explained by the smaller elements capturing large concentrated loads and therefore increasing the standard deviation of the element loads within a given panel component. Although these load concentrations will need to be addressed as the design progresses, the relatively coarse FEM used for global loads development may not be well-suited for this task. Based on these observations the 2σ method should be avoided and the 0σ and 1σ method should be further investigated.

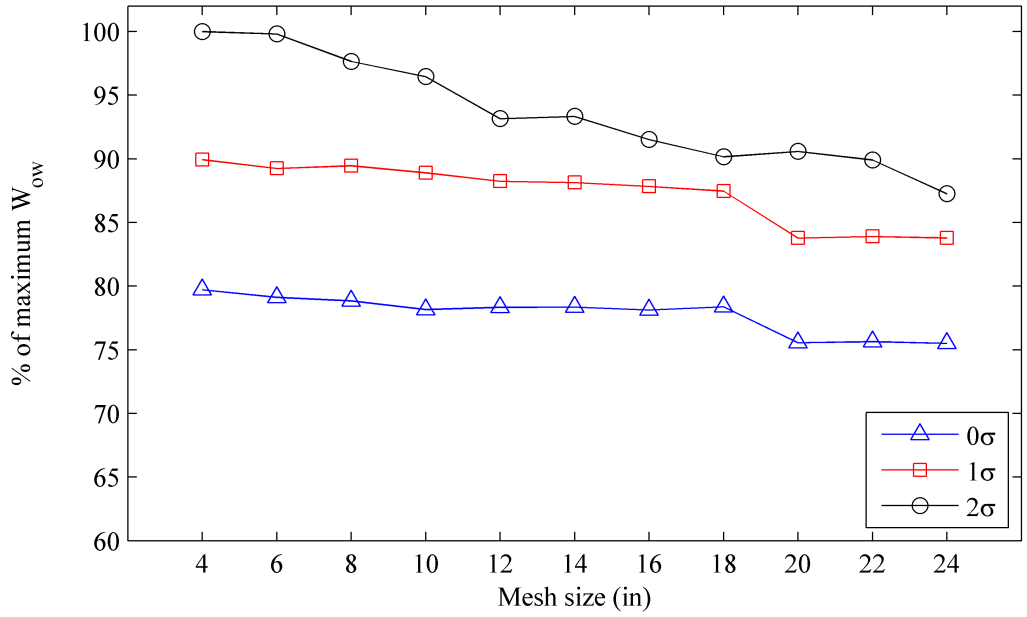

Figure 21: Sensitivity of outboard wing structural weight with respect to the mesh size and statistical loading option.

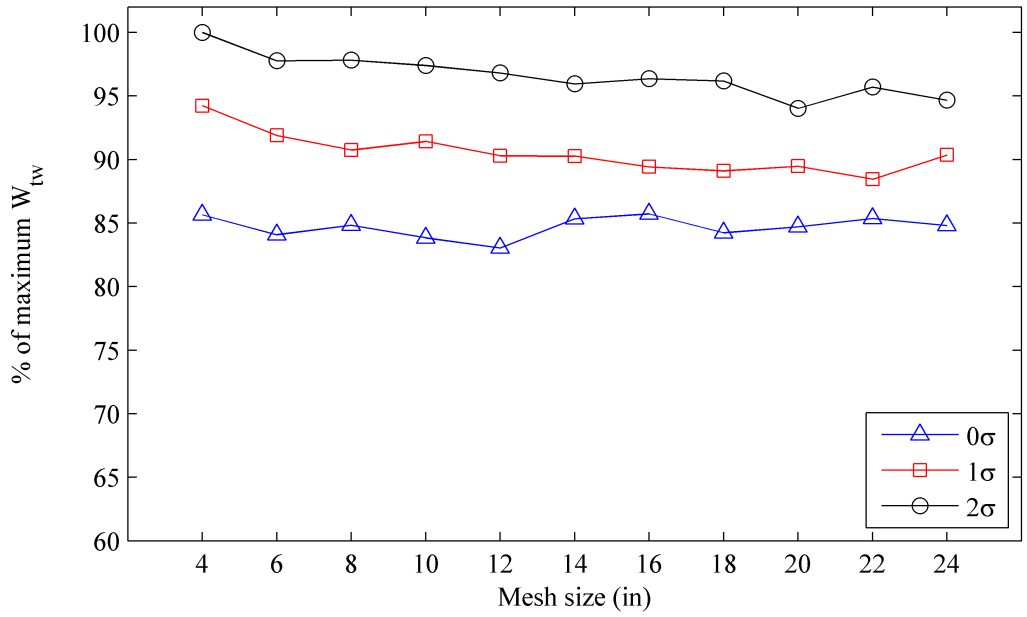

Figure 22: Sensitivity of trapezoidal wing structural weight with respect to the mesh size and statistical loading option.

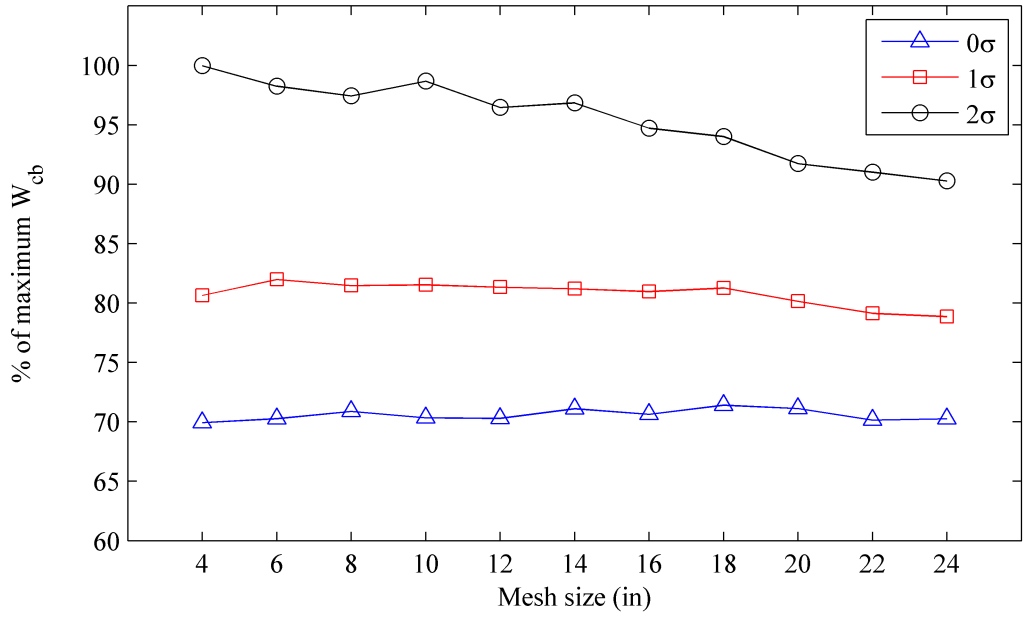

Figure 23: Sensitivity of centerbody structural weight with respect to the mesh size and statistical loading option.

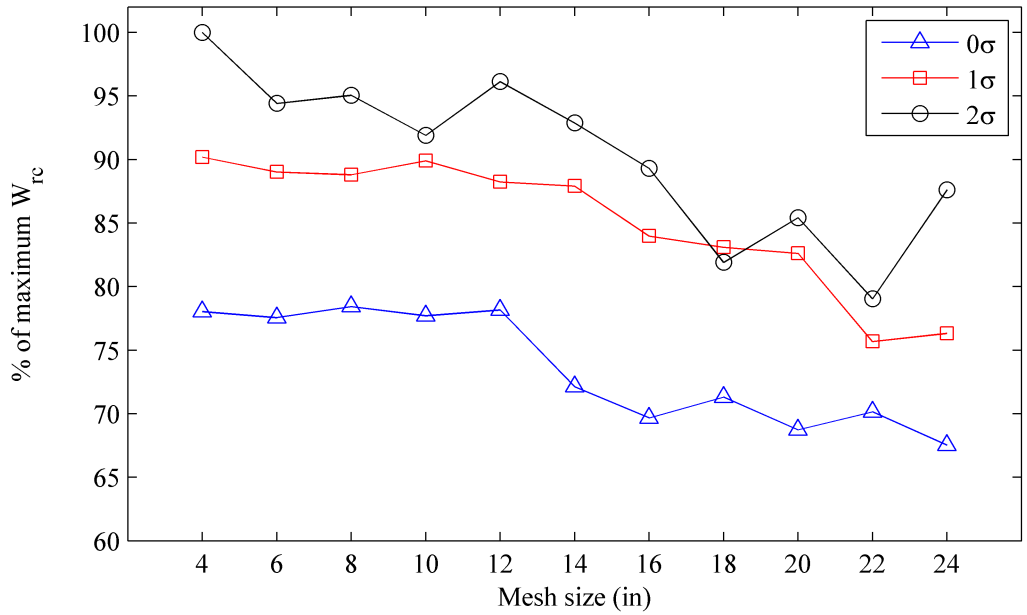

Figure 24: Sensitivity of rear centerbody structural weight with respect to the mesh size and statistical loading option.

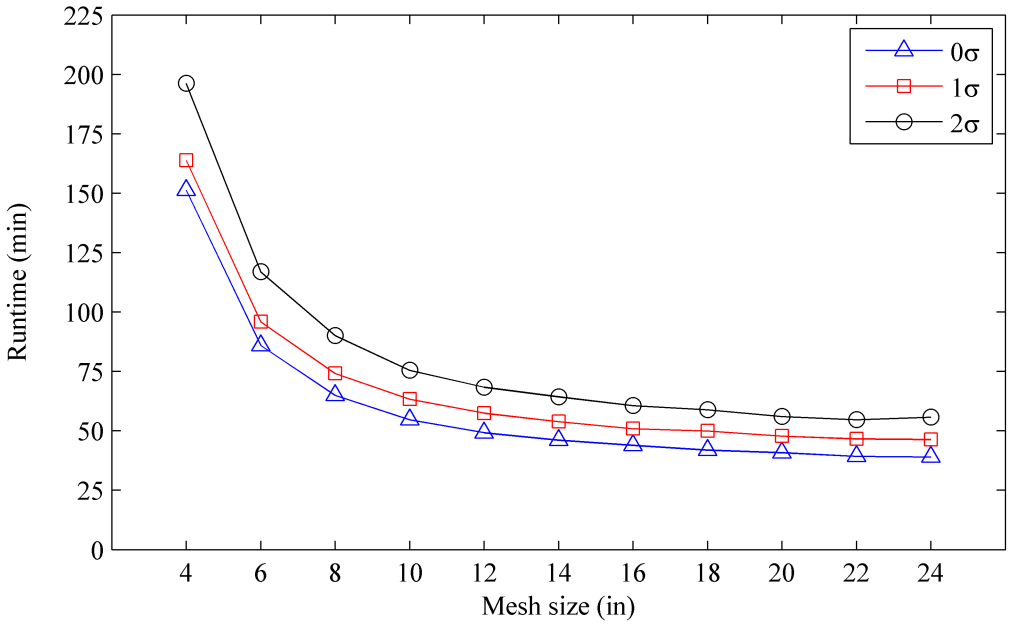

Figure 25: Impact of changing the mesh size on the runtime of the M&S environment.

Below a mesh size of eighteen inches the outboard wing weight in Figure 21 appears relativity constant for the 0σ and 1σ loading options. The trapezoidal wing and centerbody weights in Figures 22 and 23, respectively, appear to be consistent across all mesh sizes. Notice that the 0σ method is generally thirty percent below the 2σ method where in the other sections this difference is usually no more than twenty percent. The centerbody passenger cabin must resist the out-of-plane pressure loads through bending which will result in concentrated bending loads and the edges of the panel. Since the statistical loading methodology is sensitive to the extremes of the data set, the design-to loads used for structural sizing will increase and therefore lead to the larger discrepancy between the 0, 1, and 2σ methods as seen for the centerbody section in Figure 23. The rear centerbody weight is the most irregular but converges to a steady value below a mesh size of twelve inches for the 0 and 1σ methods. The total runtime as a function of the mesh size is shown in Figure 25. Considering that the environment is intended for large parametric studies, selecting a mesh size less

than twelve inches results in a significant increase in runtime. As stated earlier, the weights of all the various sections appear to be well-behaved with respect to the mesh size at values below twelve inches. For these reasons a mesh size of twelve inches was selected.

4.2 Application to Conventional Aircraft Wings

Without any historical data the M&S environment cannot be truly validated for HWB configurations. Rather, the same overall process and tools described in Chapter 3 are applied to a number of conventional aircraft wings to ensure that they are capable of providing reasonable results. In addition to this, this process can be used to develop a calibration factor that relates the load-carrying weight of an aircraft wing structure to the total as-built structural weight. It is anticipated that this calibration factor can be applied to the results of the HWB environment.

The conventional aircraft and their wing structural weights are obtained from a NASA report describing the development of the semi-empirical wing weight estimation tool PDCYL[3]. A total of eight transport aircraft were used for that study but only four are used for the current research. The four aircraft and a summary of their wing weight breakdowns are given in Table 6. The load-carrying structure, or the wing box, consists of spar caps, interspar coverings, spanwise stiffeners, spar webs, spar stiffeners, and interspar ribs. The primary structural weight includes all load-carrying items plus auxiliary spar caps and spar webs, joints and fasteners, landing gear support beam, leading and trailing edges, tips, structural firewall, bulkheads, jacket fittings, terminal fittings, and attachments. The total, or as-built, weight includes all primary weight items plus high-left devices, control surfaces, and access items.

The HWB M&S environment was generalized to accept conventional wing models from VSP and a FEM of the wing structure can quickly be generated given the

Table 6: Wing weight breakdowns for four transport aircraft[3].

Aircraft	**Load-carrying (lbs)**	**Primary (lbs)**	**Total (lbs)**
Boeing 737	5,414	7,671	10,687
Boeing 727	8,791	12,388	17,860
DC-8	19,130	27,924	35,330
L-1011	28,355	36,101	46,233

location of the spars and ribs. The process is not yet fully automated but a complete analysis can usually be performed in less than two hours by an experienced user. Data describing in detail aircraft structural arrangements, dimensions, and material properties is difficult to find in open literature, but a number of sources was used to construct representative structural models of the aircraft listed in Table 6. Niu[27] provided notional sketches of the wing's structural arrangement, upper and lower skin materials, skin stiffener types, and in some cases the rib spacing. The takeoff gross weight used for the various maneuver load cases and the engine weights for inertia relief are the same as those given in Reference [3]. The fuel weight was based on the volume of the FEM, a volume efficiency factor, and an assumed fuel density of 6.8 pounds per gallon. All of this information is summarized in Appendix B. Each analysis used a twelve inch structural mesh and both the $+2.5g$ and $-1.0g$ load cases were considered. Using the information provided by Niu, structural models of the wing load-carrying structure were defined and can be seen in Figure 26.

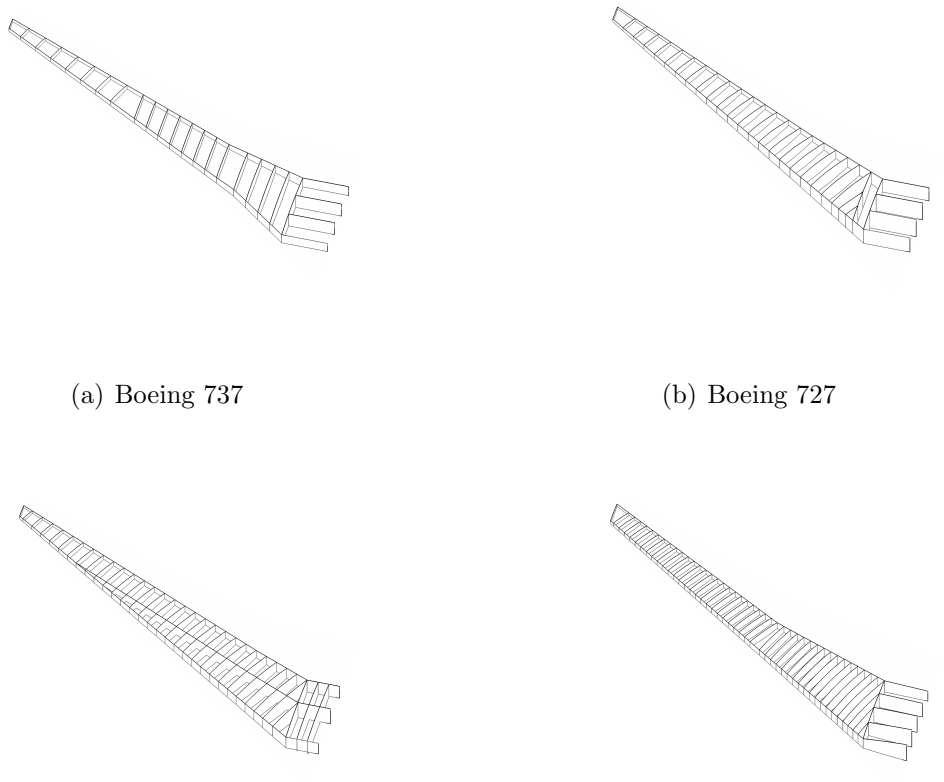

(a) Boeing 737

(b) Boeing 727

(c) DC-8

(d) L-1011

Figure 26: Structural models of conventional aircraft wings used for M&S validation (not to scale).

Like the HWB environment, only the load-carrying structure is modeled and since the wing weight breakdowns given in Table 6 separate the load-carrying weight, a direct comparison can be made between these values and the results of the M&S environment. In addition to this, a relationship between the load-carrying and total weight can be established and used as an initial calibration factor for the HWB analysis. For each of the considered aircraft, the analysis was performed with the various statistical loading options provided by HyperSizer and the results for the load-carrying weights are summarized in Table 7. In general, the M&S environment tends to underestimate the load-carrying weights of the two smallest aircraft models (Boeing 737 and Boeing 727) for all but the 2σ statistical loading option. For the larger aircraft models (DC-8 and L-1011) and the 0σ statistical loading option, the environment overestimates the load-carrying weights by approximately twelve and four percent, respectively. The 1 and 2σ statistical loading options overestimate the load-carrying weight by anywhere between fourteen and twenty-seven percent.

Table 7: Predicted load-carrying results compared to the actual values with different statistical loading options.

Aircraft	**Predicted load-carrying (lbs)**			**Error (%)**		
	0σ	1σ	2σ	0σ	1σ	2σ
Boeing 737	4,875	5,228	5,518	-9.96	-3.34	1.92
Boeing 727	8,284	8,883	9,194	-5.77	1.05	4.59
DC-8	21,461	23,364	24,376	12.18	22.13	27.42
L-1011	29,447	32,471	34,957	3.85	14.52	23.28

The data listed in Table 7 is presented graphically in Figure 27 where the actual load-carrying weights are plotted against the predicted load-carrying weights for the various statistical loading options. A perfect fit line is also plotted making it easy to see the discrepancy between the actual and predicted weights and the dashed lines represent linear trendlines with the intercepts set equal to zero for each of the data sets. Results to the right of the perfect fit line indicate overestimates of the

load-carrying weight while left of the line are underestimates. The error generally increases as the models grow in size with the largest error being associated with the DC-8 model. Based on Figure 27, the 0σ approach appears to provide best overall estimate of the actual load-carrying weight.

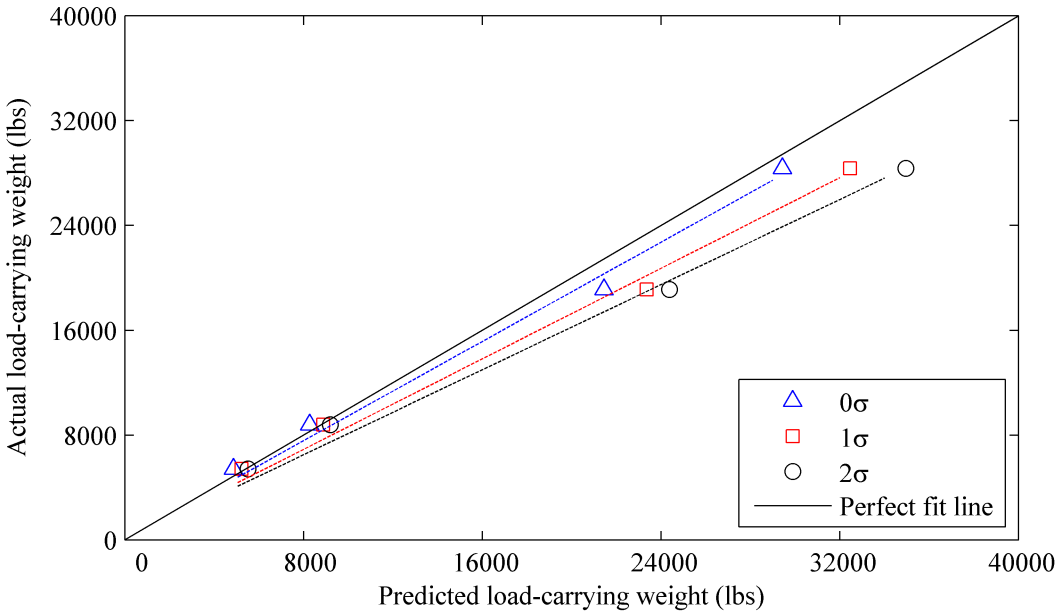

Figure 27: Actual load-carrying weight versus the predicted load-carrying weight for different statistical loading options.

The relationship between the actual total and predicted load-carrying weights is shown in Figure 28. Again, all statistical loading options provide similar results for the smaller aircraft models, but the difference between them increases as the aircraft size increases. These results also suggest that a linear relationship between the load-carrying and total structural weight.

For both the load-carrying and total weight, linear trendlines with the intercept set to equal zero were fit to the data to determine what statistical loading option provided the best prediction of actual weight as a function of the predicted weight. This simple linear relationship is given by

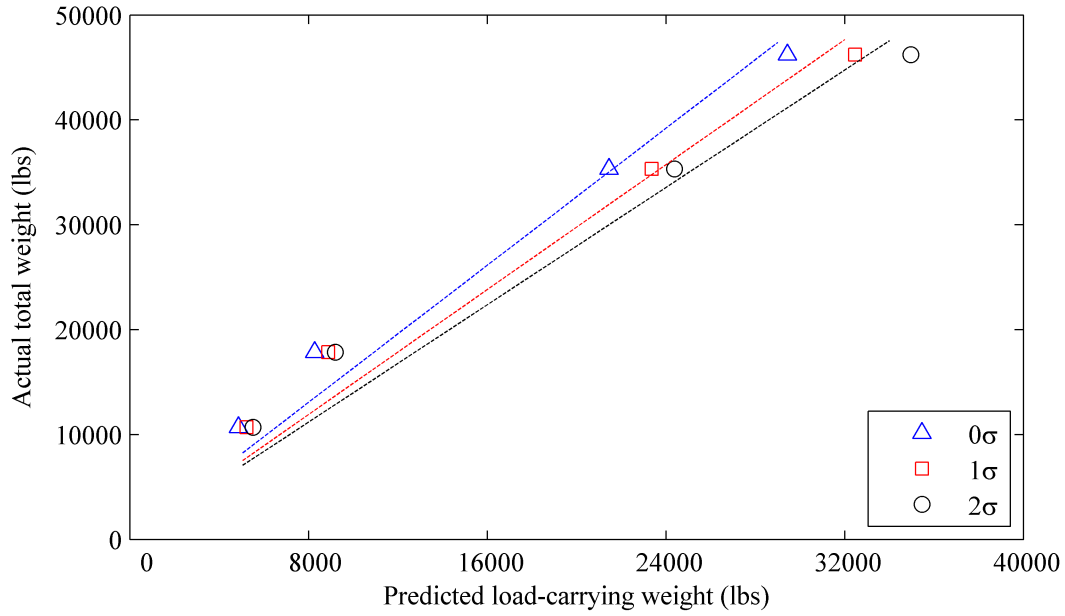

Figure 28: Actual total weight versus the predicted load-carrying weight for different statistical loading options.

$$W_{actual} = K \times W_{predicted} \tag{13}$$

where the predicted load-carrying weight $W_{predicted}$ is related to the actual weight W_{actual} (either load-carrying or total) by a single coefficient K. These trendlines are plotted as dashed lines in Figures 27 and 28 and a summary of the resulting coefficients and fit statistics are shown in Table 8.

Table 8: Summary of linear regression results for conventional wing study.

Statistical Loading	**Load-carrying**		**Total**	
	$\boldsymbol{K}$	$\boldsymbol{R^2}$	$\boldsymbol{K}$	$\boldsymbol{R^2}$
0σ	0.9469	0.9902	1.6335	0.9623
1σ	0.8638	0.9900	1.4892	0.9560
2σ	0.8121	0.9906	1.3984	0.9461

For all statistical loading options the linear model adequately fits the data as implied by the coefficients of determination R^2. This is true for both the load-carrying

and total structural weights and suggests that a single calibration factor can be used to estimate the total structural weight given the predicted load-carrying weight. The accuracy of the various statistical loading methods is determined by the calibration constant K where values closest to one provide a more accurate prediction. The 0σ statistical loading option provides the most accurate results for load-carrying weight while the other options overestimate the actual load-carrying weight. Table 8 also shows that the linear model provides an adequate relationship between the predicted-load carrying weight and the actual total structural weight. The coefficient of 1.6335 for the 0σ loading option represents the scale factor required to estimate an aircraft's total wing weight as a function of the predicted load-carrying weight.

The 0σ statistical loading method provides the best prediction of the load-carrying weight, with a maximum error of approximately twelve percent. Considering the limited amount of data regarding the details of each aircraft's structural configuration and the rather crude method of defining the structural arrangement, these results show that the overall process and analysis tools are capable of providing realistic predictions. The fundamental assumption moving forward is that since the M&S environment is based on the physics of the problem rather than historical data, it can be applied to a HWB configuration and provide accurate predictions of the load-carrying structural weight. Relating the load-carrying weight to the total structural weight is done by a calibration factor applied to load-carrying weight assuming a linear relationship. Examining the terms of the general wing weight equation and their relative size as shown in Table 2, it is clear that the bending material accounts for the majority of the wing structural weight. The structural models generated for this conventional wing study should capture most, if not all, of the bending material weight but they model none of the secondary structure which could account for twenty-five percent of the wing weight. With this in mind and considering the size of the terms in

Table 2, a calibration factor of between 1.67 and 1.33 is expected to relate the load-carrying to the total weight, depending on the amount of rib and shear size material captured by the model. Also, Figure 3 shows that a FEM model for a conventional structure may only account for forty to eighty percent of the total weight. The calibration factor of 1.6335 provided by the 0σ method is within these ranges and appears to be a reasonable value. As the structural models increase in detail and more load cases are considered, the calibration factors will approach one.

4.3 Calibration of Baseline HWB Configuration

Initially it was thought that using the 2σ loading method would be a more appropriate choice assuming the added level of conservatism might partially account for the limited number of load cases. The results of the mesh sensitivity and conventional wing study suggested otherwise. Although a calibration factor relating the load-carrying weight to the total structural weight was determined from the conventional wing study, its applicability may be limited given the unconventional configuration of the HWB. In addition to this, a relationship derived from metallic wings may not be suitable for advanced composite materials, even for a conventional configuration. If a database of conventional composite wings existed, a similar study to the one performed in Section 4.2 might yield a more appropriate calibration factor. The purpose of this section is to establish a baseline HWB configuration, asses the applicability of the calibration factor determined by the conventional wing study, and to then further refine the calibration factors if needed.

A HWB configuration developed by a Boeing study was used as a calibration point for the environment and its general characteristics and mission parameters are given in Table 9. The configuration is known as the N2A model and Reference [14] provides a more detailed description of the aircraft. Figure 29 shows the OML generated by VSP and the structural model not including the outer skins and main cabin floor.

This baseline HWB employs a blended centerbody leading edge and a three bay passenger cabin. Although not included in the model, vertical tails are placed on the rear centerbody section with pod-mounted turbofan engines mounted between them for noise shielding.

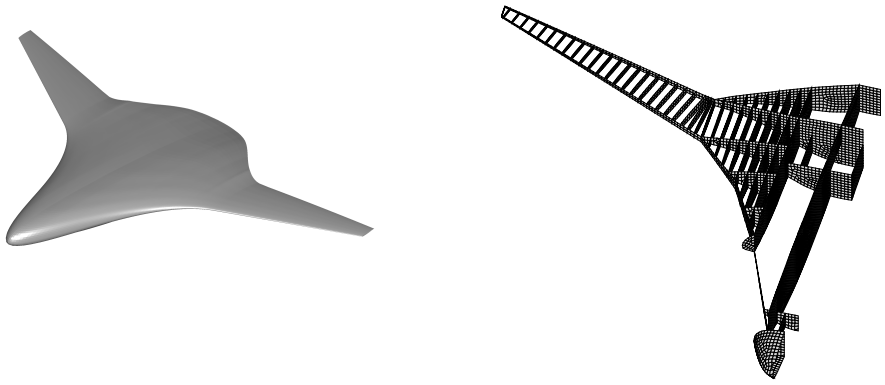

(a) OML (b) Internal structure

Figure 29: Outer mold line and internal structure of baseline HWB configuration.

Table 9: Configuration and mission data of baseline HWB configuration used for M&S calibration[14].

Baseline HWB configuration and mission data		
Range	6,000 nm	
Cruise Mach	0.8	
Wing area	9,246 ft^2	
Wingspan	213 ft^2	
Centerline length	134.5 ft	
Payload	103,000 lbs	
Mission fuel	139,900 lbs	
W_E	218,600 lbs	
W_{TO}	416,500 lbs	
Structural weight summary		
	Boeing	FLOPS
Outboard wing[†]	44,450	36,850
Rear centerbody	10,875	13,945
Centerbody	57,092	64,735
Total	**112,417**	**115,530**

[†] Includes both outboard and trapezoidal wing sections.

Table 9 also provides a structural weight summary of the aircraft categorized by the various sections. Here, the outboard wing value includes both the outboard and trapezoidal wing as defined in this research. A Boeing in-house weight estimation methodology was used to generate the Boeing results about which little detail is known. The FLOPS results were generated by a study performed by researchers at NASA LaRC and uses the methodology developed by Bradley[6] for the centerbody weight predictions and existing empirical methods for the outboard wing and rear centerbody. The FLOPS analysis assumes the centerbody structure employs the PRSEUS concept and a fifteen percent weight savings is applied to the metallic wing weights to account for composite materials. A difficult aspect of this calibration effort is the lack of detail regarding the various structural concepts and materials used throughout the aircraft. This is a common theme in any physics-based approach since all the details surrounding the design and analysis must be individually accounted for as opposed to empirically derived methods where this information is embedded in the data. For each structural component (i.e., outboard wing spars and ribs, centerbody skin panels, etc.) a structural concept, variable bounds, and materials must be defined. A summary of the structural concepts for each of the structural components is provided in Table 22. Rather than defining a number of discrete composite laminates, effective laminates were used instead which allow the thickness to be treated as a continuous variable. The variable bounds and number of permutations were selected in such as way that the resulting thicknesses would be equal to a discrete number of composite laminate stacks. The composite material properties and effective laminates can be found in Appendix A. In areas of predominantly uniaxial loading, an effective laminate consisting of mostly 0° plies is used and shear dominated areas, such as rib webs, use an effective laminate consisting of more $\pm 45^\circ$ plies. The stiffeners on the outboard and trapezoidal wings and the rear centerbody skin panels are in directed in the spanwise direction. Stiffeners on any spar or rib webs are oriented vertically. For

the centerbody skin panels, the frames of the PRSEUS concept are in the spanwise direction resulting in the stringers being oriented in the chordwise direction. The PRSEUS frames are aligned vertically for the centerbody rear and side cabin walls.

Table 10: Stiffened panel concepts and effective laminates used for the various components in the baseline HWB structural model.

Component	Panel concept	Effective laminate (EL)
Outboard wing spar webs	angle-stiffened	EL 2
Outboard wing rib webs	angle-stiffened	Shear EL
Outboard wing skin panels	z-stiffened	EL 2
Trapezoidal wing spar webs	z-stiffened	EL 2
Trapezoidal wing rib webs	t-stiffened	Shear EL
Trapezoidal wing skin panels	z-stiffened	EL 2
Rear centerbody wing spar webs	t-stiffened	EL 2
Rear centerbody wing bay wall webs	foam sandwich	EL 1 facesheets
Rear centerbody wing skin panels	z-stiffened	EL 2
Centerbody cabin rear and side wall webs	PRSEUS	EL 2
Centerbody cabin floor	PRSEUS	EL 2
Centerbody bay wall webs	foam sandwich	EL 1 facesheets
Centerbody skin panels	z-stiffened	EL 2
Landing gear spar/rib webs	z-stiffened	EL 2

The M&S environment was executed for this baseline case and the convergence of the structural weight is shown in Figure 30. Here, the results on the y-axis are the raw data from HyperSizer with no calibration factors applied. The weight quickly converges after the second iteration and remains stable for all six iterations. Although the weight converges, the environment is typically executed with three HyperSizer iterations to ensure that the loads are properly redistributed throughout the structure. This may not significantly change the overall weight results, but it was observed that it did affect the critical load case of some structural components.

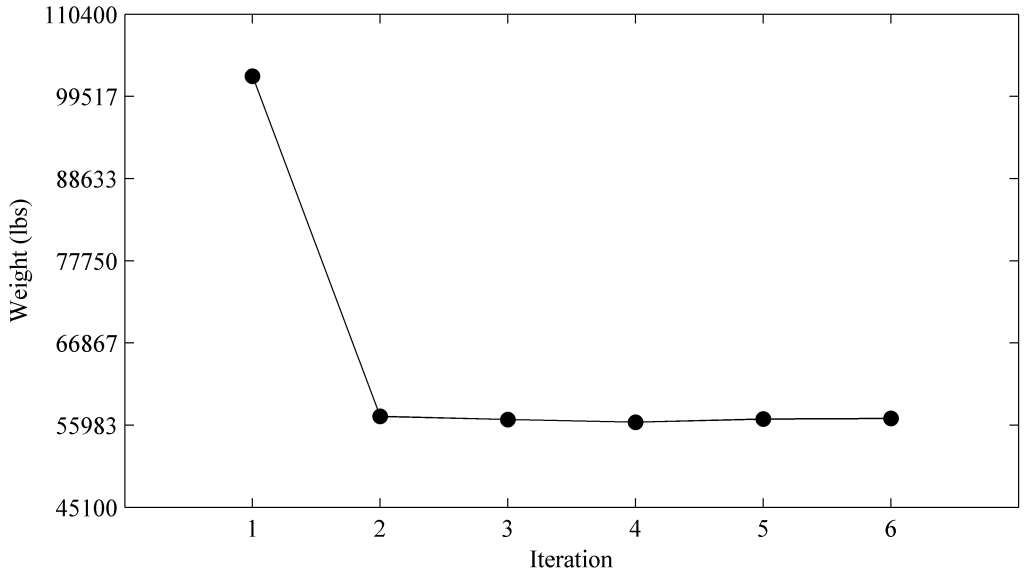

Figure 30: Convergence of structural weight for the baseline HWB configuration.

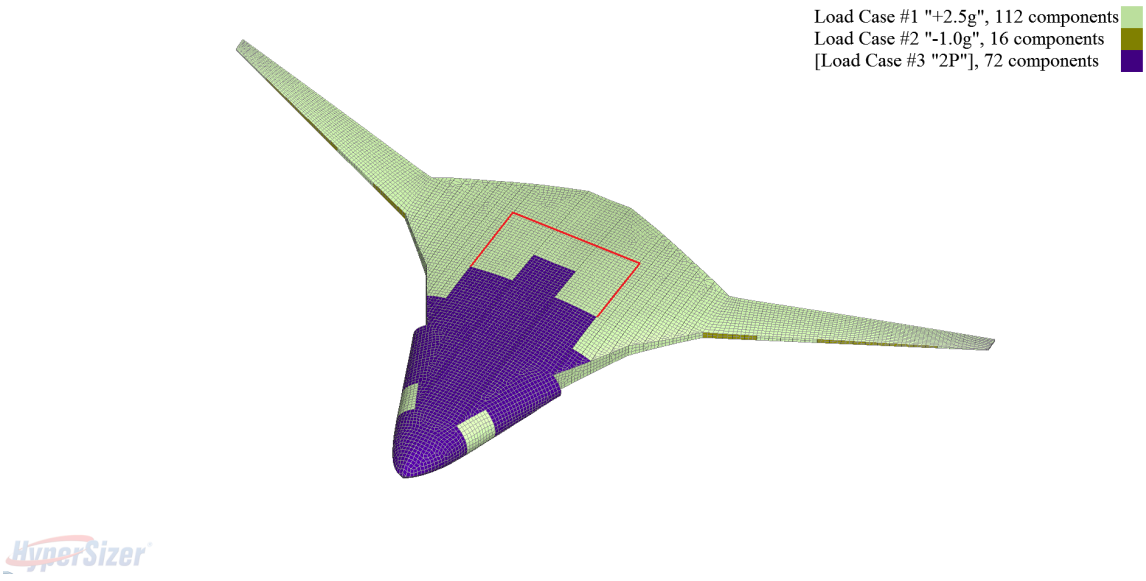

Figure 31: Critical load cases for baseline HWB configuration (reflected along centerline). The upper centerbody skin panels are outlined in red.

The critical load cases are shown in Figure 31 where the results have been reflected along the aircraft's centerline. As expected, the majority of the upper skin panels of the outboard and trapezoidal wing sections are sized by the compressive loads resulting from the $+2.5g$ maneuver. Lower skin panels near the root of the outboard wing are also sized by this load cases and the critical failure criteria is material strength. The rest of the lower skins on the outboard and trapezoidal wings are typically sized by the -1.0g maneuver and are stability critical. Without any vertical tail or propulsion system loads the critical load cases for the rear centerbody section are the two maneuver load cases. The critical load cases for the centerbody section are much more interesting since carries the wing bending loads and the internal cabin pressure. The upper skin panels in the centerbody section near the rear of the cabin, outlined in red, are sized by the $+2.5g$ maneuver including the $1P$ internal pressure. This is a direct result of the loads from the outboard wings and is a unique feature of the HWB. This supports the assumption that the weight of the centerbody section will be sensitive to the outboard wing parameters. The panels are the forward portion of the centerbody structure are sized by the $2P$ load case. The lower centerbody skin panels are also sized by the $2P$ load case where the spars surrounding the main gear skin cutout are sized by the compressive loads from the -1.0g maneuver. Critical failure modes for the centerbody skin are typically maximum strain in the spanwise direction. Optimum unit weights for the PRSEUS panels in the centerbody section are generally between two and three pounds per square foot, where the heavier panels are associated with those sized by the $+2.5g$ maneuver.

Deflections for the $2P$ load case can be seen in Figure 32. The maximum of 2.32 inches occurs in the front portion of the upper centerbody skin just behind the flight deck. Vertical deflection results for the $+2.5g$ maneuver are shown for the entire model in Figure 33 with a maximum wing tip deflection of 137 inches. The deflection results for the centerbody upper skin for this same load case are shown in Figure 33(b). Here

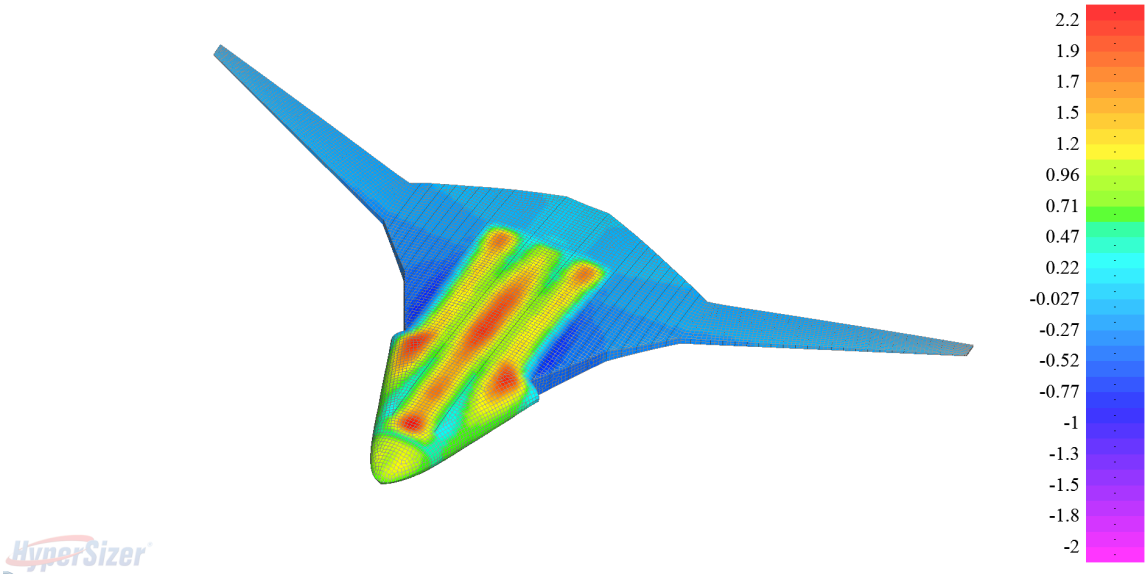

Figure 32: Deflection results for the baseline HWB configuration for the $2P$ load case (reflected along centerline). The maximum deflection of 2.32 inches occurs near the front of the upper centerbody skin just behind the flight deck.

(a) Wing tip (b) Centerbody skin

Figure 33: Deflection results for baseline HWB configuration during the $+2.5g$ maneuver for the (a) wingtip and (b) upper centerbody skin (reflected along centerline). The maximum wing tip deflection is 137 inches. The maximum centerbody deflection of 1.66 inches occurs near the rear of the upper skin.

you can again see the impact of the compressive loads from the outboard wings. In this case, the maximum deflection occurs in the rear panels where the largest compressive loads from the outboard wings are experienced. From an aerodynamic perspective, it may be important to take these structural deflections into consideration. During a steady-state cruise, the deflections will be less in magnitude but display the same overall deflection shape as seen in Figures 32 and 33(b). These deflections may

adversely affect the vehicles aerodynamic cruise performance and it may be necessary to place a deflection limit on the centerbody skin panels.

The structural weight results for the baseline HWB configuration produced by the M&S environment can be seen in Table 11. The results with a calibration factor K of one represent the raw data from HyperSizer. These results are expected to be significantly less than the Boeing and FLOPS results since the detail of the structural model was limited (e.g., no leading or trailing edges). Raw results similar to the Boeing and FLOPS data would be a cause for concern since it would mean the load-carrying structure is significantly oversized. The last column shows the results using the calibration factor derived from the conventional wing study. A K factor of 1.634 results in a total structural weight prediction of about eighteen percent below the averaged Boeing and FLOPS results.

Table 11: Baseline HWB weight results using the calibration factor derived from the conventional wing study.

Component	**Boeing**	**FLOPS**	**M&S** $(0\sigma, K = 1)$	**M&S** $(0\sigma, K = 1.634)$
Outboard wing	44,450	36,850	21,211	34,648
Centerbody	57,092	64,735	30,440	49,724
Rear centerbody	10,875	13,945	5,061	8,267
Total	**112,417**	**115,530**	**56,712**	**92,639**

Using the Boeing data as the baseline to determine the required calibration factors, Equation 12 becomes

$$W_{airframe} = 2.095W_{ow} + 2.095W_{tw} + 1.876W_{cb} + 2.149W_{rc} \tag{14}$$

and will be used for all further analysis. The resulting calibrations factors are larger than the one derived from the conventional wing study, but are still well within

reasonable limits. A number of things could be refined to bring the calibration factors to an expected range of 1.33 to 1.67. First, the model assumed that composites were used for the entire load-carrying structure, whereas the Boeing and FLOPS studies may use a mixture of metallic and composites materials. Second, the material properties and strength allowables of the composite materials were "textbook" values. Given the limited use of composite materials thus far in load-carrying structures, it is common to use conservative strength allowables as opposed to metallic structures since their properties are well understood and supported by decades of use. These refinements would decrease the calibration factors but at this point they will not significantly impact the overall trends produced by the M&S environment.

CHAPTER V

RESULTS AND DISCUSSION

In this chapter, the M&S environment formulated in Chapter 3 is used to examine a number of problems regarding HWB structural weight estimation. In the first section, the results from an existing HWB vehicle scaling study are compared to those produced by the current environment with particular focus given to the centerbody section. With no historical data to truly validate results, if a number of independent analyses provide similar results, each using their own unique procedure and modeling tools, the confidence in these HWB structural weight predictions may be improved. In the second section, the M&S environment is used to identify the design parameters that significantly contribute to the variability of the HWB structural weight. Here, emphasis is placed upon the sensitivity of the centerbody structural weight with respect to the design parameters of the outboard wing section. The next section concludes the chapter with a means to provide the prediction capability of the M&S environment to an aircraft conceptual design tool without the computational cost.

5.1 HWB Vehicle Scaling Study

Nickol[25] performed an HWB study that investigated the scalability of the configuration and at what vehicle sizes the HWB outperformed a tube-and-wing in terms of fuel burn. In conjunction with this study, the HWB centerbody structural weight tool described in Section 2.3 developed by Gern[8] was used to provide structural weight estimates. A total of five HWB aircraft were defined for the analyses and provide a data set for comparison. The overall approach taken by Gern was similar to one described in this research effort. A number of physics-based analysis methods, including finite element analysis and doublet-lattice aerodynamics, were integrated to

form a parametric analysis environment. The main differences between Gern and the M&S environment formulated in Chapter 3 are the detail of the structural model and the structural sizing routine. Gern uses Nastran's design and optimization routine to size the thickness of the elements and provide a relationship between the centerbody weight and the available design parameters. Another Boeing study, other than the one used in this work, was then used to calibrate the Nastran weight results to provide an estimate of the as-built structural weight. The same load cases were used by Gern but the aerodynamic loads were estimated by a doublet-lattice aerodynamic tool.

The models developed by Nickol and Gern were reproduced by the current M&S environment as accurately as possible given the description provided by their publications. The dimensions of the centerbody cabins for the various HWB configurations were provided by Dr. Gern to enable a more accurate evaluation. The HWB aircraft are defined by their passenger capacity and range from 98 to 400 passengers. A summary of the configuration parameters is provided in Table 12. Both studies assume a composite PRSEUS centerbody structural concept and the material properties and concepts used for the HWB calibration case are used here. The planforms use a linear rather than blended centerbody leading edge and a centerbody front spar that is the full depth of the OML. The structural arrangements of each of the HWB models can be seen in Figure 34.

Table 12: Configuration parameters for HWB scaling study.

Aircraft	**HWB98**	**HWB160**	**HWB216**	**HWB301**	**HWB400**
Number of passengers	98	160	216	301	400
W_{TO} **(lbs)**	101,000	166,100	286,900	542,600	693,600
b **(ft)**	142	180	210	240	260
$c_{r,cb}$ **(ft)**	65.7	80.7	105	118	135
l_{cabin} **(ft)**	41.7	52.4	64.8	82.0	99.2
w_{cabin} **(ft)**	32.1	39.7	41.3	46.3	70.0
$\Lambda_{LE,cb}$	51.7°	50.4°	54.9°	56.0°	51.5°

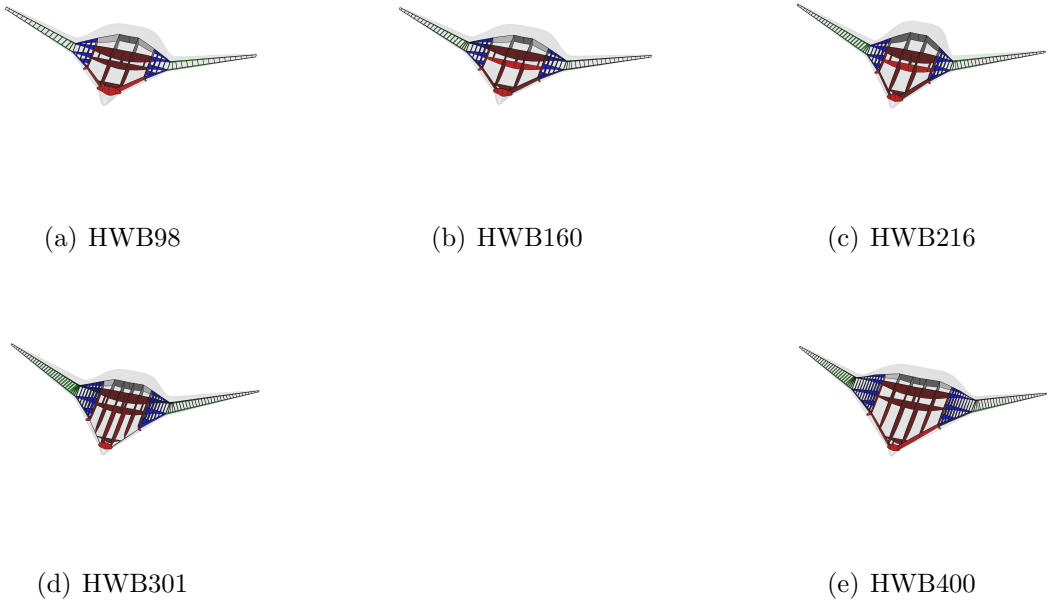

(a) HWB98 (b) HWB160 (c) HWB216

(d) HWB301 (e) HWB400

Figure 34: Structural arrangements of the various HWB models used for the vehicle scaling study (images not to scale).

The predicted centerbody structural weights for both Gern and the current M&S environment using the 0σ statistical loading method are given in Table 13. Both three and five bay cabin arrangements were considered and the percent difference is relative to the M&S (0σ) results. The average difference between the two methods for the three bay models is approximately five percent with the largest occurring at the HWB400. The average difference of the five bay results is approximately nine percent with both the HWB160 and HWB301 five bay models differing by slightly more than eleven percent. The results in Table 13 are presented in graphical form in Figure 35 and the relationship between the centerbody weight and number of passengers can be observed. Results by Gern show that a five bay cabin arrangement always provides the minimum weight solution while the M&S environment shows the same except for the HWB98 aircraft. For the smaller aircraft, the number of cabin bays, and therefore cabin bay width, may be determined more by the passenger cabin arrangement rather than the lightest weight, especially given the relatively small

weight increase for the three bay configuration. The difference between the three and five bay cabin models becomes more pronounces as the vehicle increases in size. This is a result of the increased span distance between the cabin bay walls which increases bending moments at the panel edges and the design-to loads during structural sizing. The recommended transition point between a three and five bay cabin is between two and three hundred passengers. This implies that the aircraft designer should configure the cabins of smaller HWB vehicles for passenger comfort or cargo arrangement. As the cabin increases in size it should be optimized for weight reduction. The centerbody structural weight methodology currently employed in FLOPS and given by Equation 3 is also displayed in Figure 35. It is both interesting and encouraging that the centerbody weight predictions of all three methods display the same behavior as the vehicle increases in size. All three methods were developed independently where each used structural models of different detail, employed different analysis tools, and used different HWB calibration models.

Table 13: Summary of centerbody structural weight results for the HWB scaling study.

Aircraft	**Gern**		**M&S (0σ)**		**% difference**		**FLOPS**
	3-bay	**5-bay**	**3-bay**	**5-bay**	**3-bay**	**5-bay**	
HWB98	14,770	14,236	15,432	15,547	4.48	9.21	14,928
HWB160	25,218	22,633	25,987	25,318	3.05	11.9	26,528
HWB216	36,231	34,538	37,357	35,545	3.11	5.81	41,659
HWB301	57,673	49,838	59,490	55,555	3.15	11.5	69,513
HWB400	145,343	111,950	160,590	106,852	10.5	-4.55	128,003

The impact on the number of cabin bays was further investigated by analyzing the various HWB configurations in Table 12 using five discrete settings for the number of cabin bays. For each vehicle the number of cabin bays was varied from two to six except for the HWB400 where the number of bays was from four to eight. For each vehicle an optimum number of cabin bays in terms of centerbody structural weight

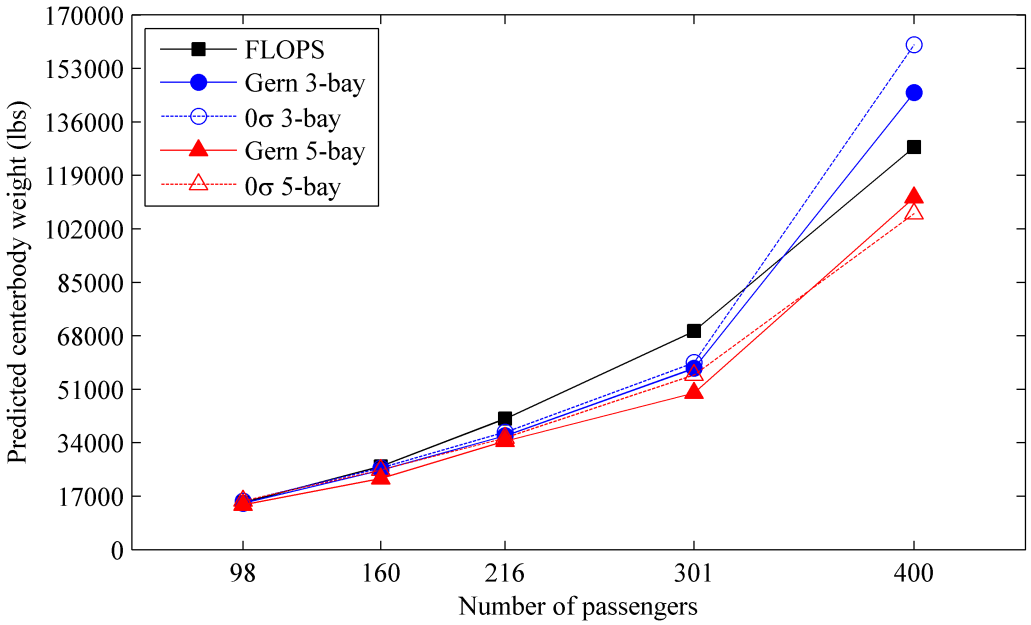

Figure 35: Comparison of the centerbody structural weights as a function of the number of passengers.

was observed and displayed a response as the one show in Figure 36. The lowest setting of cabin bays always resulted in the largest weight due to the increased span of the centerbody skin between the bay walls. The highest setting of cabin bays never provided the minimum weight although it was significantly lighter than the minimum setting. Although the span distance of the centerbody skin continuously decreases as the number of cabin bays increases, the weight penalty associated with the added cabin bay walls exceeds any weight savings in the skin. Table 14 presents the results of this cabin bay sensitivity study. As expected, the optimum number of cabin bays increases as the vehicle increases in size but the resulting cabin bay width remains between approximately eight to nine feet. This information can be used as a general design rule for initial cabin arrangements of HWB configurations. While this value may be slightly lower than the fuselage width of a conventional narrow-body aircraft, the design engineer can refine cabin arrangement as needed. If the cabin bay width is to be increased it is important to take the sensitivity of the centerbody structural

weight shown in Figure 36 into consideration.

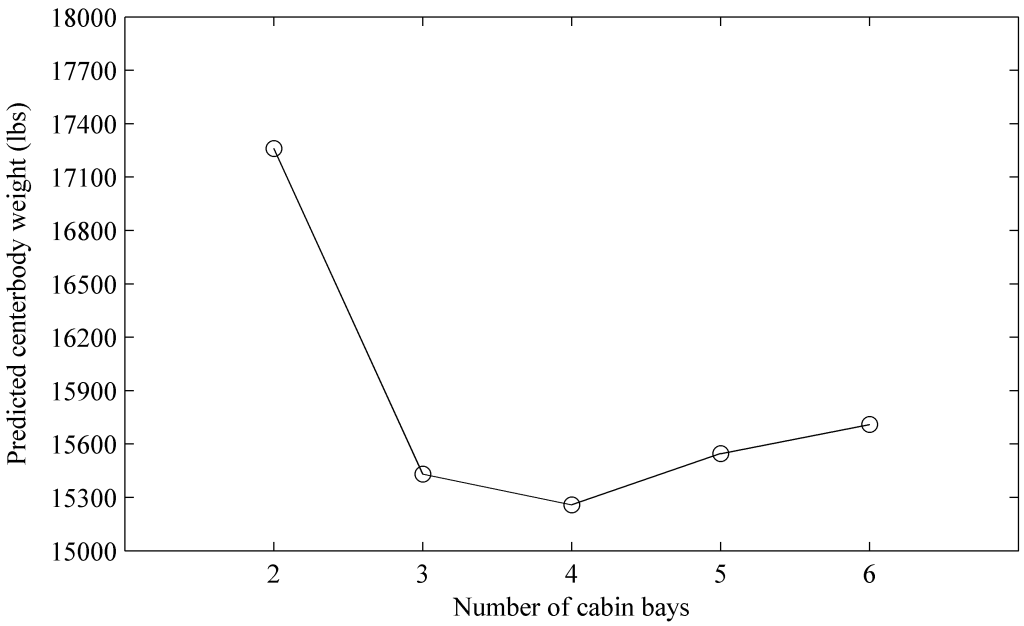

Figure 36: Optimum bay width for HWB98 vehicle.

Table 14: Optimum number of cabin bays for each of the HWB aircraft used in the vehicle scaling study.

Aircraft	**Number of cabin bays**	w_{bay} **(ft)**
HWB98	4	8.03
HWB160	5	7.94
HWB216	5	8.26
HWB301	5	9.26
HWB400	7	8.75

5.2 Identification of Key Design Parameters

Early in the development of a new product, having knowledge of the design parameters that significantly impact the metrics of interest is critical for the engineering and decision-making process. This is especially true during conceptual design where the most design freedom exists but the knowledge about the design is at a minimum. It is also during this stage that decisions will be made that affect the entire life cycle of the product. In the context of aircraft design and structural weight estimation, inaccurate estimations could jeopardize the mission requirements or result in costly design changes. Over a long period of conventional tube-and-wing aircraft construction, critical design parameters are fairly well established and usually appear in the statistical equations used for weight estimation. Again, this relies upon decades of experience and historical data which is nonexistent for HWB type configurations. It has already been shown in Section 4.3 that portions of the centerbody structure are sized by the maneuver load cases. The internal loads in these sections will be a function of the outboard wing size and shape, the ultimate load factor, and the vehicle weight during the maneuver. The goal of this section is to characterize this relationship and determine if the outboard wing parameters are as significant as those defining the overall size and shape of the centerbody.

Various statistical methods are commonly used to identify which factors of a data set are significant with respect to a desired response. One of these methods, known as Analysis of Variance (ANOVA), can be performed using the M&S environment where the design parameters, or factors, can be easily varied to generate the response data necessary to perform the statistical analysis. Creating this data set was accomplished through well established Design of Experiments (DOE) techniques. Performing an ANOVA usually requires the use of two level factorial designs to capture the linear relationship between the data points. Given the number of variables intended to be considered in this study, a full factorial design resulting in 2^n test cases would be too

computationally expensive. If high-order interactions between the design parameters are assumed to be negligible, fractional factorial designs can be used to gather information about the main effects and low-order interactions for much less computational effort. These types of designs are commonly used for screening experiments which is equivalent to identifying the key design parameters as in this study[23].

The M&S provides a total of thirteen design variables to define the OML shape, eight of which are associated with the outboard wing. In additional to these parameters, another eleven parameters are needed to fully define the structural arrangement, resulting in a total of twenty-four independent variables. If only considering the outboard wing parameters, the total number can be reduced to ten assuming that certain structural parameters are assumed to take typical values. For example, the front and rear spar positions on the outboard wing can be assumed to be positioned by leading and trailing edge surfaces. Common values for front and rear spar positions as a percentage of the chord are twelve and sixty percent, respectively. The ten outboard wing factors and their minimum and maximum bounds considered for this first screening test are shown in Table 15.

Table 15: Outboard wing factors and minimum and maximum bounds for the first ANOVA.

Variable	Minimum	Nominal	Maximum
b_{ow} (ft)	66.5	71.5	76.5
$\Lambda_{LE,ow}$	20.0°	28.0°	36.0°
$c_{r,ow}$ (ft)	26.0	32.0	38.0
$c_{t,ow}$ (ft)	5.00	7.50	10.0
$(t/c)_{r,ow}$	0.08	0.10	0.12
$(t/c)_{t,ow}$	0.058	0.078	0.098
ϕ_{ow}	0.0°	4.0°	8.0°
θ_{ow}	-3.0°	0.0°	3.0°
$y_{rib,ow}$ (ft)	2.0	3.0	4.0
$y_{rib,tw}$ (ft)	2.0	3.0	4.0

The DOE was a resolution IV fractional factorial design which required a total

of 129 test cases. With a resolution IV design no main effects are aliased with any other main effect or any two-factor interaction, but the two-factor interactions may be aliased with one another. After the data was generated a series of ANOVAs were performed for each response of interest. The ANOVA results are quantified by the F-statistic which is a ratio of the explained variance to the unexplained. In general, the larger the value the more statistically significant the factor is. The following results are presented in such as way that the factors are sorted according to their F-statistic, where each value has been normalized by the sum of the F-statistics of each factor. In this way, the horizontal axis displays the percent of variability that each factor accounts for, and the line plot represents the cumulative total starting from the most significant factor and then progressing downwards. Only the top fifteen factors and interactions are shown.

The first ANOVA results in Figure 37 are generated from varying the outboard wing parameters only and observing the response of the centerbody structural weight. One noticeable result is that the two-factor interactions account for the most of the displayed results. The only main effects that can be seen are the outboard wing root chord $c_{r,ow}$, span b_{ow}, and leading edge sweep $\Lambda_{LE,ow}$. The significance of the two-factor interactions implies that the impact of changing the two parameters together is more significant than changing them independently. The most statistically significant result is an interaction between the span of the outboard wing and the outboard wing chord $b_{ow} \times c_{r,ow}$.

Although certain set of parameters were identified as being statistically significant with respect to the centerbody structural weight, a true measure of their significance will better measured when they are included in an ANOVA with centerbody size and shape parameters. The same DOE as before was used but this time the parameters in Table 16 are used. The intent of this study is to determine if the factor identified when only varying the outboard wing are still significant when compared with the

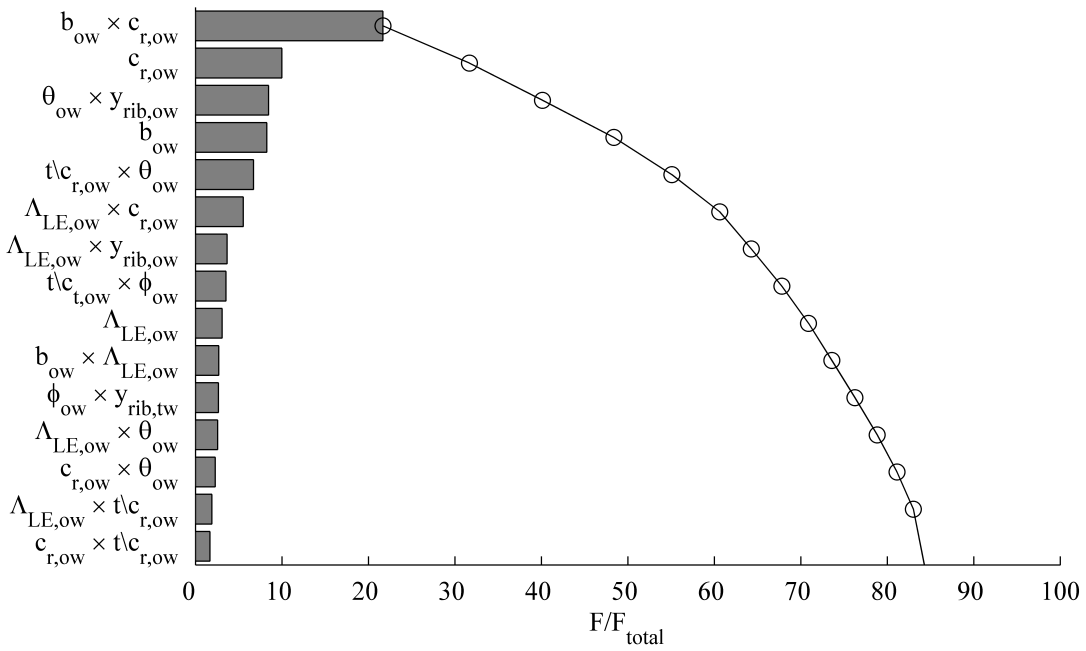

Figure 37: ANOVA results for centerbody weight while only varying outboard wing parameters ($F_{total} = 165$).

general size of the centerbody.

Table 16: Variables and maximum and minimum bounds for outboard wing and centerbody ANOVA.

Variable	Minimum	Nominal	Maximum
$\boldsymbol{b_{ow}}$ **(ft)**	66.5	71.5	76.5
$\boldsymbol{\Lambda_{LE,ow}}$	20.0°	28.0°	36.0°
$\boldsymbol{c_{r,ow}}$ **(ft)**	26.0	32.0	38.0
$\boldsymbol{c_{t,ow}}$ **(ft)**	5.00	7.50	10.0
$\boldsymbol{\phi_{ow}}$	0.0°	4.0°	8.0°
$\boldsymbol{\Lambda_{LE,cb}}$	62.0°	65.0°	68.0°
$\boldsymbol{c_{r,cb}}$ **(ft)**	129.6	134.6	139.6
$\boldsymbol{l_{cabin}}$ **(ft)**	89.22	94.22	99.22
$\boldsymbol{w_{cabin}}$ **(ft)**	30.75	35.75	40.75
$\boldsymbol{W_{TO}}$ **(lbs)**	436,500	461,500	486,500

The ANOVA results from varying both the outboard wing and centerbody parameters are shown in Figure 37. The most significant result is the interaction between

the length and width of the cabin $l_{cabin} \times w_{cabin}$. Based on a visual inspection, all the statistically significant parameters appear to be the ones associated with only the centerbody, with the overall width of the cabin w_{cabin} being the most significant. This is due to using a fixed number of bays during this experiment so as the width increased, so did the span between the cabin bay walls. Closer examination of the raw data showed that the top twelve factors shown in Figure 38 yielded an F-statistic of greater than three, which is a common threshold for rejecting the null hypothesis that the factor is not statistically significant. Outboard wing parameters in this category are the outboard wing root chord $c_{r,ow}$, leading edge sweep $\Lambda_{LE,ow}$, span b_{ow}, and wing twist ϕ_{ow}. While they may be considered for statistical modeling purposes, they most likely will not be a key driver of the centerbody structural weight. Additional ANOVA results for the other HWB sections can be found in Appendix C.

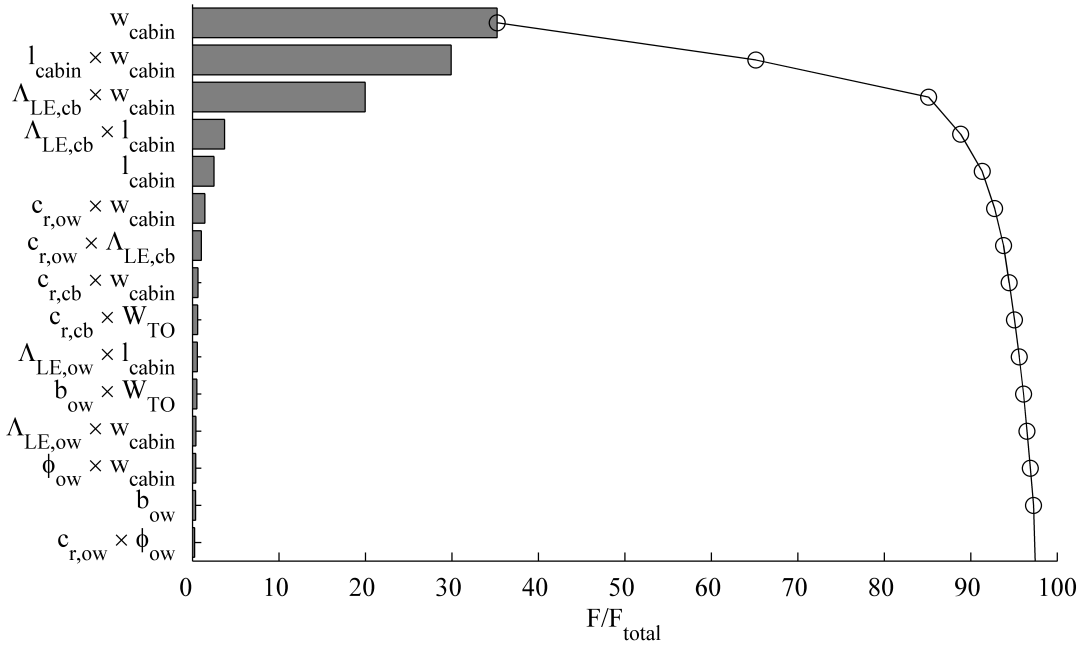

Figure 38: ANOVA results for the centerbody weight while varying both outboard wing and centerbody parameters ($F_{total} = 716$).

5.3 Development of HWB Structural Weight Surrogate Models

The goal of this research effort was in part to provide an improved HWB structural weight prediction methodology that could be employed during the conceptual design phase. The M&S environment formulated in this work satisfies the first portion of that goal, but considering its computational cost, it may not be well-suited for direct implementation into an iterative aircraft sizing routine. Although the execution time of the environment may be small relative to a high-order aerodynamic analysis, an aircraft sizing routine may require many updated structural weight estimations per design point as the aircraft scales to meet the mission requirements. Enabling this feature will require that the weight estimation procedure be parametric in order to remain sensitive to the aircraft's geometry and any other critical aspects. Given the integrated and parametric capability of the M&S environment and the key design parameters identified by the previous study, it is hypothesized that analytical equations can be formed that accurately model the physics-based environment. These equations, or surrogate models, can augment traditional aircraft sizing routines and provide improved HWB structural weight estimations without the computational effort.

The general procedure for formulation of these surrogate models was to intelligently generate a set of data using Design of Experiment (DOE) techniques and the M&S environment. The required number of data points and type of DOE will depend upon the number key factors, the number of levels each factor will take, and the desired prediction accuracy of the surrogate model. Using the results presented in Section 5.2 the key factors that should be included in the surrogate models can be chosen. A variable range for each factor was chosen so that they spanned the variables bounds of the aircraft used in the HWB scaling study. The nine factors and their variable bounds are given in Table 17. Using the actual cabin dimensions as inputs would

immediately result in many failed cases in the corner of the design space. Instead, the number of passengers is used and the cabin sizing routine within FLOPS is used to generate the cabin dimensions. This allows a wide range of passenger classes to be examined without the chance of failed cases due to incompatible cabin dimensions. The width of the cabin bays has a significant impact on the centerbody structural weight as shown in the HWB scaling study. Although, if this parameter is used as an independent input, the FLOPS cabin sizing routine may override the value to obtain an integer value for the number of cabin bays. Instead, the number of cabin bays was used as an input to avoid this issue.

Table 17: Factors and variable bounds for the HWB structural weight surrogate models.

Variable	Minimum	Nominal	Maximum
n_{pax}	100	275	450
n_{bay}	3	4	5
W_{TO} (lbs)	100,000	400,000	700,000
ϕ_{ow}	0.0°	2.0°	4.0°
b_{ow} (ft)	46.5	61.5	76.5
$\Lambda_{LE,ow}$	25.0°	31.0°	37.0°
$c_{r,ow}$ (ft)	12.0	19.5	27.0
$c_{t,ow}$ (ft)	3.0	4.5	6.0
$\Lambda_{LE,cb}$	50.0°	55.0°	60.0°

The DOE consisted of a face-centered central composite design which consists of a center point, factorial points at the corners of the design space, and face points. The type of design allows estimates of the quadratic terms and two factor interactions if present in the data. Based on the results of the ANOVAs, two-factor interactions are significant in all the responses. The required number of test cases for this design is given by $2^n + 2n + 1$ where n is the number of factors and requires a total of 531 cases for the nine variables. A Latin Hypercube space filling design was used to fill the interior of the design space and increase the resolution of the model. An additional 219 Latin Hypercube points were added to the DOE now totaling 750

cases. In anticipation of the nonlinear design space, an additional 300 random cases were added to provide more points for a nonlinear statistical modeling approach. Of the 1,050 attempted cases, 899 were successful. Most of the failed cases occurred when the largest outboard wing was paired with the smallest cabin size. In this situation the span of the trapezoidal wing section was too small to place any ribs and the structural arrangement routine failed. That was the only corner that consistently failed and accounted for 88 of the 151 failed cases.

Even before the data fitting process began a number of problems were anticipated. First, it became apparent that as a result of the OML parameterization scheme, the root chord of the outboard wing had a significant impact on the shape and position of the outboard wing. Since the outboard wings are positioned relative to points on the root chord and the centerbody rear wall, as the root chord changes the spanwise position of the wings, and hence the span of the trapezoidal wing section, change. Although this method works well for the planform and structural definition, it is generally cause for concern when producing statistical models. Another concern was the result of the discrete optimization process used within HyperSizer. The structural optimization routine relies upon a full factorial combination of the panel variables at each level to generate a pool of candidate designs. As the number of levels increases, the variable will become more like a continuous parameters but the number of candidate designs and computational effort will increase dramatically. Providing variable bounds and a useful number of factors to cover a wide range of possible HWB configurations can quickly result in tens of thousands of candidate designs that will be analyzed for every single component. As a result, the number of levels per variable was usually limited to between five and ten, which would already produce close to 10,000 candidate designs for certain structural concepts. This discrete combination of candidates produces some "jagged" trends in the design space. While the overall trend may be clearly observable, statistical models will have difficult capturing this

behavior. This may be beneficial since the jaggedness is artificial and the surrogate models will capture the underlying continuous behavior while smoothing out the data, although the adverse effect will be that the statistical models display poor fit statistics.

The surrogate modeling method of choice is an Artificial Neural Network (ANN) since the independent parameters include a discrete variable and they are better suited for this as opposed to a Response Surface Equation. ANNs relate the input variables to the set of response by a set of filters or hidden layers. At each hidden layer an optimal number of hidden nodes will exist that provide the best predictive capability. The responses of interest observed during the DOE was the structural weight of the centerbody, trapezoidal and outboard wings, rear centerbody, and the overall airframe weight as calculated by Equation 14. The resulting centerbody cabin area was also recorded so that surrogate models would be a function of this variable rather than the number of passengers. For response the number of hidden nodes for a single hidden layer was optimized using a MATLAB based ANN toolbox. The number of hidden nodes was determined by optimizing the surrogate model in terms of the Model Fit Error MFE, Model Representation Error MRE, actual by predicted and residual by predicted plots.

The fit statistics for the ANN predicting the centerbody structural weight is provided below in Figure 39. Desirable values for the MFE and MRE means are near zero and a standard deviation of less than one. The MFE meets these thresholds where the MRE is slightly outside the desirable limits. The actual by predicted plot shows the data for the most part evenly distributed and very close to the perfect line, except for a small number of outliers in the data set used for validation. The ANN fit statistics for the other response variables are provided in Appendix C. For all other responses the fit statistics were not as sufficient as desired. Standard deviations for a number of the responses, most notably the trapezoidal and outboard

wings, were well above one and there was also a noticeable amount of clumping in the actual by predicted and residual by predicted plots. The fits for the rear centerbody and total airframe structural weight provided better results, although still above a desirable limit. As mentioned earlier, these types of results were predicted given the significance of the outboard wing root chord, which would cause the clumping, and the discrete nature of the HyperSizer optimization process leading to higher MFE and MRE values. This does not necessarily invalidate the models usefulness. If the underlying physical trends and relationships between design parameters are being adequately captured by the surrogate models, they could still be for initial design space exploration and first-order structural weight estimates. Fortunately, the centerbody structural weight response was best fit with an ANN which was the most desirable result when this research effort was initiated.

The ANNs can be gathered to form a prediction profiler where the dependent responses of interest are plotted on the vertical axis and the independent modeled variables are along the horizontal axis. As can be seen in Figure 40, the prediction profiler shows the partial derivatives of the modeled variable around the current point indicted by red crosshairs. This type of plot is usually interactive and provides a means for rapid trade studies but even in static form it contains a wealth of information. The sensitivity of each response with respect to each design parameters can be immediately observed in addition to the overall relationship.

The centerbody structural weight is predominately driven by the overall cabin area which was also shown by the ANOVA study. Although shown to be statistically significant by the ANOVA analysis, the outboard wing parameters appear to have little impact compared to the cabin area with the outboard wing sweep providing the largest sensitivity. The aircraft takeoff gross weight has a significant impact on all sections except the centerbody since it is predominately sized by the static $2P$ load case which is independent of the aerodynamic loads. The small sensitivity between

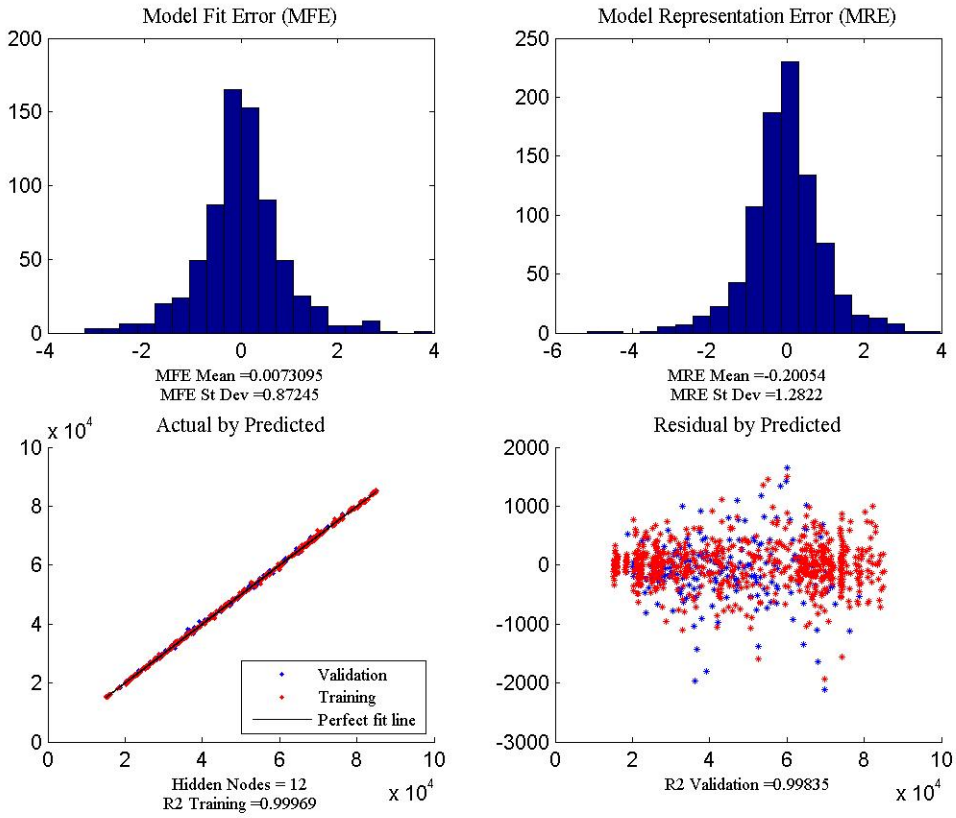

Figure 39: Summary of fit statistics for the centerbody structural weight ANN.

the centerbody structural and aircraft gross weight is due to sections shown in Figure 31 that are sized by the wind bending loads, which are a function of the aircraft weight and load factor.

The total airframe weight $W_{airframe}$ provided the next best statistical fit and here the prediction profiler shows that the cabin area and takeoff gross weight are again critical parameters. Although for this response, the outboard wing parameters of wing twist ϕ_{ow}, leading edge sweep $\Lambda_{LE,ow}$, and root chord $c_{r,ow}$ are equally significant. Notice the impact the outboard wing root chord $c_{r,ow}$ has on the various responses. In this case, as the chord length increases, the structural weights tend to decrease, in the outboard and trapezoidal wings in particular. This is most likely due to the fact that as the root chord increases the thickness of the wing also increases given a constant

thickness-to-chord ratio. Increased wing thicknesses are usually advantageous from a structural perspective and the sizing routine appears to be capturing this scenario. The surrogate models have been implemented as MATLAB functions and are given in Appendix D.

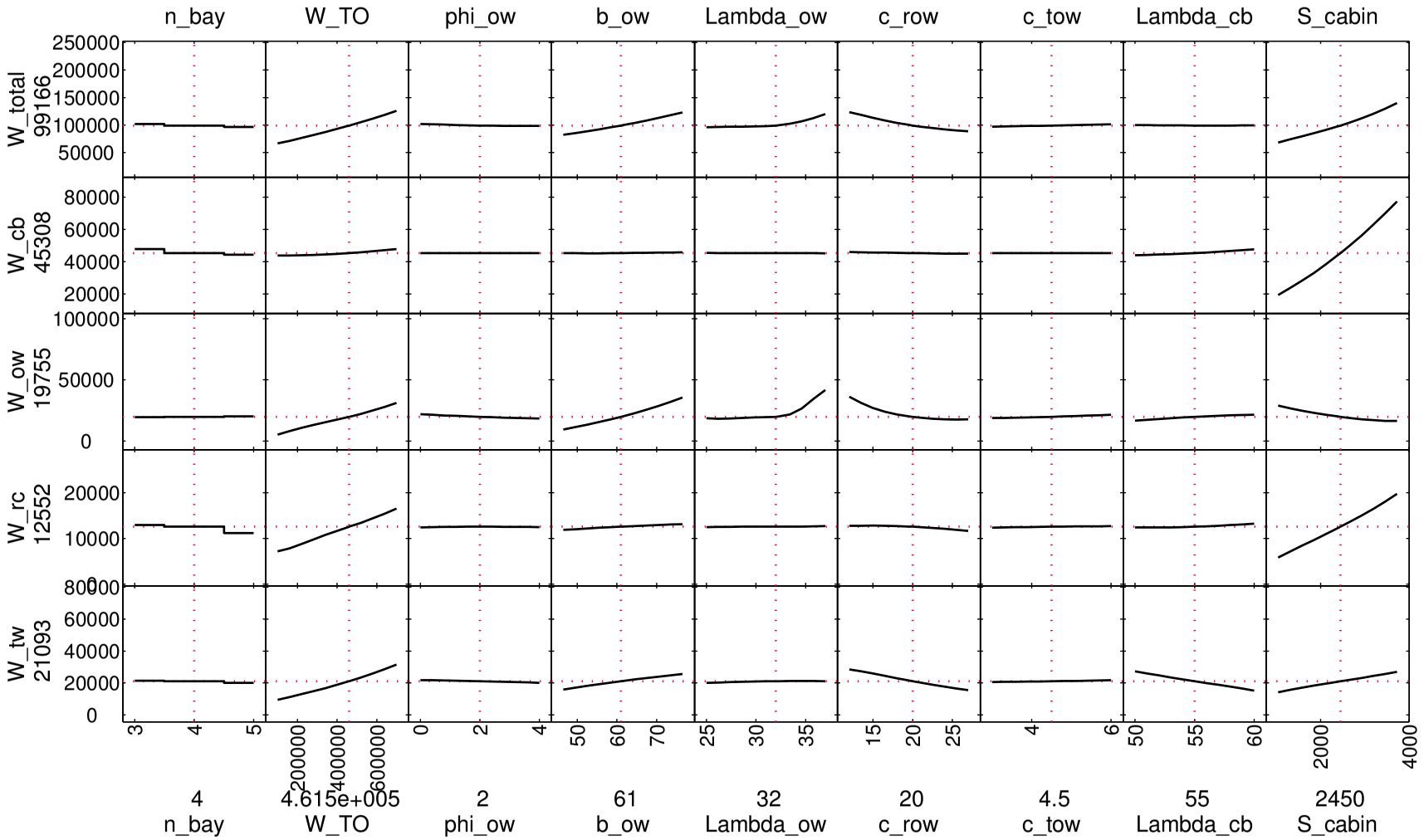

Figure 40: Prediction profiler generated from the Artificial Neural Networks showing the relationships between the structural weight and the design parameters.

CHAPTER VI

CONCLUSIONS

In the final chapter of this thesis, the research objectives presented in Chapter 1 are reviewed and discussed. The overall approach to the various objectives is reviewed as well as any key findings and lessons learned. The next section concludes the thesis with a series of recommendations for future work. The recommendations may propose revisiting certain parts of the research effort and suggesting alternatives methods to improve the results or gain further insight to the problem at hand. Also included is a discussion regarding the applicability of the M&S environment formulated as part of this thesis to other aircraft concepts.

6.1 Summary of Research

The work presented in this thesis originated when engineers at NASA LaRC offered a graduate student fellowship for work in the area of HWB structural weight estimation. The HWB concept was receiving a significant amount of attention given its potential performance advantages but the uncertainty surrounding the centerbody structural weight estimations was a major cause for concern. At the time, it was thought that the centerbody weight estimation methodology within FLOPS did not adequately model the different aspects of the HWB centerbody and another independent approach to the problem was needed.

The first objective of this thesis was to develop a parametric and physics-based modeling and simulation environment for HWB structural weight estimation. A review of the literature revealed that main challenges associated with this task, beyond the lack of historical data, are adequately modeling the geometry and the physics of the HWB centerbody section. The three-axis loading conditions present in the

centerbody are a unique feature of the HWB and result from a combination of wing bending loads and internal cabin pressure. With these challenges and critical aspects in mind, Chapter 3 formulated a M&S environment utilizing a set of analysis tools appropriate for HWB concepts. This included parametric geometry which provided a common model for potential flow aerodynamic tools and high-order finite element analysis. The end result of this objective provided a new HWB structural weight estimation tool that is sensitive to more design parameters and can be used during the conceptual design phase.

The procedure and analysis tools contained in the HWB M&S environment were then applied to a number of historical wings to validate the model. The load-carrying wing structure of four aluminum subsonic transports was modeled and the predicted structural weights were compared to the actual data. The predicted values for the load-carrying structural weight agreed well with the historical data using the 0σ statistical loading method. This was an encouraging result considering the limited knowledge regarding the structural details of the actual design and the few number of load cases. If reasonable values were chosen for such parameters as rib spacing and spar location, the structural weight was primarily dependent upon the overall size, shape, and weight of the aircraft. During this study a linear relationship was found relating the load-carrying to the total structural wing weight. The resulting calibration factor not only served as a starting point for the baseline HWB model, it substantiated the approach of modeling only the HWB load-carrying structure and assuming it would capture the trends in the design space.

A baseline HWB configuration was defined used as a calibration point for the M&S environment. The calibration factor derived from the conventional wing study was first applied but yielded results approximately eighteen percent below the expected value. This result was not unanticipated since the applicability of a calibration factor derived from metallic wings and then applied to an unconventional configuration

using advanced materials was always uncertain. Although, refining the theoretical composite material properties used for the calibration study to perhaps reflect the uncertainty surrounding their performance would be an easy implementation from a programming standpoint and would reduce the required calibration factors in Equation 14.

With the M&S calibration the next two research objectives could be accomplished. First, results from an independent HWB structural weight estimation study were obtained and used for a comparative analysis. The results showed good agreement in both the magnitude of the numbers and the relationship to the overall vehicle size. This is a very encouraging result given that these studies were performed independently, used different analysis tools, and used a different HWB baseline calibration point. This study also revealed that there appears to be a constant cabin bay width of between eight and nine feet that provides a minimum weight solution for HWB centerbody section as the vehicle scales among different passenger classes.

One early question that arose when this research effort was initiated was "How much do the outboard wings really matter to the centerbody?" To answer this question, statistical modeling techniques were first used to identify the critical design parameters of the outboard wing with respect to the centerbody structural weight. A first ANOVA study was performed which examined only outboard wing parameters and a smaller number of critical parameters, including the outboard wingspan b_{ow}, leading edge sweep $\Lambda_{LE,ow}$, wing twist ϕ_{ow}, root chord $c_{r,ow}$, and finally tip chord $c_{t,ow}$ were chosen for further consideration. Another ANOVA study was performed that used these outboard wing parameters in addition to parameters defining the centerbody cabin size. Results showed the outboard wing parameters were not nearly as critical as the centerbody size but technically statistically significant. Also revealed during study was the two-factor interactions significantly contribute to the variability of the centerbody structural weight and needed to be adequately accounted for during

the surrogate modeling process.

The last objective of this thesis was to enable the features of the new HWB structural weight estimation M&S environment to be utilized during the conceptual design phase and existing aircraft sizing routines. This objective was accomplished by the use of surrogate modeling where the response parameters were the structural weight of the various HWB sections. The fit of the ANN were less than desired, but were sufficient enough to predict the centerbody structural weight and observe trends in the design space by the use of a prediction profiler. The observed trends of the centerbody weight with respect to the outboard wing parameters supported the earlier observation that the outboard wings had little effect on the centerbody structural weight, at least when compared to the cabin area.

6.2 Recommendations for Future Work

A number of immediate improvements could be made to the M&S environment such as refinement of the material properties or adding load cases. The clumping observed during the surrogate model fitting process is most likely due to the root chord of the outboard wing driving most of the structural response given its significance to the planform parameterization process. A variable transformation might account for this behavior in the surrogate models and improve the fit statistics and predictive capability.

The overall approach and the analysis tools utilized for this HWB environment could be extended to other aircraft configurations. The overall method formulation in Chapter 3 is general in the sense that the HWB geometry and structural model just need to be replaced, the physics of the analysis remain unchanged.

Due to the number of design parameters provided by the environment and the high-order analysis tools, the environment is sensitive to many degrees-of-freedom.

This feature could make the environment an excellent test platform for the development of uncertainty quantification methods related to the structural sizing process. Rather than producing a single determinant structural weight prediction, statistical distributions could be placed on the uncertain parameters such as the material properties or the tolerance of the structural dimensions. This would result in a statistical distribution of structural weight and provide a traceable and quantifiable approach to structural weight estimation of unconventional aircraft configurations.

APPENDIX A

MATERIAL PROPERTIES

A.1 Isotropic Materials

Table 18: Material properties for conventional wing study.

Material	Aluminum 7075	Aluminum 2024
$\boldsymbol{E_t}$ **(Msi)**	10.4	10.5
$\boldsymbol{E_c}$ **(Msi)**	10.5	10.7
$\boldsymbol{G}$ **(Msi)**	4.0	4.0
$\boldsymbol{\nu_t}$	0.300	0.313
$\boldsymbol{\nu_c}$	0.313	0.338
$\boldsymbol{\sigma_{tu}}$ **(ksi)**	78.0	64.0
$\boldsymbol{\sigma_{ty}}$ **(ksi)**	70.0	47.0
$\boldsymbol{\sigma_{cy}}$ **(ksi)**	70.0	39.0
$\boldsymbol{\sigma_{su}}$ **(ksi)**	42.0	39.0
$\boldsymbol{\rho}$ $(\frac{\boldsymbol{lbs}}{\boldsymbol{in^3}})$	0.101	0.101

A.2 Composite Materials

Table 19: Lamina stiffness properties.

Material	AS4/3502 Tape
$\boldsymbol{E_{t1}}$ **(Msi)**	19.3
$\boldsymbol{E_{t2}}$ **(Msi)**	1.35
$\boldsymbol{E_{c1}}$ **(Msi)**	18.0
$\boldsymbol{E_{c2}}$ **(Msi)**	1.41
$\boldsymbol{\nu_{t12}}$	0.34
$\boldsymbol{\nu_{c12}}$	0.34
$\boldsymbol{G_{12}}$ **(Msi)**	0.543
$\boldsymbol{G_{13}}$ **(Msi)**	0.543
$\boldsymbol{G_{23}}$ **(Msi)**	0.543
$\boldsymbol{\rho}$ $(\frac{\boldsymbol{lbs}}{\boldsymbol{in^3}})$	0.057

Table 20: Lamina strength allowables.

Material	AS4/3502 Tape
$\boldsymbol{\sigma_{tu1}}$ **(ksi)**	205
$\boldsymbol{\sigma_{tu2}}$ **(ksi)**	6.28
$\boldsymbol{\sigma_{cu1}}$ **(ksi)**	171
$\boldsymbol{\sigma_{cu2}}$ **(ksi)**	26.2
$\boldsymbol{\sigma_{su12}}$ **(ksi)**	13.4
$\boldsymbol{\sigma_{su13}}$ **(ksi)**	8.25
$\boldsymbol{\sigma_{su23}}$ **(ksi)**	4.51
$\boldsymbol{\sigma_{su3}}$ **(ksi)**	4.85

Table 21: Lamina strain allowables.

Material	AS4/3502 Tape
$\boldsymbol{\varepsilon_{tu1}}$ **(μin/in)**	13,250
$\boldsymbol{\varepsilon_{tu2}}$ **(μin/in)**	16,000
$\boldsymbol{\varepsilon_{cu1}}$ **(μin/in)**	10,725
$\boldsymbol{\varepsilon_{cu2}}$ **((μin/in)**	16,000
$\boldsymbol{\varepsilon_{su12}}$ **(μin/in)**	27,000

Table 22: Material properties of effective laminates.

Name	EL 1	EL 2	Shear EL
Ply percentages (0/±45/90)	(45/43/12)	(62/30/8)	(32/60/8)
$\boldsymbol{E_{t1}}$ **(Msi)**	10.5	13.2	8.10
$\boldsymbol{E_{t2}}$ **(Msi)**	5.02	3.99	4.65
$\boldsymbol{E_{c1}}$ **(Msi)**	9.82	12.4	7.62
$\boldsymbol{E_{c2}}$ **(Msi)**	4.78	3.84	4.43
$\boldsymbol{\nu_{t12}}$	0.43	0.42	0.55
$\boldsymbol{\nu_{c12}}$	0.43	0.42	0.55
$\boldsymbol{G_{12}}$ **(Msi)**	2.54	1.86	3.20
$\boldsymbol{G_{13}}$ **(Msi)**	0.547	0.543	0.545
$\boldsymbol{G_{23}}$ **(Msi)**	0.547	0.543	0.544
$\boldsymbol{\rho}$ **(**$\frac{lbs}{in^3}$**)**	0.057	0.057	0.057

APPENDIX B

CONVENTIONAL AIRCRAFT INFORMATION

Table 23: Skin stiffener type, rib spacing, and spar locations used for conventional wing study. Spar locations are given as a fraction of the chord length and are the values used at the root of the wing[27].

Aircraft	**Skin stiffener**	**Rib spacing (in)**	**Front spar**	**Middle spar**	**Rear spar**
Boeing 737	z	31	0.10	N/A	0.63
Boeing 727	z	28	0.17	N/A	0.61
DC-8	z	32	0.13	0.39	0.58
L-1011	z	21	0.10	N/A	0.60

Table 24: Aircraft takeoff weights, materials, and fuel weights used for conventional wing study[3]. Aluminum 7075 was used for all ribs and spars.

Aircraft	$\boldsymbol{W_{TO}}$ **(lbs)**	**Fuel weight (lbs)**	**Upper skin material**	**Lower skin material**
Boeing 737	100,800	16,043	Aluminum 7075	Aluminum 2024
Boeing 727	160,000	23,120	Aluminum 7075	Aluminum 2024
DC-8	335,000	80,249	Aluminum 7075	Aluminum 7075
L-1011	409,000	119,688	Aluminum 7075	Aluminum 7075

Table 25: Engine weight and locations used for conventional wing study[3]. Engine locations are given as a fraction of the wing semispan.

Aircraft	**Weight per engine (lbs)**	**Engine 1 location**	**Engine 2 location**
Boeing 737	4,083	0.34	N/A
Boeing 727	N/A	N/A	N/A
DC-8	6,765	0.35	0.60
L-1011	9,195	0.41	N/A

APPENDIX C

ADDITIONAL RESULTS AND SURROGATE MODEL FIT STATISTICS

C.1 Additional ANOVA Results

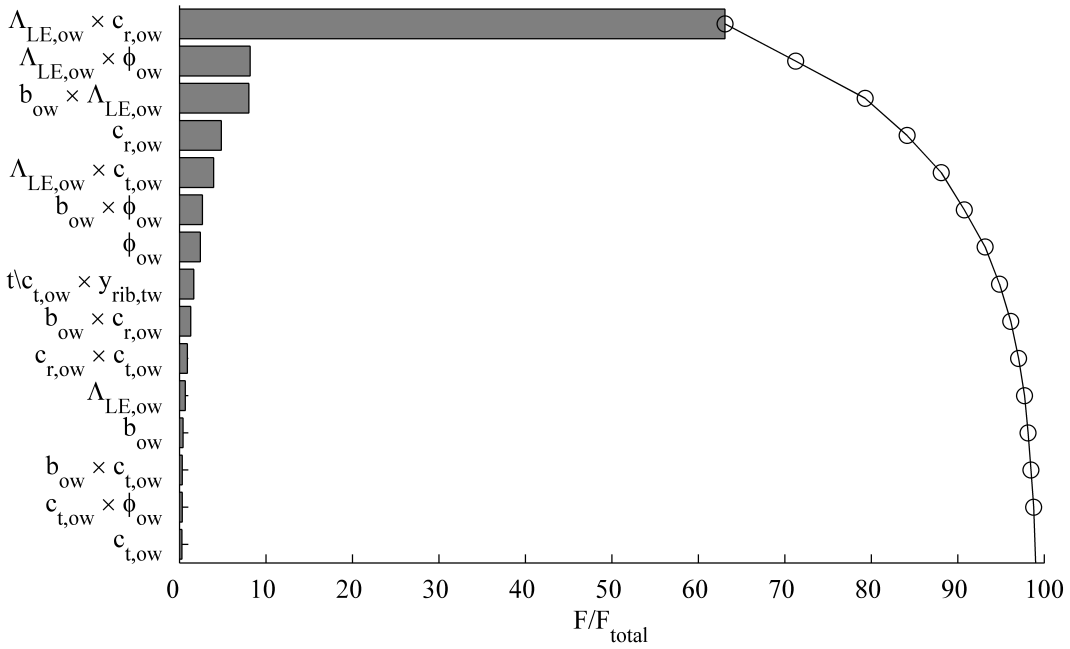

Figure 41: ANOVA results for the outboard wing weight while only varying outboard wing parameters ($F_{total} = 807$).

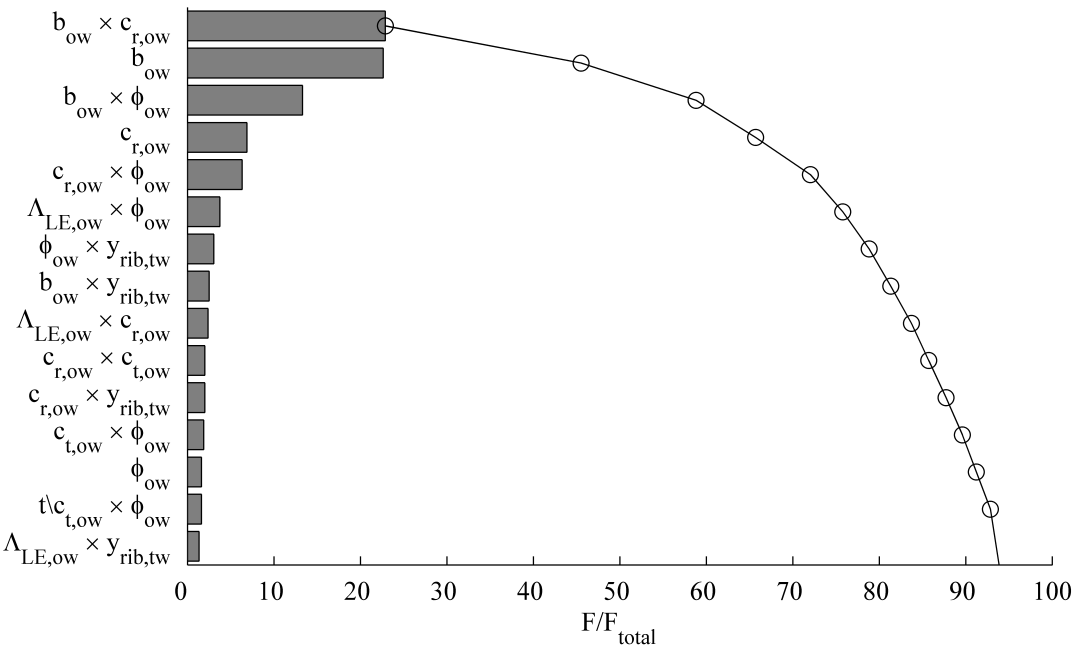

Figure 42: ANOVA results for the trapezoidal wing weight while only varying outboard wing parameters ($F_{total} = 784$).

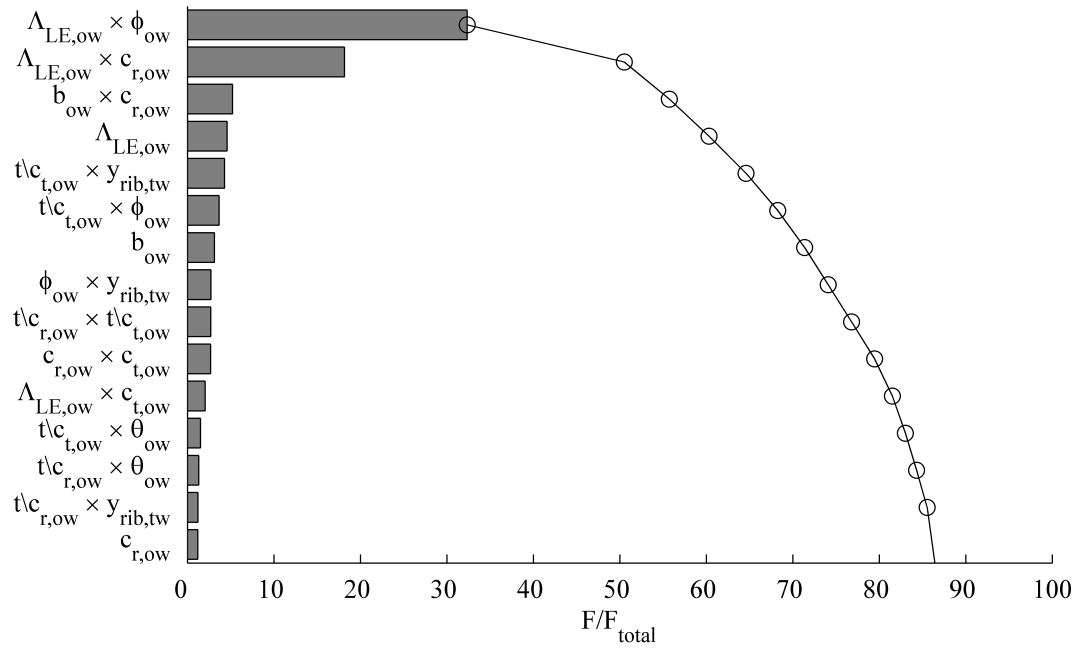

Figure 43: ANOVA results for rear centerbody weight while only varying outboard wing parameters ($F_{total} = 145$).

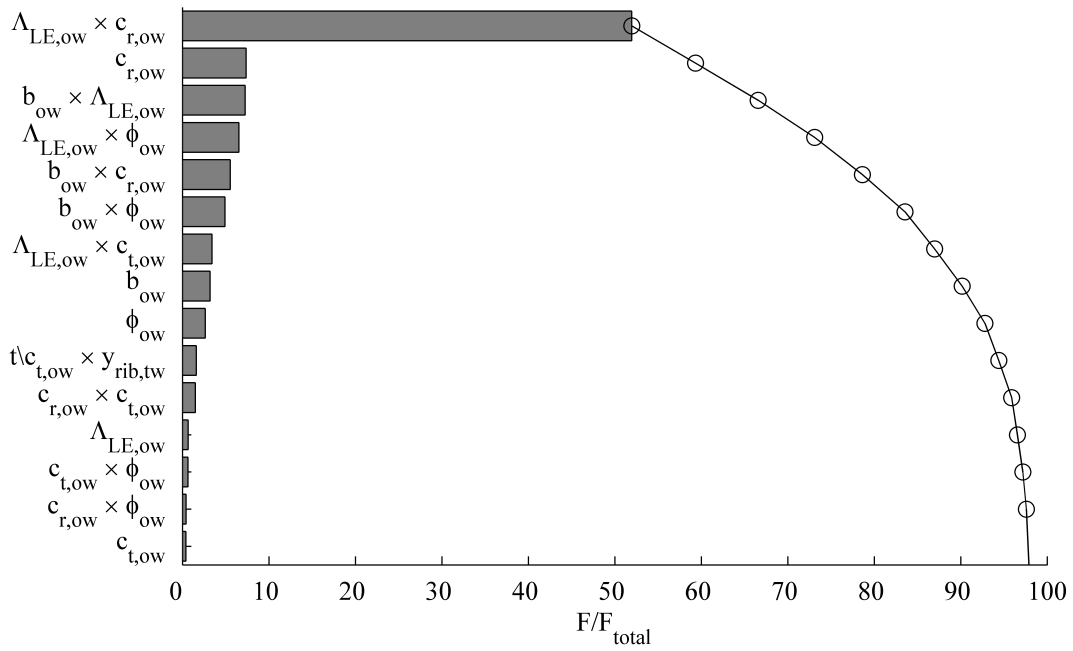

Figure 44: ANOVA results for total structural weight while only varying outboard wing parameters ($F_{total} = 782$).

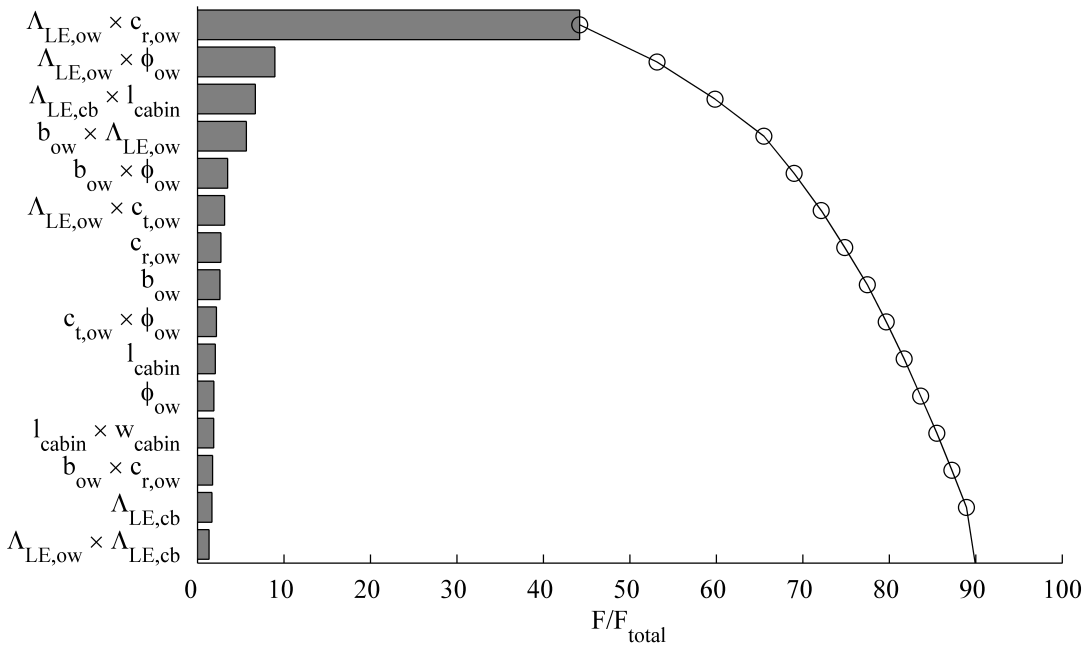

Figure 45: ANOVA results for the total structural weight while varying both outboard wing and centerbody parameters ($F_{total} = 716$).

C.2 Surrogate Model Fit Statistics

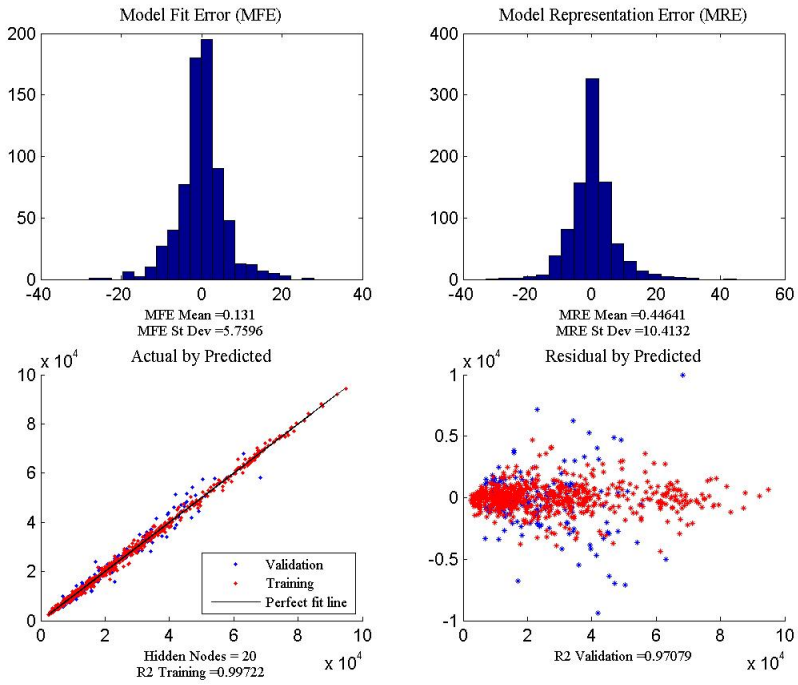

Figure 46: Summary of fit statistics for the outboard wing structural weight ANN.

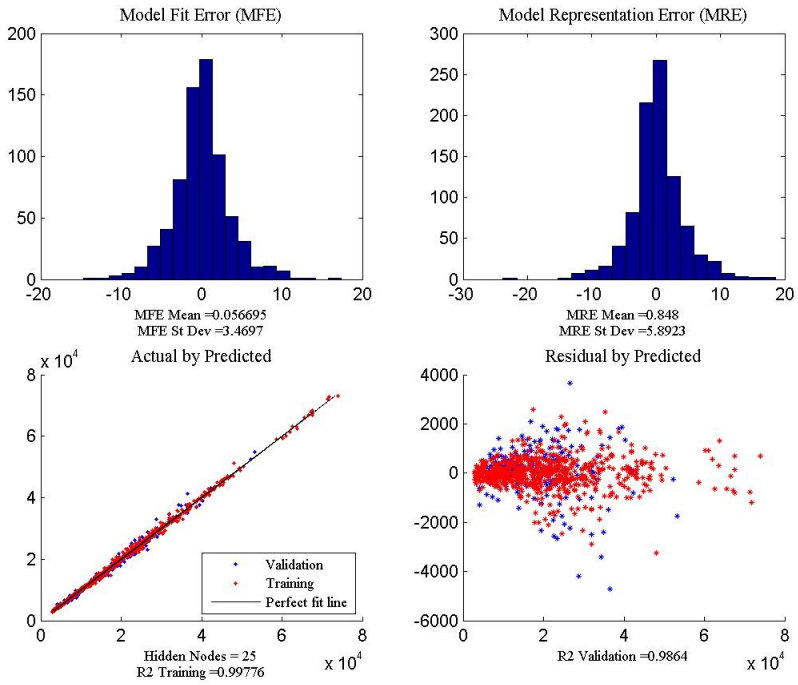

Figure 47: Summary of fit statistics for the trapezoidal wing structural weight ANN.

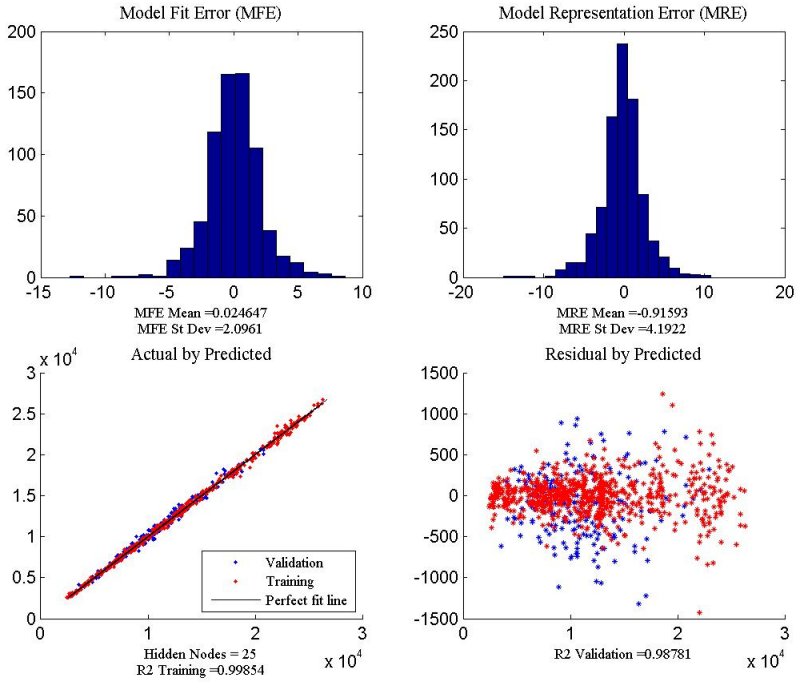

Figure 48: Summary of fit statistics for the rear centerbody structural weight ANN.

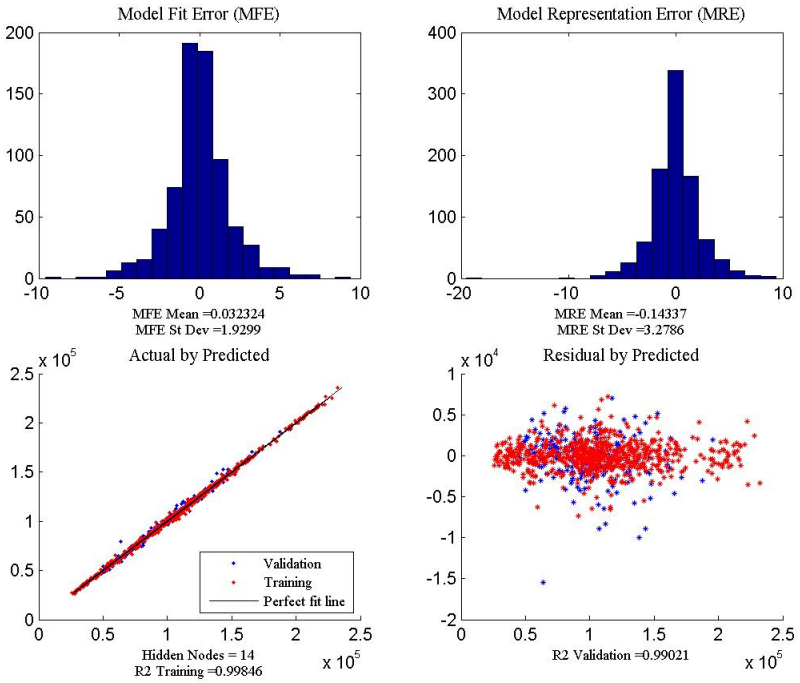

Figure 49: Summary of fit statistics for the total airframe structural weight ANN.

APPENDIX D

MATLAB IMPLEMENTATION OF HWB STRUCTURAL WEIGHT SURROGATE MODELS

The following sections contain MATLAB functions that implement the Artificial Neural Networks developed in Section 5.3. Each function returns the predicted structural weight as a function of the nine design variables contained in the columns of the $n \times m$ matrix *inputs*. Each row contains a unique setting of the design variables and the response matrix will be $n \times 1$. The columns reserved for each design variable in the matrix *inputs* can be seen in Table 26.

Table 26: Matrix structure and variable description for MATLAB implemented surrogate models.

Column	Symbol	MATLAB Variable	Description
1	n_{bay}	nbay	Number of centerbody cabin bays
2	W_{TO}	WTO	Aircraft takeoff gross weight
3	ϕ_{ow}	phiOW	Twist angle at tip of outboard wing
4	b_{ow}	bOW	Span of the outboard wing section
5	$\Lambda_{LE,ow}$	LambdaOW	Sweep angle of outboard wing leading edge
6	$c_{r,ow}$	crOW	Chord length at root of outboard wing section
7	$c_{t,ow}$	ctOW	Chord length at tip of outboard wing section
8	$\Lambda_{LE,cb}$	LambdaCB	Sweep angle of centerbody leading edge
9	S_{cabin}	Scabin	Area of the passenger cabin

D.1 Centerbody Structural Weight

```
function WcbANN=WcbANNFUN(inputs)
%expand input array out to its component vectors:
LambdaCB=inputs(:,8);
LambdaOW=inputs(:,5);
Scabin=inputs(:,9);
WTO=inputs(:,2);
bOW=inputs(:,4);
crOW=inputs(:,6);
ctOW=inputs(:,7);
nbay=inputs(:,1);
phiOW=inputs(:,3);

nruns=size(inputs,1);
%evaluate function:
logsig=@(n) 1./(1 + exp(-n));
WcbANN=10610.1750594986390-51210.7515808091780.*1./(1+exp(-1.*...
(1.9572085089592+0.9627018216035.*nbay-0.0000019628500.*WTO+...
0.0236907299990.*phiOW+0.0507062172733.*bOW+0.0177111080996.*...
LambdaOW-0.0769456921275.*crOW-0.0205823395961.*ctOW-...
0.1091715414532.*LambdaCB+0.0001814327445.*Scabin)))+...
118963.6052651059600.*1./(1+exp(-1.*(0.1914985844791-...
0.5750625505560.*nbay+0.0000007960762.*WTO-0.0074100135558.*phiOW-...
0.0170451877669.*bOW+0.0018183670343.*LambdaOW+0.0345286576087.*...
crOW+0.0140543835305.*ctOW+0.0482392623709.*LambdaCB+...
0.0001792570717.*Scabin)))+58253.5123953756990.*1./(1+exp(-1.*...
(0.1680509921795+0.1624533405524.*nbay+0.0000027267241.*WTO+...
0.0149497753253.*phiOW-0.0244121529207.*bOW+0.0238744245747.*...
LambdaOW+0.0207467592270.*crOW-0.0077446695203.*ctOW-...
0.0281605636409.*LambdaCB-0.0003252400602.*Scabin)))+...
80345.5060437966600.*1./(1+exp(-1.*(3.9698501164985-0.0242665636380.*...
```

```
nbay-0.0000011424600.*WTO+0.0089562501912.*phiOW-0.0127523182787.*...
bOW+0.0198966103720.*LambdaOW+0.0168819868781.*crOW-...
0.0119819179984.*ctOW-0.0796126883855.*LambdaCB+0.0000655931486.*...
Scabin)))-95094.9923290675210.*1./(1+exp(-1.*(0.2123274513577-...
0.4113776724882.*nbay+0.0000016673651.*WTO-0.0096667971981.*phiOW+...
0.0168083341960.*bOW+0.0012039246787.*LambdaOW+0.0380739556819.*...
crOW+0.0090275405833.*ctOW+0.0132936964938.*LambdaCB-...
0.0001369900725.*Scabin)))-61643.7876788545400.*1./(1+exp(-1.*...
(-2.4448703347424-0.8309549506950.*nbay+0.0000025919544.*WTO-...
0.0223269185707.*phiOW-0.0233764311622.*bOW-0.0177607788740.*...
LambdaOW+0.0609841228454.*crOW+0.0148863907932.*ctOW+...
0.0857255290327.*LambdaCB-0.0001780516182.*Scabin)))-...
100690.5728505053600.*1./(1+exp(-1.*(3.6518562708066+...
0.7106173976485.*nbay-0.0000006944852.*WTO-0.0007263020254.*phiOW+...
0.0146359478629.*bOW-0.0004897393890.*LambdaOW-0.0117756874131.*...
crOW-0.0060900890260.*ctOW-0.0464631982469.*LambdaCB-...
0.0008595493345.*Scabin)))+104129.2035760976600.*1./(1+exp(-1.*...
(-3.1454703252983+0.3728265224798.*nbay-0.0000004281343.*WTO+...
0.0003090467126.*phiOW-0.0035978610418.*bOW-0.0049024110969.*...
LambdaOW+0.0085309323732.*crOW+0.0019567474447.*ctOW+...
0.0143434419537.*LambdaCB+0.0005821056657.*Scabin)))+...
132239.5530183911000.*1./(1+exp(-1.*(-0.4062328942866-...
0.0299301224449.*nbay-0.0000009596107.*WTO-0.0086118443203.*phiOW+...
0.0189324373457.*bOW-0.0228522329228.*LambdaOW-0.0293599541588.*...
crOW+0.0073090956602.*ctOW+0.0289947611021.*LambdaCB+...
0.0000223433263.*Scabin)))-135325.5924020594400.*1./(1+exp(-1.*...
(0.5943020990762+0.0493785534291.*nbay-0.0000006928705.*WTO+...
0.0033815026871.*phiOW-0.0287383989932.*bOW-0.0105706755692.*...
LambdaOW-0.0101767449277.*crOW+0.0025161283447.*ctOW+...
0.0177739575500.*LambdaCB+0.0000439883360.*Scabin)))+...
105021.1100525670500.*1./(1+exp(-1.*(-1.1501918097378+...
0.4334896663852.*nbay+0.0000025604858.*WTO+0.0002386748418.*phiOW+...
```

```
0.0010954977755.*bOW-0.0208248810060.*LambdaOW-0.0440980820990.*...
crOW-0.0080665343176.*ctOW+0.0107203236003.*LambdaCB-...
0.0003845088561.*Scabin)))-46556.3959771144070.*1./(1+exp(-1.*...
(-2.1474455860769+0.8790762807865.*nbay+0.0000036224607.*WTO+...
0.0023867853769.*phiOW-0.0066743003411.*bOW-0.0238964454392.*...
LambdaOW-0.0536588043707.*crOW-0.0111320873036.*ctOW+...
0.0058020843173.*LambdaCB-0.0005102566121.*Scabin)));
```

D.2 Outboard Wing Structural Weight

```
function WowANN=WowANNFUN(inputs)
%expand input array out to its component vectors:
LambdaCB=inputs(:,8);
LambdaOW=inputs(:,5);
Scabin=inputs(:,9);
WTO=inputs(:,2);
bOW=inputs(:,4);
crOW=inputs(:,6);
ctOW=inputs(:,7);
nbay=inputs(:,1);
phiOW=inputs(:,3);

nruns=size(inputs,1);
%evaluate function:
logsig=@(n) 1./(1 + exp(-n));
WowANN=39673.3183607141620-164620.5866324089300.*1./(1+exp(-1.*(...
2.2123429711298+0.1072996734792.*nbay-0.0000011258212.*WTO+...
0.0662614528794.*phiOW+0.0127310489611.*bOW-0.0126948900357.*LambdaOW...
-0.1116597249481.*crOW+0.0603116629708.*ctOW+0.0222614309131.*...
LambdaCB-0.0004501067575.*Scabin)))+139162.6758716515300.*1./(1+exp...
(-1.*(2.3497329403932-0.0922161291318.*nbay+0.0000005812952.*WTO-...
0.0384758649043.*phiOW-0.0364709684961.*bOW+0.1544608436916.*LambdaOW...
-0.2215586470379.*crOW-0.1823624041604.*ctOW-0.0396869575133.*...
```

```
LambdaCB+0.0005598744970.*Scabin)))+80752.4909626994340.*1./(1+exp...
(-1.*(-0.7346397614329+0.0572832361645.*nbay+0.0000044435568.*WTO-...
0.0515209129330.*phiOW+0.0459557297859.*bOW-0.1565240784734.*LambdaOW...
-0.0992857034528.*crOW-0.0464348543663.*ctOW+0.0424308217588.*...
LambdaCB-0.0004709924876.*Scabin)))+282078.2646123530600.*1./(1+exp...
(-1.*(13.3587882912133+0.0079216614247.*nbay-0.0000016342591.*WTO-...
0.0061222047506.*phiOW-0.0307445415142.*bOW-0.3779755833413.*LambdaOW...
+0.1315807830302.*crOW-0.0800481017428.*ctOW-0.0015937883725.*...
LambdaCB+0.0001286951891.*Scabin)))-77820.9510737284000.*1./(1+exp...
(-1.*(2.7321146249467-0.0261191465011.*nbay+0.0000036302041.*WTO-...
0.0849318116248.*phiOW-0.0273682904777.*bOW-0.0573851753776.*LambdaOW...
+0.0536379816237.*crOW+0.5081645890749.*ctOW-0.0133254218963.*...
LambdaCB+0.0001607010583.*Scabin)))+162790.8544727840100.*1./(1+exp...
(-1.*(-0.4530265493642+0.0143882027590.*nbay-0.0000012735493.*WTO-...
0.0083204717278.*phiOW-0.0122542787595.*bOW+0.0115998226676.*LambdaOW...
-0.0112784470862.*crOW+0.0053717778201.*ctOW+0.0072937728733.*...
LambdaCB+0.0003278394761.*Scabin)))+257692.6493896893200.*1./(1+exp...
(-1.*(0.9085692859449+0.0712276356170.*nbay-0.0000006949242.*WTO+...
0.0121004047274.*phiOW+0.0201154067984.*bOW-0.2431820978547.*LambdaOW...
+0.2346549770777.*crOW+0.1391115807468.*ctOW+0.0409429197291.*...
LambdaCB-0.0004946167834.*Scabin)))+152568.9012228282800.*1./(1+exp...
(-1.*(3.6647994841283+0.0447553919042.*nbay+0.0000022078758.*WTO+...
0.0564311342128.*phiOW+0.0262899090684.*bOW-0.0993129985787.*LambdaOW...
-0.0643313540184.*crOW-0.0037149346986.*ctOW+0.0007723806290.*...
LambdaCB-0.0002137336990.*Scabin)))+122131.8226199238300.*1./(1+exp...
(-1.*(3.2772608380049-0.0083196145956.*nbay-0.0000030692470.*WTO+...
0.0739232906036.*phiOW+0.0228463369739.*bOW-0.1323876607055.*LambdaOW...
+0.1553978655063.*crOW+0.0287389363970.*ctOW-0.0224322086586.*...
LambdaCB+0.0001105522861.*Scabin)))+74381.7585849429600.*1./(1+exp...
(-1.*(3.8960502943074-0.1000027824023.*nbay-0.0000010948935.*WTO+...
0.3333065284896.*phiOW-0.0170903799602.*bOW-0.0263301471953.*LambdaOW...
+0.0092998308779.*crOW-0.0414738628931.*ctOW-0.0434546666513.*...
```

```
LambdaCB+0.0008838534857.*Scabin)))-55502.1534958320480.*1./(1+exp...
(-1.*(8.2702731527522+0.0555772595836.*nbay-0.0000031118823.*WTO-...
0.0530162559769.*phiOW+0.0326345093058.*bOW-0.0204616234640.*LambdaOW...
-0.0322669746786.*crOW-0.0088147559139.*ctOW-0.1434145654717.*...
LambdaCB-0.0003127172089.*Scabin)))+137104.7293264903100.*1./(1+exp...
(-1.*(-20.1293297846172-0.0402421170445.*nbay+0.0000016588709.*WTO-...
0.0125505023787.*phiOW+0.0425730413506.*bOW+0.6335482630815.*LambdaOW...
-0.2552679695383.*crOW+0.0884371934684.*ctOW-0.0145455261312.*...
LambdaCB-0.0000278199482.*Scabin)))-48345.3454973395130.*1./(1+exp...
(-1.*(-2.3668882351784+0.1089904858444.*nbay+0.0000004119723.*WTO-...
0.2576186236117.*phiOW+0.0313273748663.*bOW+0.0563708232223.*LambdaOW...
-0.0182400028494.*crOW+0.0802477152874.*ctOW-0.0048340128042.*...
LambdaCB-0.0001270040837.*Scabin)))+111853.0852784791500.*1./(1+exp...
(-1.*(-7.3104725737831+0.0053601987873.*nbay-0.0000008550182.*WTO+...
0.2094617519089.*phiOW+0.0344091383906.*bOW+0.1476521584353.*LambdaOW...
-0.0313740333989.*crOW+0.0149027857815.*ctOW-0.0165130900813.*...
LambdaCB+0.0001871886676.*Scabin)))-170921.6331491442700.*1./(1+exp...
(-1.*(5.1522028086723+0.0420080331770.*nbay-0.0000011112727.*WTO-...
0.0119168617093.*phiOW+0.0049080734834.*bOW-0.3458597792251.*LambdaOW...
+0.2390987537505.*crOW+0.0748102215092.*ctOW+0.0337146125343.*...
LambdaCB-0.0003323385431.*Scabin)))+105854.3655019370800.*1./(1+exp...
(-1.*(4.7900618969763+0.0997607919500.*nbay-0.0000018359138.*WTO+...
0.0620819602577.*phiOW+0.0007040180997.*bOW-0.0694275583930.*LambdaOW...
-0.1005200792331.*crOW+0.1180651558416.*ctOW+0.0125117084802.*...
LambdaCB-0.0004059034134.*Scabin)))-218092.6409796448400.*1./(1+exp...
(-1.*(-3.9346962037548+0.0536430483109.*nbay-0.0000032341480.*WTO+...
0.1017754018419.*phiOW+0.0329576174481.*bOW+0.0675834295914.*LambdaOW...
-0.0728492400094.*crOW-0.1263877923177.*ctOW+0.0105911496201.*...
LambdaCB-0.0002323817097.*Scabin)))-403400.0151005411200.*1./(1+exp...
(-1.*(5.4595589060339-0.0053237534415.*nbay-0.0000006595048.*WTO+...
0.0743336433717.*phiOW-0.0066319766585.*bOW-0.1050446133699.*...
LambdaOW-0.0055320471328.*crOW-0.0290612307219.*ctOW-...
```

```
0.0148155931865.*LambdaCB+0.0002095891705.*Scabin)))-...
225056.4739020119600.*1./(1+exp(-1.*(-2.6277736527347-...
0.0523321840103.*nbay+0.0000016661656.*WTO+0.0702103153641.*phiOW-...
0.0155021742126.*bOW+0.0147874371400.*LambdaOW+0.0188123903167.*crOW-...
0.0003773788692.*ctOW+0.0372774484994.*LambdaCB+0.0003805490659.*...
Scabin)))-139749.5430645617600.*1./(1+exp(-1.*(9.5384235130584-...
0.0100439422811.*nbay-0.0000038195154.*WTO+0.0724110095962.*phiOW-...
0.0274239993453.*bOW-0.2290255764699.*LambdaOW+0.1713581661707.*crOW-...
0.0379393199759.*ctOW-0.0322008906368.*LambdaCB+0.0003307527959.*...
Scabin)));
```

D.3 Trapezoidal Wing Structural Weight

```
function WtwANN=WtwANNFUN(inputs)
%expand input array out to its component vectors:
LambdaCB=inputs(:,8);
LambdaOW=inputs(:,5);
Scabin=inputs(:,9);
WTO=inputs(:,2);
bOW=inputs(:,4);
crOW=inputs(:,6);
ctOW=inputs(:,7);
nbay=inputs(:,1);
phiOW=inputs(:,3);

nruns=size(inputs,1);
%evaluate function:
logsig=@(n) 1./(1 + exp(-n));
WtwANN=11982.3708550893730+68814.9367825134100.*1./(1+exp(-1.*...
(-2.2719259210291-0.2097682311501.*nbay+0.0000028083994.*WTO+...
0.0207280637023.*phiOW+0.0217006127877.*bOW-0.0064894615222.*LambdaOW...
-0.0001144456987.*crOW+0.0205467537272.*ctOW+0.0328620600928.*...
LambdaCB-0.0007672251816.*Scabin)))-51675.9695161101260.*1./(1+exp...
```

```
(-1.*(2.8383807680820-0.5111674966041.*nbay-0.0000017071323.*WTO-...
0.0028277688260.*phiOW-0.0151496089795.*bOW+0.0170015827137.*LambdaOW...
+0.0190663978909.*crOW+0.0775799806722.*ctOW-0.0036812883925.*...
LambdaCB+0.0001142872408.*Scabin)))-40003.3127907521920.*1./(1+exp...
(-1.*(0.6193701757034-0.2368523926141.*nbay+0.0000012915205.*WTO-...
0.2650332799114.*phiOW+0.0038619100471.*bOW+0.0096734645484.*LambdaOW...
-0.0676024368257.*crOW-0.3043580576694.*ctOW+0.0102465534383.*...
LambdaCB+0.0001450701485.*Scabin)))-31902.4447876915110.*1./(1+exp...
(-1.*(3.3481236828186-0.2198457783429.*nbay-0.0000007400861.*WTO-...
0.0417279387909.*phiOW+0.0166171975140.*bOW-0.0388437960599.*LambdaOW...
-0.0376687303778.*crOW-0.1612480046238.*ctOW-0.0239231202283.*...
LambdaCB+0.0001715450018.*Scabin)))+64293.4002101759620.*1./(1+exp...
(-1.*(-10.1562331636958+0.1380975854051.*nbay+0.0000032227412.*WTO-...
0.0115638104827.*phiOW+0.0108572082777.*bOW-0.0322335875517.*LambdaOW...
-0.0009284828697.*crOW-0.0312352907377.*ctOW+0.1935575220262.*...
LambdaCB-0.0001586496723.*Scabin)))-70193.5045776280310.*1./(1+exp...
(-1.*(-3.2762653931006+0.1325593429216.*nbay+0.0000009921360.*WTO+...
0.0061074266501.*phiOW+0.0286168720399.*bOW-0.0494047228738.*LambdaOW...
+0.0098569774288.*crOW-0.0424858642536.*ctOW+0.0571115813279.*...
LambdaCB-0.0001985870858.*Scabin)))+82687.8476567980400.*1./(1+exp...
(-1.*(7.6805061787411+0.0838885811388.*nbay-0.0000009695713.*WTO+...
0.0072075862345.*phiOW-0.0035875657995.*bOW-0.0783464965136.*LambdaOW...
+0.0631120020883.*crOW+0.0292777761723.*ctOW-0.1051476951575.*...
LambdaCB+0.0003100536300.*Scabin)))-62301.2140099819880.*1./(1+exp...
(-1.*(1.4054693296375+0.0445693920774.*nbay+0.0000001910225.*WTO+...
0.1296590971387.*phiOW-0.0163602989322.*bOW-0.0188717733284.*LambdaOW...
+0.0499835650922.*crOW-0.0158753466232.*ctOW-0.0242689158032.*...
LambdaCB+0.0002332812580.*Scabin)))-86969.7825800481080.*1./(1+exp...
(-1.*(1.4883740776072-0.1814282225609.*nbay+0.0000020187657.*WTO-...
0.0209750527823.*phiOW+0.0096144325534.*bOW+0.0188735374334.*LambdaOW...
-0.0309949811703.*crOW+0.1536265124427.*ctOW-0.0535155372445.*...
LambdaCB-0.0002585923593.*Scabin)))-51916.6987167047480.*1./(1+exp...
```

```
(-1.*(-3.7351869677818+0.0299633855430.*nbay+0.0000038166072.*WTO-...
0.0195654597032.*phiOW-0.0004091563590.*bOW-0.0410986261372.*LambdaOW...
-0.0725728575277.*crOW+0.0125781334039.*ctOW+0.1056205820600.*...
LambdaCB-0.0007422147821.*Scabin)))-75221.3198988192600.*1./(1+exp...
(-1.*(-2.3718223303540-0.0469099998018.*nbay-0.0000025430170.*WTO+...
0.0389005016023.*phiOW+0.0300441715989.*bOW+0.0132429360559.*LambdaOW...
+0.0655628274075.*crOW+0.0297913237335.*ctOW-0.0143720223966.*...
LambdaCB+0.0001521580838.*Scabin)))-50008.4750770771130.*1./(1+exp...
(-1.*(1.5826509015865+0.1388833053097.*nbay-0.0000014354661.*WTO-...
0.0384970275059.*phiOW+0.0402738738626.*bOW-0.0728473123044.*LambdaOW...
+0.0187683776473.*crOW-0.0242232014828.*ctOW-0.0296630522932.*...
LambdaCB+0.0001653110782.*Scabin)))+45200.9318628013930.*1./(1+exp...
(-1.*(-4.3919589774966-0.1948486994255.*nbay-0.0000005084270.*WTO+...
0.2327532619346.*phiOW-0.0161204246811.*bOW+0.0302656462199.*LambdaOW...
+0.0022154123472.*crOW-0.1335268069664.*ctOW+0.1254617256349.*...
LambdaCB-0.0003040490068.*Scabin)))+144493.0671008702500.*1./(1+exp...
(-1.*(-2.8181367053407-0.0185701942492.*nbay+0.0000036443335.*WTO-...
0.0248595482942.*phiOW+0.0120394037138.*bOW-0.0206129950133.*LambdaOW...
-0.1264506120945.*crOW+0.0219483092844.*ctOW+0.0609620511186.*...
LambdaCB-0.0004016560276.*Scabin)))-54219.6488870360770.*1./(1+exp...
(-1.*(6.1949536258734+0.0177043042052.*nbay+0.0000013346986.*WTO-...
0.1435826938953.*phiOW-0.0482454976577.*bOW-0.0142134163297.*LambdaOW...
+0.0017827080469.*crOW+0.0997899393085.*ctOW-0.0764716556717.*...
LambdaCB-0.0001383400628.*Scabin)))+94089.7276926388730.*1./(1+exp...
(-1.*(-1.7593328182310-0.2828638016703.*nbay-0.0000003956603.*WTO-...
0.0115166066881.*phiOW+0.0075718673724.*bOW+0.0218502265808.*LambdaOW...
+0.0836650248195.*crOW-0.0131741159604.*ctOW+0.0342624142534.*...
LambdaCB-0.0002070580109.*Scabin)))-107206.5964412038200.*1./(1+exp...
(-1.*(-2.2584778033407-0.1097394204326.*nbay+0.0000023418000.*WTO+...
0.0483640102995.*phiOW-0.0168774458631.*bOW+0.0199064533047.*LambdaOW...
-0.0044718447919.*crOW-0.0500688537615.*ctOW+0.0413718968450.*...
LambdaCB-0.0000849647779.*Scabin)))+89342.1289973872480.*1./(1+exp...
```

```
(-1.*(1.6877120524607+0.0855496652624.*nbay+0.0000019957426.*WTO-...
0.1827019007008.*phiOW+0.0007380440669.*bOW-0.0233670653791.*LambdaOW...
+0.0133525397415.*crOW+0.1545003479859.*ctOW-0.0591159096422.*...
LambdaCB-0.0000242764761.*Scabin)))-92349.5996113203730.*1./(1+exp...
(-1.*(1.4814872491014+0.2173945757702.*nbay+0.0000012477816.*WTO-...
0.0432990876934.*phiOW+0.0228506081191.*bOW-0.0392499338485.*LambdaOW...
-0.0079255733914.*crOW-0.0052200659510.*ctOW-0.0536264755076.*...
LambdaCB-0.0005159516736.*Scabin)))+53013.1605153791970.*1./(1+exp...
(-1.*(-0.3378560186330+0.0249993218336.*nbay+0.0000005519626.*WTO+...
0.1593590425775.*phiOW+0.0007390002993.*bOW-0.0778610740384.*LambdaOW...
+0.0056333853967.*crOW+0.1013515494890.*ctOW+0.0216793430516.*...
LambdaCB-0.0000366794352.*Scabin)))-87405.6970631351290.*1./(1+exp...
(-1.*(1.4568051404892+0.2358778933575.*nbay-0.0000012029198.*WTO+...
0.0949445679707.*phiOW-0.0198911516846.*bOW-0.0235907445750.*LambdaOW...
+0.0367602649338.*crOW+0.1567361121872.*ctOW+0.0053147462361.*...
LambdaCB-0.0003034297208.*Scabin)))+77980.0404245992390.*1./(1+exp...
(-1.*(2.7273989712629+0.2588171056024.*nbay-0.0000018926171.*WTO-...
0.0221276058778.*phiOW-0.0188833298548.*bOW+0.0455852577488.*LambdaOW...
+0.0981660142713.*crOW+0.0147210583921.*ctOW-0.0779442831419.*...
LambdaCB+0.0003688682423.*Scabin)))+101082.7642565038400.*1./(1+exp...
(-1.*(9.7500004145330+0.1093788024204.*nbay-0.0000005198320.*WTO-...
0.0534703528546.*phiOW+0.0038531497906.*bOW-0.0239795719834.*LambdaOW...
-0.0060108251665.*crOW+0.0994243674375.*ctOW-0.2208446647819.*...
LambdaCB+0.0003411004493.*Scabin)))-48195.0008173141250.*1./(1+exp...
(-1.*(-3.2269875641386-0.0399387556513.*nbay+0.0000005771416.*WTO+...
0.1580874626378.*phiOW+0.0220300371826.*bOW+0.0641373395043.*LambdaOW...
+0.0039544222443.*crOW+0.2920119362236.*ctOW+0.0055284511086.*...
LambdaCB+0.0001052133337.*Scabin)))+90804.3371328358770.*1./(1+exp...
(-1.*(2.3197874344156-0.1393410861126.*nbay-0.0000011621368.*WTO+...
0.0628328133201.*phiOW+0.0105415917050.*bOW+0.0270044614420.*LambdaOW...
-0.0265323875901.*crOW-0.0616693805235.*ctOW-0.0494800529941.*...
LambdaCB+0.0000755904292.*Scabin)));
```

D.4 Rear Centerbody Structural Weight

```
function WrcANN=WrcANNFUN(inputs)
%expand input array out to its component vectors:
LambdaCB=inputs(:,8);
LambdaOW=inputs(:,5);
Scabin=inputs(:,9);
WTO=inputs(:,2);
bOW=inputs(:,4);
crOW=inputs(:,6);
ctOW=inputs(:,7);
nbay=inputs(:,1);
phiOW=inputs(:,3);

nruns=size(inputs,1);
%evaluate function:
logsig=@(n) 1./(1 + exp(-n));
WrcANN=-6309.2820095304223-31363.1592888666600.*1./(1+exp...
(-1.*(-0.5159518402505+0.9027191172059.*nbay-0.0000009265345.*WTO-...
0.0060757617898.*phiOW+0.0371488999872.*bOW-0.0146498928035.*LambdaOW...
-0.0829793256064.*crOW+0.0022900038001.*ctOW-0.0444035927554.*...
LambdaCB-0.0002063007175.*Scabin)))+28848.0425945242900.*1./(1+exp...
(-1.*(-0.4065191442024-0.5237806958411.*nbay+0.0000002606904.*WTO-...
0.2205629563505.*phiOW+0.0129938164124.*bOW+0.0047248709988.*LambdaOW...
+0.0093468772436.*crOW+0.0066887399567.*ctOW+0.0041025072248.*...
LambdaCB+0.0003804473823.*Scabin)))+29680.4642375825460.*1./(1+exp...
(-1.*(-2.4316994178027+1.0961637651766.*nbay-0.0000014741647.*WTO-...
0.0465761839875.*phiOW+0.0019953953500.*bOW-0.0079543614167.*LambdaOW...
-0.0543422403433.*crOW+0.0201149551589.*ctOW+0.0344151195203.*...
LambdaCB-0.0008094323465.*Scabin)))+35893.2725251045780.*1./(1+exp...
(-1.*(-2.0592983349551+0.7621721453621.*nbay+0.0000014423933.*WTO-...
0.2490996021210.*phiOW+0.0112042323247.*bOW+0.0048237738058.*LambdaOW...
```

```
+0.0058914484007.*crOW+0.0146582961405.*ctOW-0.0217670176530.*...
LambdaCB+0.0000541584922.*Scabin)))-41429.4425829669490.*1./(1+exp...
(-1.*(2.2582442098063+0.2578410757755.*nbay+0.0000014795493.*WTO-...
0.0455585206347.*phiOW+0.0016156216115.*bOW-0.0377428919608.*LambdaOW...
-0.0347970591192.*crOW+0.0062866500414.*ctOW+0.0002213768908.*...
LambdaCB-0.0003375126945.*Scabin)))+28710.0745134201020.*1./(1+exp...
(-1.*(4.0427917657179-0.3325339468557.*nbay+0.0000004418988.*WTO+...
0.0304940050798.*phiOW+0.0160876507270.*bOW-0.0188610452654.*LambdaOW...
+0.0143162055041.*crOW+0.0214049225511.*ctOW-0.0735874377426.*...
LambdaCB+0.0004047416344.*Scabin)))+14913.3522385330560.*1./(1+exp...
(-1.*(3.0435027853567-0.7377161282549.*nbay-0.0000010078448.*WTO+...
0.1230499293256.*phiOW-0.0139609122870.*bOW+0.1248377892842.*LambdaOW...
+0.0652562841620.*crOW+0.0092647808135.*ctOW-0.0918578074237.*...
LambdaCB+0.0004267499876.*Scabin)))+26728.5986616798730.*1./(1+exp...
(-1.*(-1.6075916812973-0.4614820562923.*nbay-0.0000022621703.*WTO+...
0.0788581875149.*phiOW-0.0257279151480.*bOW-0.0097282048842.*LambdaOW...
+0.0378273644267.*crOW-0.0139418030441.*ctOW+0.0989521278035.*...
LambdaCB-0.0004409555309.*Scabin)))+45056.4167515806770.*1./(1+exp...
(-1.*(0.3420557715533+0.1920353635015.*nbay-0.0000007431078.*WTO-...
0.0076269477165.*phiOW-0.0224196389412.*bOW-0.0029796310688.*LambdaOW...
+0.0037800676418.*crOW+0.0164999746224.*ctOW-0.0139094355326.*...
LambdaCB+0.0004818168855.*Scabin)))+28707.0979887416290.*1./(1+exp...
(-1.*(-1.5694655336721+0.5457269727701.*nbay+0.0000021804608.*WTO-...
0.0755286786991.*phiOW+0.0154985024769.*bOW-0.1076893039006.*LambdaOW...
-0.0574494951772.*crOW-0.0284039573314.*ctOW+0.0527081751922.*...
LambdaCB-0.0002478058424.*Scabin)))-19720.3608790010480.*1./(1+exp...
(-1.*(-0.0729580380897-0.0870509562138.*nbay-0.0000005169079.*WTO+...
0.0871323505325.*phiOW+0.0197194387829.*bOW-0.0468896651092.*LambdaOW...
-0.0030425460261.*crOW+0.0028868257779.*ctOW+0.0037758242200.*...
LambdaCB+0.0005209280272.*Scabin)))-32526.1460776521740.*1./(1+exp...
(-1.*(7.7179800574832-0.1207625992844.*nbay+0.0000008942150.*WTO-...
0.1116154957797.*phiOW-0.0192357057400.*bOW-0.0044167406968.*LambdaOW...
```

```
-0.0278979357264.*crOW-0.0319690444377.*ctOW-0.1072337575265.*...
LambdaCB+0.0001213584607.*Scabin)))-32966.4822182117350.*1./(1+exp...
(-1.*(-0.7866249536530+0.5568306430205.*nbay-0.0000033904666.*WTO+...
0.0261003176717.*phiOW-0.0080994848923.*bOW+0.0015400166685.*LambdaOW...
+0.0093387650121.*crOW-0.0056460646849.*ctOW-0.0332512097947.*...
LambdaCB+0.0004679881032.*Scabin)))+20800.1402389521320.*1./(1+exp...
(-1.*(-0.6710673300732+0.3957530825524.*nbay-0.0000028706830.*WTO-...
0.0179690549974.*phiOW+0.0418326424436.*bOW-0.1128353390683.*LambdaOW...
-0.0000690000936.*crOW+0.0047696037794.*ctOW+0.0266822974659.*...
LambdaCB-0.0000550393470.*Scabin)))+24543.0296454260930.*1./(1+exp...
(-1.*(-3.9132158494220-0.3804430998446.*nbay-0.0000000770376.*WTO+...
0.0207566406020.*phiOW-0.0035904856889.*bOW+0.0275701685668.*LambdaOW...
-0.0356808319185.*crOW+0.0036004867684.*ctOW+0.0819776648512.*...
LambdaCB+0.0001138442865.*Scabin)))-15746.0129796186630.*1./(1+exp...
(-1.*(0.7448270101025+0.0046568495428.*nbay-0.0000014519484.*WTO-...
0.0140553565160.*phiOW-0.0090883559580.*bOW-0.0228017689874.*LambdaOW...
+0.0135458408602.*crOW+0.1903649345649.*ctOW-0.0106108549258.*...
LambdaCB-0.0000127720195.*Scabin)))-66582.3141065427040.*1./(1+exp...
(-1.*(0.5571119835090+0.0608302479774.*nbay+0.0000049296048.*WTO-...
0.0000045813468.*phiOW-0.0065461812189.*bOW+0.0212453291090.*LambdaOW...
-0.0250639430054.*crOW-0.0200344338408.*ctOW+0.0136641564699.*...
LambdaCB-0.0002472471442.*Scabin)))-44363.2662724064650.*1./(1+exp...
(-1.*(-5.5782410224105+0.1464693098031.*nbay+0.0000034389932.*WTO-...
0.0438965764054.*phiOW+0.0115987048737.*bOW-0.0308026165827.*LambdaOW...
+0.0118847072860.*crOW-0.0240002547712.*ctOW+0.0799862140533.*...
LambdaCB+0.0000927675817.*Scabin)))-41125.4374166680060.*1./(1+exp...
(-1.*(2.2488151260883-0.8114557294214.*nbay-0.0000013418015.*WTO-...
0.1169543458020.*phiOW+0.0017250035818.*bOW+0.0056829547151.*LambdaOW...
-0.0227510961965.*crOW-0.0101034886476.*ctOW+0.0159086007934.*...
LambdaCB+0.0001990421751.*Scabin)))+16516.8698075805110.*1./(1+exp...
(-1.*(7.4667493864716-0.3698032209177.*nbay+0.0000017293152.*WTO-...
0.1895715509160.*phiOW-0.0323068854868.*bOW+0.0348379459502.*LambdaOW...
```

```
-0.0425888705141.*crOW-0.0253222070538.*ctOW-0.1019094088756.*...
LambdaCB+0.0003549770526.*Scabin)))+35967.7603733392460.*1./(1+exp...
(-1.*(-3.8512067213275-0.0271142174006.*nbay+0.0000012330991.*WTO-...
0.0296490257666.*phiOW+0.0284016250583.*bOW-0.0680043478435.*LambdaOW...
+0.0473086576459.*crOW-0.0215010359450.*ctOW+0.0612723918854.*...
LambdaCB+0.0000837440003.*Scabin)))-36257.8329307594760.*1./(1+exp...
(-1.*(-3.8664743454618+1.1615745699346.*nbay-0.0000009988316.*WTO-...
0.1519607263524.*phiOW+0.0009207812686.*bOW+0.0096025783144.*LambdaOW...
-0.0064296593817.*crOW+0.0154403857618.*ctOW+0.0233990971354.*...
LambdaCB-0.0003253511697.*Scabin)))+45298.4949830406110.*1./(1+exp...
(-1.*(0.4225773216602+0.6089015560866.*nbay+0.0000001529074.*WTO+...
0.0023320322000.*phiOW+0.0283033016657.*bOW+0.0004245433036.*LambdaOW...
-0.0719655225327.*crOW+0.0124465696674.*ctOW-0.0637623168107.*...
LambdaCB+0.0002293188656.*Scabin)))+31569.1877879251510.*1./(1+exp...
(-1.*(0.2268233803557+0.2615689017586.*nbay+0.0000070872285.*WTO-...
0.0149608742752.*phiOW-0.0123499064331.*bOW+0.0023491894504.*LambdaOW...
-0.0587016301896.*crOW-0.0326205011431.*ctOW+0.0201428889939.*...
LambdaCB-0.0004339336595.*Scabin)))+33736.0174030973070.*1./(1+exp...
(-1.*(2.1659579685900-0.0967472529222.*nbay+0.0000009082379.*WTO+...
0.0865904511106.*phiOW-0.0305898119047.*bOW+0.0712774832785.*LambdaOW...
-0.0348431588576.*crOW+0.0114229514735.*ctOW-0.0403174895435.*...
LambdaCB-0.0000191218448.*Scabin)));
```

D.5 Total Airframe Structural Weight

```
function WairframeANN=WairframeANNFUN(inputs)
%expand input array out to its component vectors:
LambdaCB=inputs(:,8);
LambdaOW=inputs(:,5);
Scabin=inputs(:,9);
WTO=inputs(:,2);
bOW=inputs(:,4);
crOW=inputs(:,6);
```

```
ctOW=inputs(:,7);
nbay=inputs(:,1);
phiOW=inputs(:,3);

nruns=size(inputs,1);
%evaluate function:
logsig=@(n) 1./(1 + exp(-n));
WairframeANN=296253.8856810655000+336286.4923544407400.*1./(1+exp...
(-1.*(-4.8193866241852-0.2954915706764.*nbay-0.0000003815870.*WTO-...
0.0078776398264.*phiOW+0.0089053844924.*bOW+0.0156346134037.*LambdaOW...
+0.0770678716379.*crOW+0.0162132484192.*ctOW-0.0148222397294.*...
LambdaCB+0.0006376306442.*Scabin)))+175381.2775871119500.*1./(1+exp...
(-1.*(-2.4005924313909+0.0030413901654.*nbay+0.0000049120963.*WTO-...
0.0528317036602.*phiOW+0.0150449105417.*bOW-0.0477009188971.*LambdaOW...
-0.1496039678188.*crOW-0.0103728420382.*ctOW+0.0506024837423.*...
LambdaCB-0.0003011072574.*Scabin)))-121038.1890879898900.*1./(1+exp...
(-1.*(2.5020628930193-0.0314716521719.*nbay+0.0000029387885.*WTO-...
0.1694434718692.*phiOW-0.0297318615461.*bOW-0.0712092318224.*LambdaOW...
+0.0254807504762.*crOW-0.1002268148519.*ctOW+0.0297062633325.*...
LambdaCB-0.0000136752913.*Scabin)))+435272.5018719831700.*1./(1+exp...
(-1.*(4.3930146486364-0.0525907415331.*nbay+0.0000007728189.*WTO-...
0.0219869798310.*phiOW-0.0316175287887.*bOW-0.0590536117212.*LambdaOW...
+0.0742859499742.*crOW-0.0211113608604.*ctOW-0.0182097510916.*...
LambdaCB+0.0002289444595.*Scabin)))+349953.7773386215600.*1./(1+exp...
(-1.*(1.4486527764886+0.0130274934871.*nbay+0.0000009300537.*WTO+...
0.0228891906904.*phiOW-0.0120062582402.*bOW+0.0719098194534.*LambdaOW...
-0.0812703905407.*crOW-0.0019352405219.*ctOW-0.0160874366799.*...
LambdaCB+0.0001320661677.*Scabin)))-691040.7753933228100.*1./(1+exp...
(-1.*(0.7437219176432+0.0827136485190.*nbay+0.0000011296049.*WTO-...
0.0302399262790.*phiOW-0.0154977590958.*bOW-0.0202435291291.*LambdaOW...
-0.0285898655001.*crOW-0.0197542842261.*ctOW+0.0133134566003.*...
LambdaCB-0.0002180523914.*Scabin)))-198534.6461859939400.*1./(1+exp...
```

```
(-1.*(5.3999550566678-0.0859088590213.*nbay+0.0000020928474.*WTO+...
0.0593608506765.*phiOW-0.0447174427006.*bOW-0.0171381602194.*LambdaOW...
-0.0137035890319.*crOW-0.0289162539724.*ctOW-0.0351314046192.*...
LambdaCB+0.0002145765513.*Scabin)))+246297.2464258320700.*1./(1+exp...
(-1.*(-2.5596672711427+0.2746110909202.*nbay-0.0000000272851.*WTO+...
0.0358298960340.*phiOW+0.0001159219411.*bOW-0.0111021556143.*LambdaOW...
-0.0317685876933.*crOW-0.0164057568110.*ctOW+0.0288048290439.*...
LambdaCB+0.0005744832347.*Scabin)))-189500.4101634032600.*1./(1+exp...
(-1.*(1.9771682955281-0.0308103154206.*nbay-0.0000000233658.*WTO-...
0.0571686733442.*phiOW-0.0023792202308.*bOW-0.0098362824779.*LambdaOW...
-0.0728154197256.*crOW+0.0017926061847.*ctOW-0.0226563484954.*...
LambdaCB+0.0008189862489.*Scabin)))+155365.4841043305400.*1./(1+exp...
(-1.*(10.1986310632804+0.0017284650994.*nbay-0.0000009722995.*WTO-...
0.0120421836352.*phiOW-0.0488935171875.*bOW-0.2302698413847.*LambdaOW...
+0.0319967873324.*crOW-0.0795241775995.*ctOW+0.0084293945322.*...
LambdaCB+0.0000804528624.*Scabin)))-123717.6651163854400.*1./(1+exp...
(-1.*(12.4681572537420-0.0017022603905.*nbay-0.0000018816935.*WTO+...
0.0207188760619.*phiOW-0.0482472083971.*bOW-0.3336220182560.*LambdaOW...
+0.1898019713502.*crOW-0.0473971460484.*ctOW-0.0116543944255.*...
LambdaCB+0.0002039544947.*Scabin)))-189163.3422216278900.*1./(1+exp...
(-1.*(-1.9657085282541+0.0389514743528.*nbay+0.0000001103139.*WTO+...
0.1554290197112.*phiOW-0.0084473432831.*bOW-0.0094175710329.*LambdaOW...
-0.0337877813140.*crOW-0.0518718822085.*ctOW+0.0498087980794.*...
LambdaCB+0.0003498921770.*Scabin)))-207463.5313545801000.*1./(1+exp...
(-1.*(-3.9125375405019+0.0275150871837.*nbay+0.0000020148892.*WTO+...
0.0300002497957.*phiOW+0.0493900036175.*bOW+0.1449389767643.*LambdaOW...
-0.0580817344592.*crOW+0.0754696920032.*ctOW-0.0136362790636.*...
LambdaCB-0.0000539032589.*Scabin)))-380819.0942198347800.*1./(1+exp...
(-1.*(-1.0836002928707+0.0087928380234.*nbay-0.0000035480181.*WTO+...
0.0389210216057.*phiOW+0.0085440774181.*bOW+0.0074756828568.*LambdaOW...
+0.0774145747284.*crOW+0.0355790554670.*ctOW-0.0222486088455.*...
LambdaCB+0.0001377251042.*Scabin)));
```

REFERENCES

[1] Akay, E., "Conceptual level fem based wing weight estimation," Master's thesis, University of Texas at Austin, Austin, TX, August 2010.

[2] Anderson, J. D., *The Airplane: A History of its Technology.* Reston, VA: American Institute of Aeronautics and Astronautics, 2002.

[3] Ardema, M. D., Chambers, M. C., Patron, A. P., Hahm, A. S., Miura, H., and Moore, M. D., "Analytical fuselage and wing weight estimation of transport aircraft," Tech. Rep. NASA TM-110392, National Aeronautics and Space Administration, May 1996.

[4] Babikian, R., "The historical fuel efficiency characteristics of regional aircraft from technological, operational, and cost perspectives," Master's thesis, Massachusetts Institute of Technology, June 2001.

[5] Bailey, A. R., Boynton, R., Cate, D. M., and Hargrave, J. T., *Introduction to Aircraft Weight Engineering.* Society of Allied Weight Engineers, 1996.

[6] Bradley, K. R., "A sizing methodology for the conceptual design of blended-wing-body transports," Tech. Rep. NASA CR-2004-213016, Langley Research Center, Hampton, Virginia, September 2004.

[7] Collier, C. S., "Stiffness, thermal expansion, and thermal bending formulation of stiffened, fiber-reinforced composite panels," in *AIAA/ASME/ASCE/AHS/ACS 34th Structures, Dynamics, and Materials Conference*, no. AIAA-1993-1569, (La Jolla, CA), 19-22 April 1993.

[8] Gern, F. H., "Finite element based hwb centerbody structural optimization and weight prediction," in *53rd AIAA/ASME/ASCE/AHS/ASC Structures, Structural Dynamics, and Materials Conference*, no. AIAA 2012-1606, (Honolulu, HA), 23-26 April 2012.

[9] Giles, G. L., "Equivalent plate analysis of aircraft wing box structures with general planform geometry," Tech. Rep. NASA-TM-87697, National Aeronautics and Space Administration, March 1986.

[10] Giles, G. L., "Further generalization of an equivalent plate representation for aircraft structural analysis," *Journal of Aircraft*, vol. 26, pp. 67–74, January 1989.

[11] Giles, G. L., "Equivalent plate modeling for conceptual design of aircraft wing structures," in *1st AIAA Aircraft Engineering, Technology and Operations Congress*, no. AIAA 95-3945, (Los Angeles, CA), 19-21 September 1995.

[12] Howe, D., "The prediction of aircraft wing mass," *Proceedings of the Institution of Mechanical Engineers*, vol. 210, pp. 135–145, 1996.

[13] Howe, D., "Blended wing body airframe mass prediction," *Proceedings of the Institution of Mechanical Engineers*, vol. 215, pp. 319–331, 2001.

[14] Kawai, R., Brown, D., Roman, D., Odle, R., Spakovszky, Z., and Papamoschou, D., "Acoustic prediction methodology and test validation for an efficient low-noise hybrid wing body subsonic transport," tech. rep., Boeing Phantom Works, 2008.

[15] Kundu, A. K., *Aircraft Design*. No. 27 in Cambridge Aerospace Series, Cambridge University Press, 2010.

[16] Li, V. and Velicki, A., "Advanced prseus structural concept design and optimization," in *12th AIAA/ISSMO Multidisciplinary Analysis and Optimization Conference*, no. AIAA 2008-5840, (Victoria, British Columbia Canada), 10-12 September 2008.

[17] Liebeck, R., "Design of the blended wing body subsonic transport," *Journal of Aircraft*, vol. 41, pp. 10–25, January-February 2004.

[18] Loftin, L. K., *Quest for Performance: The Evolution of Modern Aircraft*. Washington, D.C.: National Aeronautics and Space Administration, 1985.

[19] Lovejoy, A. E., "Optimization of blended wing body composite panels using both nastran and genetric algorithm," Tech. Rep. NASA/CR-2006-214515, National Aeronautics and Space Administration, Hampton, VA, October 2006.

[20] Mukhopadhyay, V., "Structural concepts study of non-circular fuselage configurations," in *SAE/AIAA World Aviation Congress*, no. WAC-67, (Los Angeles, CA), 22-24 October 1996.

[21] Mukhopadhyay, V., "Blended-wing-body (bwb) fuselage structural design for weight reduction," in *46th AIAA/ASME/ASCE/AHS/ASC Structures, Structural Dynamics and Materials Conference*, no. AIAA 2005-2349, (Austin, TX), 18-21 April 2005.

[22] Mukhopadhyay, V., Sobieszczanski-Sobieski, J., Kosaka, I., and Vanderplaats, G. N., "Analysis, design, and optimization of noncylindrical fuselage for blended-wing-body vehicle," *Journal of Aircraft*, vol. 41, pp. 925–930, July-August 2004.

[23] Myers, R. H., Montogomery, D. C., and Anderson-Cook, C. M., *Response Surface Methodology: Process and Product Optimization using Designed Experiments*. John Wiley & Sons, Inc., 2009.

[24] Nickol, C. L., "Silent aircraft initiative concept risk assessment," Tech. Rep. NASA/TM-2008-215112, Langley Research Center, Hampton, Virginia, February 2008.

[25] Nickol, C. L., "Hybrid wing body configuration scaling study," in *50th AIAA Aerospace Sciences Meeting including the New Horizons Forum and Aerospace Exposition*, no. AIAA 2012-0337, (Nashville, TN), 09-12 January 2012.

[26] Nickol, C. L. and McCullers, L. A., "Hybrid wing body configuration system studies," in *47th AIAA Aerospace Sciences Meeting Including The New Horizons Forum and Aerospace Exposition*, no. AIAA 2009-931, (Orlando, FL), 5-8 January 2009.

[27] Niu, M. C., *Airframe Structural Design: Practical Design Information and Data on Aircraft Structures*. Hong Kong Conmilit Press Ltd., 2nd ed., 1999.

[28] Padula, S. L., Robinson, J. H., and Eldred, L. B., "Structural analysis in a conceptual design framework," in *53rd AIAA/ASME/ASCE/AHS/ASC Structures, Structural Dynamics and Materials Conference*, no. 2012-1753, (Honolulu, HI), 23-26 April 2012.

[29] Pincha, P. J., "Algorithmic mass-factoring of finite element model analyses, an update: Grid-density sensitivity," in *42nd Annual Conference of the Society of Allied Weight Engineers, Inc.*, no. 1524, (Anaheim, CA), 23-25 May 1983.

[30] Raymer, D. P., *Aircraft Design: A Conceptual Approach*. AIAA Education Series, Washington, D.C.: American Institute of Aeronautics and Astronautics, fourth ed., 2006.

[31] Samareh, J. A., "Discrete data transfer technique for fluid-structure interaction," in *18th AIAA Computational Fluid Dynamics Conference*, no. AIAA 2007-4309, (Miami, FL), 25-28 June 2007.

[32] Shanley, F. R., *Weight-Strength Analysis of Aircraft Structures: The Rand Corporation*. McGraw-Hill, 1952.

[33] Smith, H., "College of aeronautics blended wing body development programme," in *ICAS 2000 Congress*, 2000.

[34] Staton, R., "Constrained regression analysis-a new approach to statistical equation development," in *28th Annual Conference*, no. 0762, (San Francisco, CA), Society of Allied Weight Engineers, Inc., 5-8 May 1969.

[35] Staton, R., "Fuselage basic shell weight prediction," in *33rd Annual Conference*, no. 1019, (Fort Worth, TX), Society of Allied Weight Engineers, Inc., 6-8 May 1974.

[36] The Boeing Company, "787 Dreamliner–Program Fact Sheet." http://www.boeing.com/commercial/787family/programfacts.html, 16 February 2010.

[37] Velicki, A. and Jegley, D., "Prseus development for the hybrid wing body," in *AIAA Centennial of Naval Aviation Forum "100 Years of Achievement and Progress"*, no. AIAA 2011-7024, (Virginia Beach, VA), 21-22 September 2011.

[38] Velicki, A. and Thrash, P., "Advanced structural concept development using stitched composites," in *49th AIAA/ASME/ASCE/AHS/ASC Structures, Structural Dynamics, and Materials Conference*, no. AIAA 2008-2329, (Schaumburg, IL), 7-10 April 2008.

[39] Velicki, A., Thrash, P., and Jegley, D., "Airframe development for the hybrid wing body aircraft," in *47th AIAA Aerospace Sciences Meeting Including The New Horizons Forum and Aerospace Expedition*, no. AIAA 2009-932, (Orlando, FL), 5-8 January 2009.

[40] Yovanof, N. P., Velicki, A., and Li, V., "Advanced structural stability analysis of a noncircular, bwb-shaped vehicle," in *50th AIAA/ASME/ASCEAHS/ASC Structures, Structural Dynamics, and Materials Conference*, no. AIAA 2009-2452, (Palm Springs, CA), 4-7 May 2009.